UNIVERSITÁ DEGLI STUDI DI PADOVA

CISAS "G. Colombo"

(Center of Studies and Activities for Space)

Ph.D. School STMS

Science Technologies and Measures for Space

Curriculum: Mechanical Measures for Engineering and Space (MMIS)

Ph.D. Thesis

Performance characterization of propulsion systems for spacecraft applications

Head of the Ph.D. School

Prof. Giampiero Naletto

Tutor

Eng. Daniele Pavarin

Co-tutors

Eng. Alberto Bettella

Eng. Marco Manente

Ph.D. Student

Federico Moretto

CYCLE XXIII — 2011

Sommario

Oggetto del programma di ricerca è l'analisi delle prestazioni di propulsori ibridi attraverso campagne sperimentali condotte su motori in scala ridotta e completa. Le misure effettuate sono state acquisite attraverso un apposito sistema di diagnostica, composto da sensori per la misura dei valori di pressione in differenti sezioni del sistema propulsivo, sensori per il monitoraggio delle quantità impiegate di combustibile e comburente, e sensori per definire le condizioni fisiche dell'ossidante: protossido d'azoto auto-pressurizzato.

Durante questa esperienza condotta al CISAS nell'ambito della propulsione chimica, svariate prove sperimentali sono state condotte per studiare le problematiche che concernono il funzionamento di motori ibridi: *a*) test di scarica ossidante, per la messa a punto del circuito idraulico, del funzionamento della valvola principale e delle prestazioni del sistema di iniezione; *b*) test di accensione, per investigare le problematiche connesse con le fasi iniziali della combustione; *c*) test a fuoco, per lo studio del motore durante il completo funzionamento.

Tutta la strumentazione necessaria è stata accuratamente progettata e prodotta con tali finalità: la facility sperimentale, il banco di test e le diverse versioni dei sottosistemi del motore. Una consistente mole di lavoro è stata portata a termine, e ha permesso la verifica degli effetti di diverse soluzioni progettuali sulle prestazioni finali sviluppate dagli endoreattori testati.

Una prima campagna sperimentale su motori in scala ridotta ha servito come "banco prova" per prendere confidenza con i sistemi propulsivi chimici, per la calibrazione della diagnostica e per evidenziare le iniziali caratteristiche prestazionali: in particolare, in questa fase è stata fatta la scelta definitiva del materiale per il grano combustibile. In un secondo momento, una prima versione in scala completa del motore è stata progettata, impiegando i risultati della precedente campagna sul propulsore in scala ridotta: l'analisi delle instabilità di combustione è iniziata a partire da questa serie di test, nella quale il comportamento instabile è stato studiato e riconosciuto come effetto dell'iniezione di ossidante nella camera di combustione.

Per questo motivo, una precisa fase di studio è stata implementata per analizzare come il fluido si comporta a cavallo della piastra di iniezione: attraverso un set-up sperimentale dedicato, svariati tipi di iniettore sono stati testati in molte configurazioni diverse, nell'ottica di studiare attentamente le proprietà fisiche dell'N_2O in condizione auto-pressurizzata, così come è stato impiegato nei test del motore. I risultati di questa fase intermedia hanno permesso di aggiornare alcune soluzioni tecniche del design del motore, e migliorarne in questo modo le prestazioni sia in termini di efficienza di combustione, sia nell'attenuazione delle instabilità.

La verifica degli effetti sulle prestazioni sviluppate è stata effettuata durante due ultime campagne di test, condotte su due diverse versioni del motore. L'utilità di questo lavoro è stato anche quello di sviluppare una realistica versione "pre-volo" del motore, che ha impiegato materiali leggeri e una configurazione compatta: le campagne sperimentali sono state molto utili nella definizione delle sollecitazioni che potrebbero interessare un eventuale payload del sistema propulsivo prodotto.

Abstract

The subject of the research program described in the present work is the analysis of hybrid rocket motors performance, through different experimental campaigns, which have been conducted on both small scale and full scale versions. The diagnostics system was composed by sensors to measure the pressure levels in many different sections of the propulsion system, sensors to monitor the burned quantity of fuel and oxidizer and sensors useful to define the physical conditions of the used oxidant: liquid nitrous oxide, in auto-pressurization form.

During this experience with chemical propulsion systems at CISAS, various test types have been performed, in order to study all the problematics, which concern the functioning of a hybrid rocket: *a*) discharge tests, to set-up the hydraulic circuit, valve actuation and injection of oxidizer; *b*) ignition tests, to understand the issues that are connected with the initial burning phases; *c*) hot firing tests, to investigate the behavior of the motor during complete functioning operations.

All the needed instrumentation has been accurately and specifically designed and produced for this scope: the experimental facilities, the test bench, the different versions of the motor subsystems. A huge amount of work has been done, and it has permitted to verify the effect of many different design solutions on the final performance of the tested rockets.

An initial small scale experimental campaign served as a "test bench" in order to preliminarily verify main issues in the development of chemical propulsion systems, to calibrate the diagnostics and to highlight the initial performance characteristics of the motor: in particular, the final choice of the fuel grain material has been done in this phase. After that, a first full scale motor version has been designed, using the resulting data of the small scale tests: the analysis on the verified instabilities started from this experimental campaign, in which an unstable behavior has been investigated and assigned to the injection of oxidizer in combustion chamber. For this reason, an accurate research program has been set-up to deep analyse how the fluid enters and behaves prior and after the injection plate: in a dedicated facility,

many different injector types have been tested in different discharge conditions, in order to investigate the physical properties of N_2O in auto-pressurization form, as it is used in the tested motors. The results of this intermediate program have permitted to upgrade some technical solutions of the rocket design, and improve its performance both in terms of combustion efficiency and instabilities mitigation.

To check the effects on the developed performance, two final verification test campaigns have been carried out, on two different motor versions. This has been useful also in the developing of a real "proto-flight" motor, which adopted lightweight materials and compact configurations: the experimental campaigns have been very useful in the definition of all the stresses, that would affect a possible payload of the produced propulsion system.

Contents

List of Figures

List of Tables

Glossary

cc	Combustion Chamber
CISAS	Center for Studies and Activity for Space "G. Colombo", at University of Padua
FEM	Finite Elements Method
FFT	Fast Fourier Transform
HTM	Hybrid Thruster Model
LDA	Laser Doppler Anemometer
LIF	Laser Induced Fluorescence
PIV	Particle Image Velocimetry
TC	Thermocouple

Chapter 1

Introduction

1.1 Overview on Hybrid Rockets

In aerospace propulsion field, chemical propulsion is the most used technology to produce high values of thrust, adequate to launch, for example, payloads into orbit or to orbit maneuvering intents. In chemical propulsion a fuel and an oxidant combine in a mixing chamber; the energy obtained from this chemical process is transferred to the total flux as thermal energy. The hot exhaust gases are then expanded in a nozzle, to give the desired thrust to the vehicle. The choice of fuel/oxidant type is a basic aspect, as well as the mixing strategy. For many years the answer to this question has been represented by solid and liquid propulsion systems, but nowadays a third opportunity is coming forward: hybrid rockets.

Liquid motors use fuels and oxidants that are stored in dedicated tank in liquid form. By means of a pressurized system, or by a mechanical pump, they are conducted in a mixing chamber, where the chemical reaction of combustion takes place. These motors can generally satisfy a wide range of thrust requirements, permit throttability and assure the better efficiency, but at the expense of a considerable complexity of the system: the adducting circuit comprehends pipes, locking valves, pressure regulators, injectors, turbo-pumps and other several hydraulic components. Considering the fact that redundancy is strictly required for reliability matters, it's easy to realize that this type of propulsion systems could be too expensive for the expected purposes.

Solid rockets are in a certain way different in their intrinsic factor, so they grant advantages and troubles. In a solid motor the fuel and the oxidant are chemically premixed in the combustion chamber, to give a single solid grain of propellant. Then it is simply enough to ignite this substance to make the fuel and oxidant re-

act together, producing the high energy gases: for this reason, the required thrust performances implicate an accurate and specific design of the grain combustion port. Solid rockets provide good thrust, and they are the simplest propulsion systems among chemical propulsion; on the other hand they also suffer inefficient combustion and don't permit throttability. They are also potentially dangerous, because oxidant and fuel are mixed together, with the possibility of generating explosions (strict requirements of stocking methods and handling).

It is quite clear that an alternative solution is required to assure specific demands: at one side there are motors with good performances, but high complexity and costs; on the other side a greater ease is assured with substantial penalization of the efficiency. In general it is possible to assume that hybrid rockets can combine the safety aspects and versatility of liquid engines, as throttability, shut-off and reigniting capability, with the simplicity and advantages of solid rockets. All to the good of hybrids many aspects may be consider: propellants are inactive, so they can be easy handled, moved and stocked; there are no risks of explosions, because the combustion chamber pressure in essence depends on the oxidant mass flow rate, and not on the grain surface that is exposed to flame, as in solid motors; low environmental pollution, thanks both to the exhausted gas composition, and to the fact that an accident would not be dangerous: out of combustion chamber, the oxidant disperses in atmosphere and fuel is not reactive. Hybrid systems are surely more complex than solid motors, because they need a feed line for the oxidant, but on the other hand only a single line is necessary, so they result constructively more simple and reliable than bi-propellant liquid engines, which they approach in performances. Finally on the whole, in hybrid rockets technology recurring and non-recurring costs are much lower than both liquid and solid propulsion systems.

Besides the described advantages, hybrid rockets suffers various troubles in the time changing of the mixing ratio in the combustion zone above the fuel surface (and in consequence, of the performances), the instabilities that sometimes may occur and most of all the low regression rate, which involves wide surfaces exposed to the flame to give high level thrust (i.e. big volumes). These effects are not so bad however; as far as specific impulse is concerned, hybrid rockets actually sit on the median between liquid and solid systems. Typical performance numbers are not difficult to find: for liquid systems, impulse can range from 300s up to 400s for the SSME (Space Shuttle Main Engine); most solid systems operate at a specific impulse of 200 to 270s. Performances generated thus far for experimental hybrid test engines lie in the range of 275 to 350s. Another disadvantage to hybrids is

	Solid Rockets	**Liquid Rockets**
Simplicity	– Chemically simpler – Tolerant of fabrication errors	– Mechanically simpler – Tolerant of processing errors
Safety	– Reduced chemical explosion hazard	– Reduced fire hazard – Less prone to hard-starts
Operability	– Throttling start / stop / restart capability	– Operation requires only a single liquid
Performance	– Higher specific impulse (Isp)	– Higher fuel density – Easy inclusion of high-energy additives (Al, Be, etc.)
Environmental	– No perchlorates required – Non-toxic exhaust products	– Solid fuel presents reduced contamination hazard
Cost	– Reduced development costs – Reduced recurring costs	

Table 1.1: Advantages of hybrid technology, compared with other chemical propulsion systems.

that there will usually be unburned fuel slivers remaining after burning; however, this effect also plagues solid rockets. Clearly in many of these respects, the disadvantages of hybrid rockets are non-critical, and many are clearly not disadvantages with respect to solid systems.

In its simplest form a hybrid rocket consists of a pressure vessel (tank) containing the liquid propellant, the combustion chamber containing the solid propellant, and a valve isolating the two. When thrust is desired, a suitable ignition source is introduced in the combustion chamber and the valve is opened. The liquid propellant (or gas) flows into the combustion chamber where it is vaporized and then reacted with the solid propellant. Combustion occurs in a boundary layer diffusion flame adjacent to the surface of the solid propellant: a turbulent diffusion flame is established over this surface. Heat transfer from the flame vaporizes the fuel sustaining combustion and the fuel surface regresses in the radial direction as it is

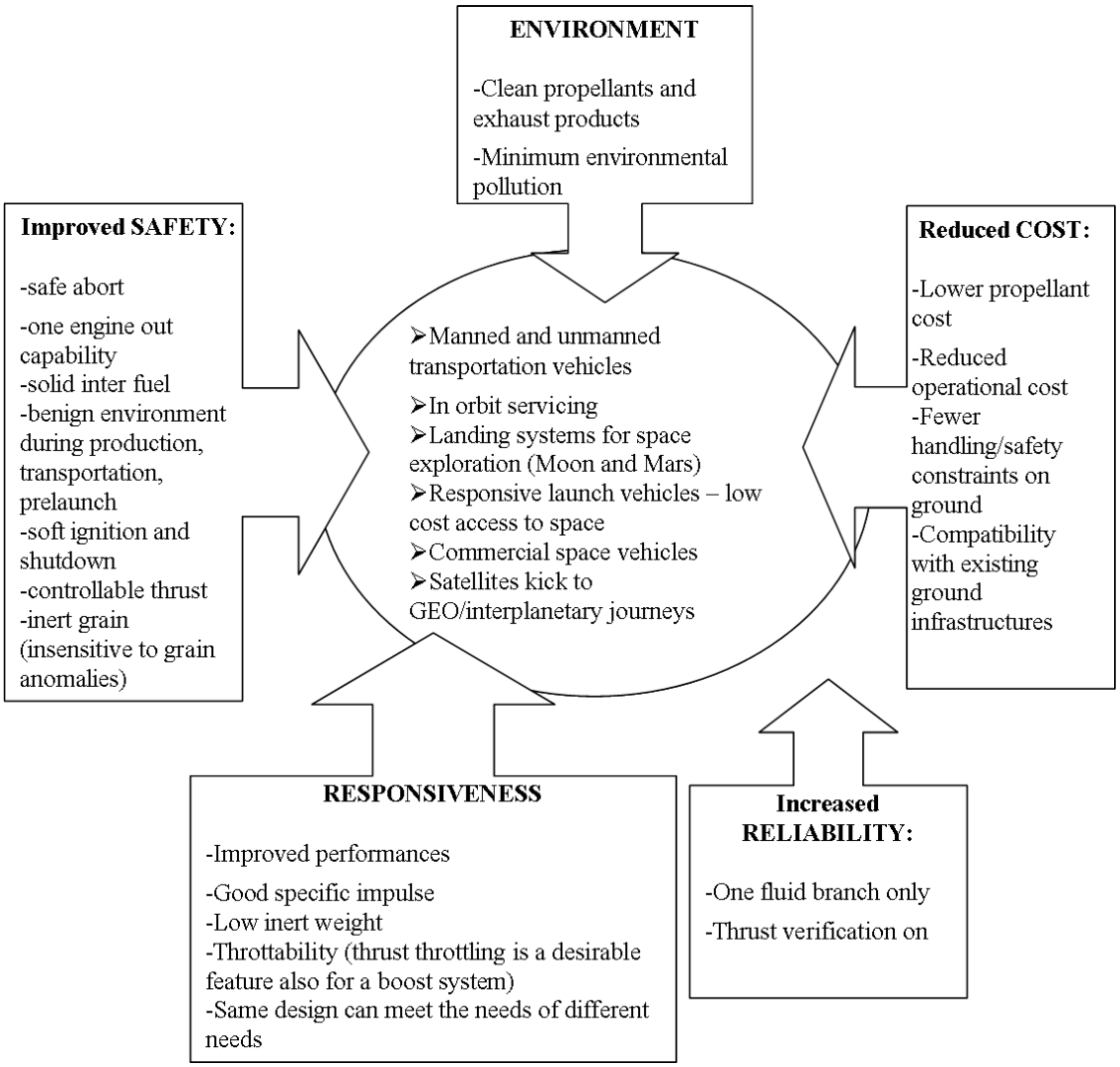

Figure 1.1: Hybrid propulsion technology key features, advantages of hybrid rockets: less expensive, environmentally safe motors that can not explode, can be shut off, restarted and throttled. Significant cost savings for larger motors.

consumed. Generally the liquid propellant is the oxidizer and the solid propellant is the fuel because solid oxidizers are problematic and lower performing than liquid oxidizers. Furthermore, using a solid fuel such as HTPB or paraffin allows for the incorporation of high-energy fuel additives such as aluminum, lithium, or metal hydrides. Common oxidizers include gaseous or liquid oxygen or nitrous oxide (N_2O). Common fuels include polymers such as polyethylene (PE), cross-linked rubber such as HTPB or liquefying fuels such as paraffin (wax). In certain applications a pressurizing system may be required.

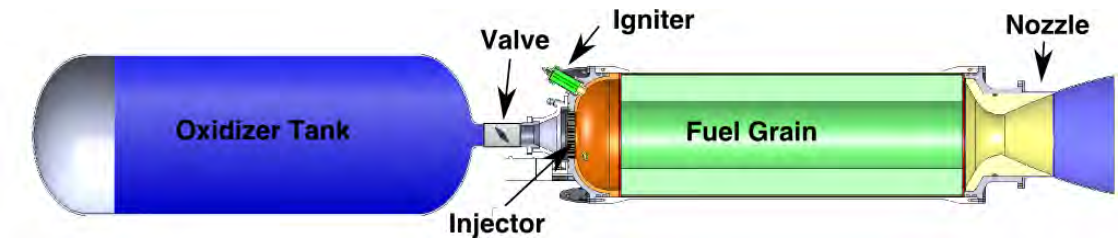

Figure 1.2: Hybrid propulsion system main components.

1.2 Scope of Work

The research program comprehends studies and experimental applications in the chemical propulsion field, with reference to hybrid motors. The scope of this work is the development of measurement techniques, to analyze the performances of a hybrid propulsion system and its functioning features, with a specific characterization of the transient phenomena. Using data from pressure measurements, the analysis is dedicated to the functioning instabilities investigation, and furthermore to the development of specific mitigation solutions. The initial phases have been dedicated to a deep experimental investigation of the motor functioning, both on a small scale and on a full scale version: during these tests the hybrid rocket functioning characteristics and issues have been identified and analyzed, to distinguish all instabilities sources and eventual scale effects. Afterwards the main instabilities causes have been deeply investigate with dedicated experimental activities, with particular attention on the oxidizer behavior in the hydraulic circuit: injection of N_2O has been studied with a specific experimental facility, to check the functioning of different injectors and different discharge conditions. On the basis of these analyses, some mitigation strategies have been studied and developed: the results of these activities have been used in the final test campaigns, that has been performed on two different full scale upgrades of the motor to test these damping techniques.

1.3 Overview of Research Program

The complete research program is described in this work, and an overview of the arguments is given in this section. The description of some distinctive performance parameters follows the introductory chapter, and it comprehends the most important values in the characterization of a propulsion system, and especially as a hybrid system is concerned: they are the combustion efficiency, the specific impulse and the different instabilities that may occur. The third chapter deals with the first

experimental phase of the research program: it describes the design of the test facility and the motor, with a complete report of the tests that have been conducted both on a small scale ground version motor and on a full scale demonstrator. The diagnostics, that have been used during the tests, are completely described and all the collected data are analyzed to precisely detect the instability phenomena that have occurred. These data have been used in the following work package, which concerns the investigation of the instabilities induced by the oxidizer feed system: it is described in chapter four. A specific test facility has been developed to verify the effect of different injector types and different discharge conditions, with a complete dedicated diagnostics set-up to monitor the fluid behavior: mass flow rate and oxidizer physical conditions. The analyses of the experimental results have been useful in the development of mitigation strategies, and these have been tested in the following test campaigns. The results are explained in the fifth chapter. Finally, the last chapter of the present work reports and summarizes the results of the research activities and draws the conclusions that can be deducted from them.

In the present work the various subjects are divided on the basis of the main described argument, but this does not strictly reflect the temporal course of the events: in some occasions, the detected problematics have required a specific research activity on particular issues to be solved, and this determined some parallel activities. The following figure illustrates how the main described subjects have been organized, and the output fluxes among the different work packages.

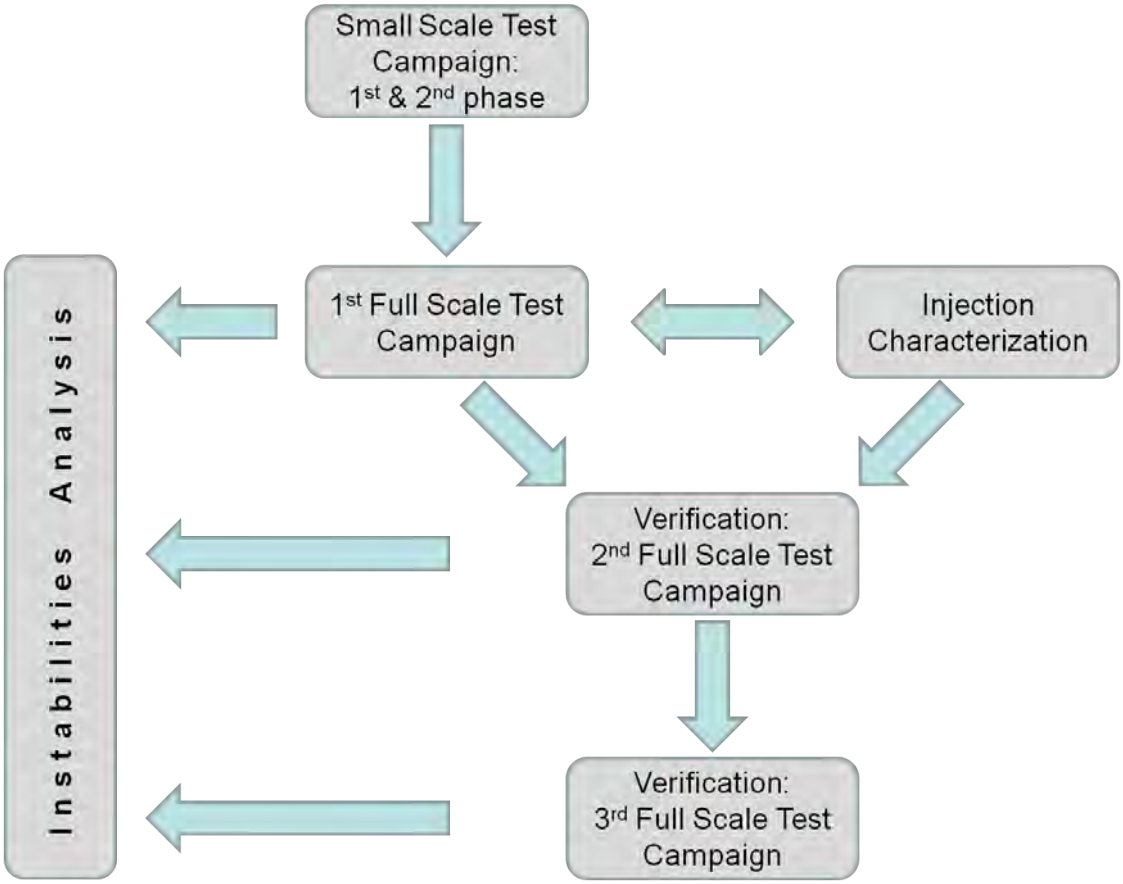

Figure 1.3: Research program work packages organization.

Chapter 2

Performance Parameters

When aerospace propulsion systems are concerned, one of the most critical aspect in choosing the appropriate technology is the evaluation of the impact that it will have on the entire vehicle. The core of an aeronautical or space rocket is the payload, and every other device or subsystem will inexorably limit it in mass and dimensions. Unfortunately all different subsystems are needed, and a compromise will be needed for each.

As the propulsive technology is concerned, there are some specific parameters that are useful in the "quality" definition, and these are described in the following sections: *combustion efficiency*, *specific impulse* and finally *combustion instabilities*. In a certain way, the first two parameters can be thought to be correlated with each other, because they express how the propellants are used during the thrust phase: the higher their value, the better the subsystem, because it would mean less propellants charged in the rocket to produce the same propulsive effect. The third parameter deals with the stresses that are induced on the entire vehicle during its functioning: a smooth application of the thrust will be less invasive on the other structures (and this also will mean a better combustion), so this will reflect in less demanding structural requirements for the rocket mechanical design.

2.1 Combustion Efficiency

Although efficiencies are not commonly used directly in designing rocket units, they permit an understanding of the energy balance of a rocket system. Their definitions are arbitrary, depending on the losses considered, and any consistent set of efficiencies, such as the one presented in this section, is satisfactory in evaluating energy losses. Two types of energy conversion processes occur in any propulsion

system, namely, the generation of energy, which is really the conversion of stored energy into available energy and, subsequently, the conversion to the form in which a reaction thrust can be obtained. The kinetic energy of ejected matter is the form of energy useful for propulsion.

As the *combustion efficiency* is concerned, in the case of chemical rockets it is the ratio of the actual and the ideal heat of reaction per unit of propellant and is a measure of the source efficiency for creating energy. In particular, with reference to the thermochemical processes occurring in the combustion chamber, it can be defined as *energy release efficiency*, and therefore it refers to the actual change in enthalpy per unit propellant mixture to the calculated change in enthalpy necessary to transform the propellants from the initial conditions to the products at the chamber temperature and pressure. The actual enthalpy change can be evaluated if the initial propellant condition and the actual composition and the temperature of the combustion gases are measured. Experimental measurements of combustion temperature and gas composition are difficult to perform accurately, and the combustion efficiency is therefore actually evaluated only in rare instances. Actual measurements on well designed rocket propulsion systems indicate efficiency values of 94 to 99%. These high values indicate that the combustion is essentially complete, that very little, if any, unreacted propellant remains, and that chemical equilibrium is indeed established.

In this research work, the combustion efficiency is evaluated from the theoretical and experimental values of the *characteristic exhaust velocity* c^*. It allows to focus on propellant and chamber performance independent of the nozzle. Development of c^* begins with the expression used for the mass flow rate at the nozzle throat: $\dot{m} = (\rho A v)_t$.

Using the stagnation conditions for temperature, pressure and density:

$$\frac{T_0}{T} = 1 + \frac{\gamma - 1}{2} M^2 \tag{2.1}$$

$$\frac{\rho_0}{\rho} = \left(1 + \frac{\gamma - 1}{2} M^2\right)^{\frac{1}{\gamma - 1}} \tag{2.2}$$

the perfect-gas law and the throat velocity: $v_t = \sqrt{\gamma R T_t}$, is it possible to express all variables of the mass flow rate in terms of chamber conditions, and the expression becomes:

$$\dot{m} = \frac{A_t p_0}{\sqrt{\gamma R T_0}} \left\{ \gamma \left(\frac{2}{\gamma + 1} \right)^{\frac{\gamma+1}{2(\gamma-1)}} \right\} = \frac{A_t p_0}{\sqrt{\gamma R T_0}} \Gamma' \tag{2.3}$$

where the expression in large brackets has been expressed as Γ'. Noting that $a_0 = \sqrt{\gamma R T_0}$ is the value of acoustic velocity in the chamber, expression 2.3 becomes:

$$\dot{m} = \frac{\Gamma'}{a_0} A_t p_0 \tag{2.4}$$

The characteristic exhaust velocity can now be defined as:

$$c^* = \frac{a_0}{\Gamma'} \tag{2.5}$$

where a_0 is the acoustic velocity in the chamber in [m/s] and Γ' is a function of γ as defined in eq. 2.3. This expression shows that c^* is a function only of temperature and gas properties in the combustion chamber (γ, R and T_0), and these values are all determined from the thermochemical reaction in the combustion chamber. In other words, is it possible to use c^* to analyze the chamber and throat independent of the nozzle.

From eq. 2.4 is it possible to develop also another expression:

$$c^* = \frac{A_t p_0}{\dot{m}} \tag{2.6}$$

where

A_t is the throat cross-sectional area in [m^2]

p_0 is the chamber pressure in [N/m^2]

$\dot{m}$ is the mass flow rate through the rocket in [kg/s]

in case of

1. isentropic flow
2. perfect gas
3. one-dimensional, steady flow

From eq. 2.6 is it possible to obtain an empirical value of c^*, which can be compared to the theoretical calculation to obtain an other expression of the combustion efficiency. Based on experience, the actual value of c^* should be 96% to 98% of the theoretical value: incomplete combustion causes this reduction.

A further parameter, which is closely connected with combustion efficiency, is the *regression rate*. This is a fundamental parameter for the hybrid rocket internal ballistic, and it describes how the solid fuel vaporizes and enter the port for combustion, and more specifically, how fast it does it or regress. A common expression to predict the behavior of the various ballistic parameters with reasonable accuracy, in case of a given length motor, is:

$$\dot{r} = a_0 G_0^n$$

where:

$\dot{r}$ is the regression rate value in [m/s]

a_0 is the regression rate coefficient incorporating grain length term

n is the regression rate exponent

G_0 is the oxidizer mass flux rate [kg/(m$^2 \cdot$ s)]

To get the best accuracy from this simplified equation, the constants a_0 and n should be determined directly from experimental data; typical experimental values of n range from 0.5 to 0.8.

2.2 Specific Impulse

The total impulse I_t is the thrust force F (which can vary with time) integrated over the burning time t.

$$I_t = \int_0^t F \, dx \tag{2.7}$$

For constant thrust and negligible start and stop transients this reduces to:

$$I_t = Ft \tag{2.8}$$

I_t is proportional to the total energy released by all the propellant in a propulsion system.

The specific impulse I_s is the total impulse per unit weight of propellant. It is an important figure of merit of the performance of a rocket propulsion system, similar in concept to the kilometers per liter parameter used with automobiles. A higher number means better performance.

If the total mass flow rate of propellant is $\dot{m}$ and the standard acceleration of gravity at sealevel go is 9.8066 m/s^2, then

$$I_s = \frac{\int_0^t F\, dt}{g_0 \int \dot{m}\, dt} \tag{2.9}$$

This equation will give a time-averaged specific impulse value for any rocket propulsion system, particularly where the thrust varies with time. During transient conditions (during start or the thrust buildup period, the shutdown period, or during a change of flow or thrust levels) values of I_s can be obtained by integration or by determining average values for F and $\dot{m}$ for short time intervals. For constant thrust and propellant flow this equation can be simplified; below, m_p is the total effective propellant mass:

$$I_s = I_t/(m_p g_0) \tag{2.10}$$

For constant propellant mass flow $\dot{m}$, constant thrust F, and negligibly short start or stop transients:

$$\begin{aligned} I_s &= F/(\dot{m} g_0) = F/\dot{w} \\ I_t/(m_p g_0) &= I_t/w \end{aligned} \tag{2.11}$$

The product $m_p g_0$ is the total effective propellant weight w and the weight flow rate is $\dot{w}$. The concept of weight relates to the gravitational attraction at or near sea level, but in space or outer satellite orbits, "weight" signifies the mass multiplied by an arbitrary constant, namely g_0. In the *Système International* (SI) or metric system of units I_s can be expressed simply in "seconds," because of the use of the constant g_0. The numerical value of I_s does not represent a measure of elapsed time, but a thrust force per unit "weight"-flow-rate.

2.3 Instabilities

The hybrid combustion process tends to produce somewhat rougher pressure versus time characteristics than either liquid or solid rocket engines. However, a well-designed hybrid will typically limit combustion roughness to approximately 2 to 3% of mean chamber pressure. In any combustion device, pressure fluctuations will tend to organize themselves around the natural acoustic frequencies of the combustion chamber or oxidizer feed system. While significant combustion pressure oscillations at chamber natural-mode acoustic frequencies have been observed

in numerous hybrid motor tests, such oscillations have not proved to be an insurmountable design problem. When pressure oscillations have occurred in hybrid motors, they have been observed to grow to a limiting amplitude which is dependent on such factors as oxidizer feed system and injector characteristics, fuel grain geometric characteristics, mean chamber pressure level, and oxidizer mass velocity. Unbounded growth of pressure oscillations, such as may occur in solid and liquid rocket motors, has not been observed in hybrid motors.

Hybrid motors have exhibited two basic types of instabilities in static test environments: oxidizer feed system-induced instability (non-acoustic), and flame holding instability (acoustic). Oxidizer feed system instability is essentially a *chugging* type, and arises when the feed system is sufficiently "soft": it stems mostly from the elastic nature of the feed systems and structures of vehicles or the imposition of propulsion forces upon the vehicle. Chugging can occur in a test facility, especially with low chamber pressure engines (0.7 to 4 MPa), because of propellant pump cavitation, gas entrapment in propellant flow, tank pressurization control fluctuations, and vibration of engine supports and propellant lines. It can be caused by resonances in the motor feed system (such as an oscillating bellows inducing a periodic flow fluctuation) or a coupling of structural and feed system frequencies. Propellant flow rate disturbances, usually at 10 to 50 Hz, give rise to low-frequency longitudinal combustion instability, producing a longitudinal motion of vibration in the vehicle. In cryogenic systems, this implies a high level of compressibility from sources such as vapor cavities or two-phase flow in feed lines combined with insufficient isolation from motor combustion processes.

The feed system instabilities can easily be recognized due to their distinct characteristics, which can be listed as follows:

1. These instabilities are mostly experienced in liquid-fed systems.

2. The pressure oscillations are much more regular in nature compared to the inherent low-frequency instabilities of hybrid rockets. The Fourier transform of the pressure signal shows a reasonably narrow bandwidth peak.

3. The driving force is a simple coupling between the feed system and combustion chamber dynamics. The vaporization delay of the oxidizer in the combustion chamber is the root cause of the positive feedback needed to produce growing pressure oscillations. The injector upstream pressure, generally, participates in the oscillatory behavior.

4. Even feed systems with isolation elements such as cavitating venturis are vulnerable to this kind of coupling due to the finite bulk modulus of the fluid in the feed lines upstream of the injector.

5. The higher modes (at multiples of the fundamental frequency) are typically also evident in the spectra.

Figure 2.1(a) illustrates feed system induced instability in a 600mm (24in) external diameter hybrid motor operated at a LOX flow rate of 10 kg/s (20 lbm/sec) with HTPB fuel. The instability is manifested by high-amplitude, periodic oscillations well below the first longitudinal (l-L) acoustic mode of the combustor. In this example the oscillation frequency is 7.5 Hz whereas the 1-L mode frequency is approximately 60 Hz. Stiffening the feed/injection system can eliminate the oscillation. This is accomplished by increasing the injector pressure drop (thus making propagation of motor pressure disturbances upstream through the feed system more difficult) and eliminating sources of compressibility in the feed system. For purposes of comparison, Fig. 2.1(b) shows a pressure-time trace from the same 600mm diameter hybrid motor exhibiting stable combustion while being operated at a LOX flow rate of 20 kg/s (40 lbm/sec) at a maximum chamber pressure of 6 MPa (900 psi).

Flame-holding instability relevant to hybrid motors was first observed during the development of solid fuel ramjets. A solid fuel ramjet is essentially a hybrid motor operating on the oxygen available in ram air. Flame-holding instabilities in hybrids are typically manifested at acoustic frequencies and appear in longitudinal modes. No acoustic instabilities in hybrid motors have been observed in higher frequency tangential or radial modes such as in solid rocket motors or liquid engines. Flame-holding instabilities arise due to inadequate flame stabilization in the boundary layer and are not associated with feed system flow perturbations. Figure 2.2(a) illustrates flame-holding instability in an 280 mm (11 in) diameter hybrid motor operated with gaseous oxygen (GOX) oxidizer and HTPB fuel, using an injector producing a conical flow field. In this test, oxygen flow was initiated through the motor at a pressure of 0.6 MPa (90 psi) for two seconds prior to motor ignition. The motor was ignited using a hydrogen torch that continued to operate for approximately one second following motor ignition. During the first second of motor operation, the hydrogen igniter flame stabilizes the motor. When the igniter flame is extinguished, the motor becomes unstable. Figure 2.2(b) illustrates operation of the same 280 mm diameter motor in which the flame-holding instability has been

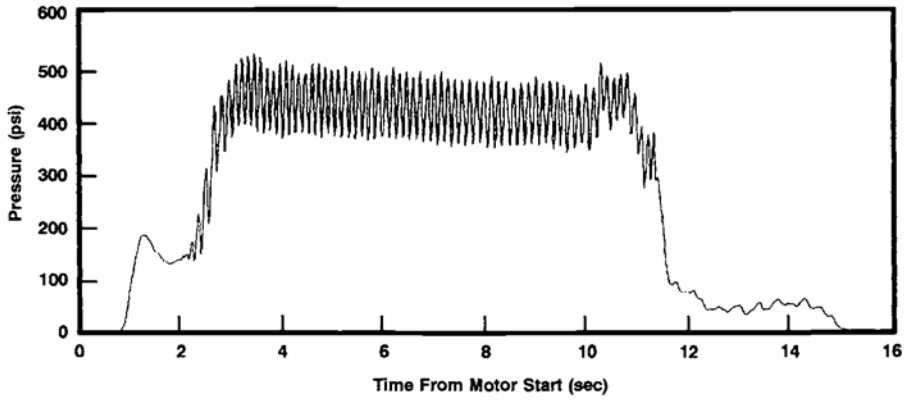

(a) Unstable combustion

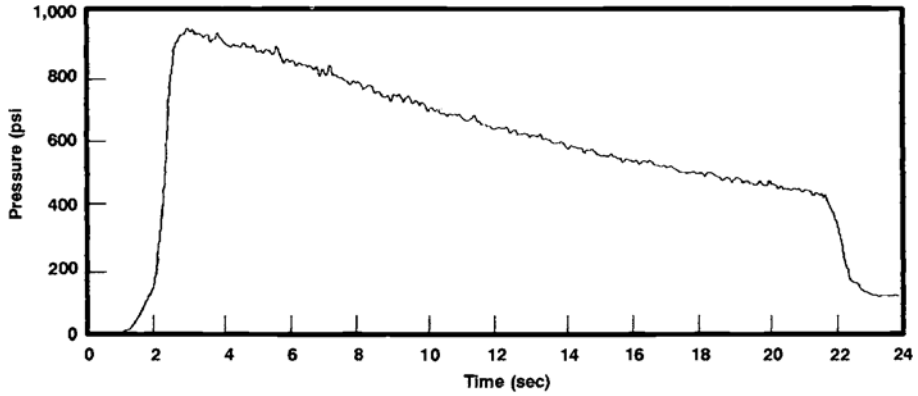

(b) Stable combustion

Figure 2.1: 2.1(a) Periodic, large-amplitude, low-frequency combustion pressure oscillations are an example of oxidizer feed system induced "chug" type combustion instability in a 24-in. diameter LOX/HTBP motor. 2.1(b) An example of stable combustion in a 24-in. diameter LOX/HTPB motor, exhibiting an overall combustion roughness level of 1.3%.

suppressed without the use of a hydrogen flame. In this case stable combustion was achieved by changing the flow field within the motor, using an injector producing an axial flow field. Figure 2.3 shows the result of decomposing the pressure versus time signal for the unstable example of Fig. 2.2(a) into its frequency components via fast Fourier transform techniques. The 1-L acoustic oscillation mode is clearly visible at approximately 150 Hz.

Comparison of the average pressure levels in Figs. 2.2(a) and 2.2(b) illustrates an interesting phenomenon. For the same motor operating conditions (oxidizer flow rate, grain geometry and composition, and throat diameter) the average pressure in the unstable motor is significantly greater than that in the stable motor. This

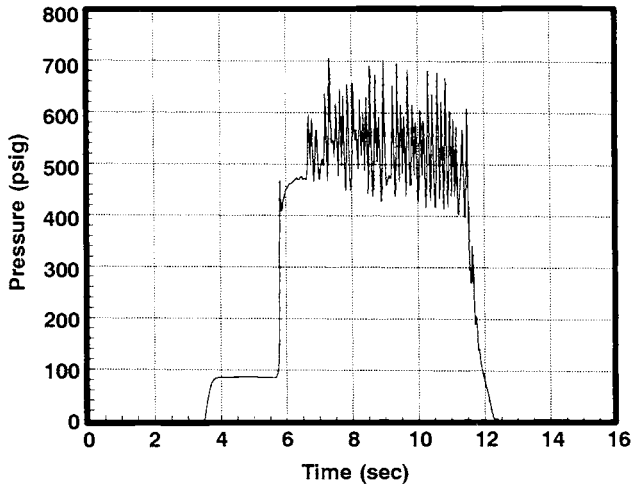

(a) Unstable combustion

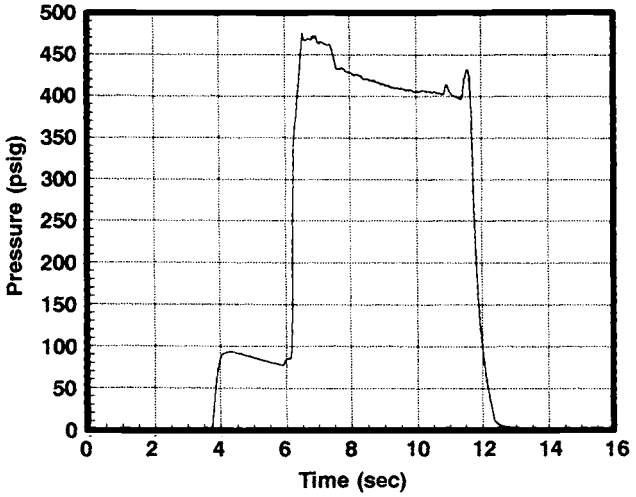

(b) Stable combustion

Figure 2.2: 2.2(a) An example of large-amplitude, high-frequency combustion pressure oscillations due to flame-holding instability in an 11-in. diameter GOX/HTPB motor. Instability during the initial one second of burn has been suppressed by the use of a pilot flame. 2.2(b) Suppression of flame-holding instability in an 11-in. diameter GOX/HTPB motor by means of strong axial injection of oxidizer.

same phenomenon has been noted in solid propellant motors and the results from intensification of heat transfer to the fuel surface due to the gas velocity at the fuel surface oscillating at high frequency. The high heating rate results in the vaporization of more fuel than would otherwise occur in equilibrium conditions, thus producing a higher average chamber pressure.

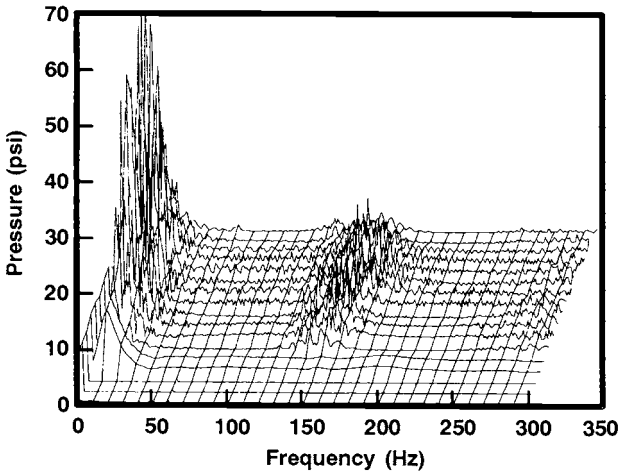

Figure 2.3: A frequency-versus-amplitude plot at successive time intervals for an ll-in, diameter GOX/HTPB motor test shows pressure oscillations in the motor 1-L acoustic mode at 150 Hz due to flame-holding instability.

Despite recent advances in understanding causes of and solutions for combustion instability in hybrid motors, development of a comprehensive, predictive theory of combustion stability remains one of the major challenges in hybrid technology development.

Chapter 3

Preparatory Experimental Activities

In any research program the experimental activity is essential for the verification of all the concepts, that have been described with numerical models. Furthermore, dealing with practical issues is useful to highlight all critical aspects in producing real systems. For these reasons, a wide experimental activity on hybrid rocket motors has been carried out at CISAS, and several versions have been successfully tested. In particular, small scale and full scale hybrid rocket tests have been performed with the specific intent of analyzing the combustion instability arising in different motor configurations.

Further paragraphs describe the experimental activities conducted for the hybrid rocket performance characterization: the design of the test facility, the motor versions and the complete preliminary test campaign: small scale and full scale tests.

3.1 Test Facility

To perform all ground experimental activities a specific test facility has been designed and set-up. The hybrid motor is installed on a dedicated test bench, which can support all the loads that come from the motor functioning: thrust, vibrations, eventual thermal stresses. Furthermore, the facility comprehends all auxiliary devices, that are needed during the test activity: hydraulic and pneumatic circuits, diagnostic and data acquisition system, service equipment (electrical power source, eventual exhaust sound damper, logistic apparatus, etc.). One of the most effective characteristics of the facility is the flexibility, so different scale motors can be tested

with reduced modification on the equipment.

3.1.1 Facility Layout

The test facility comprehends all the required equipment to perform the experiments. Fig. 3.1 reports the layout of the test area that has been set up by CISAS, and here follows a brief description of its main features:

Monitor Room It is the most important area of the facility, in which tests are managed and accurately monitored by use of video cameras and real-time diagnostics. Experimental data are then collected and analyzed briefly, to decide possible modification to perform in the following tests.

Test Room It is a closed room which contains the test bench, and where all the most important tests are performed: ignition tests, oxidizer discharge tests (cold tests) and full hot firing tests. Also the collateral procedures are performed, like oxidant tanks filling and conditioning, and post-test activities. The bench is designed to allow the mounting of both small scale and full scale motors.

Exhaust silencer During hot firing tests the exhaust gases of the motor are driven in a dedicated underground dug labyrinth, which works as a silencer system, to keep the motor sound below the imposed levels.

Work area That's an equipped area where working and small manufacturing activities take place. A workbench and work equipment are available for motor parts assembly and dismounting, so then only the final rocket positioning is necessary in the Test Room.

Other facility areas Besides the described fixtures, other equipment is required in the facility, and this comprehends some places to stock oxidant and eventual fuel reservoirs (in different and far locations), a warehouse for the material not in use, electronics and power distribution box, and protection barrages to divide the sensitive areas from the test area.

3.1.2 Test Bench Mechanical Design

In all experimental campaigns conducted by CISAS only ground tests have been performed, and they were finalized in the performance evaluation of the rockets.

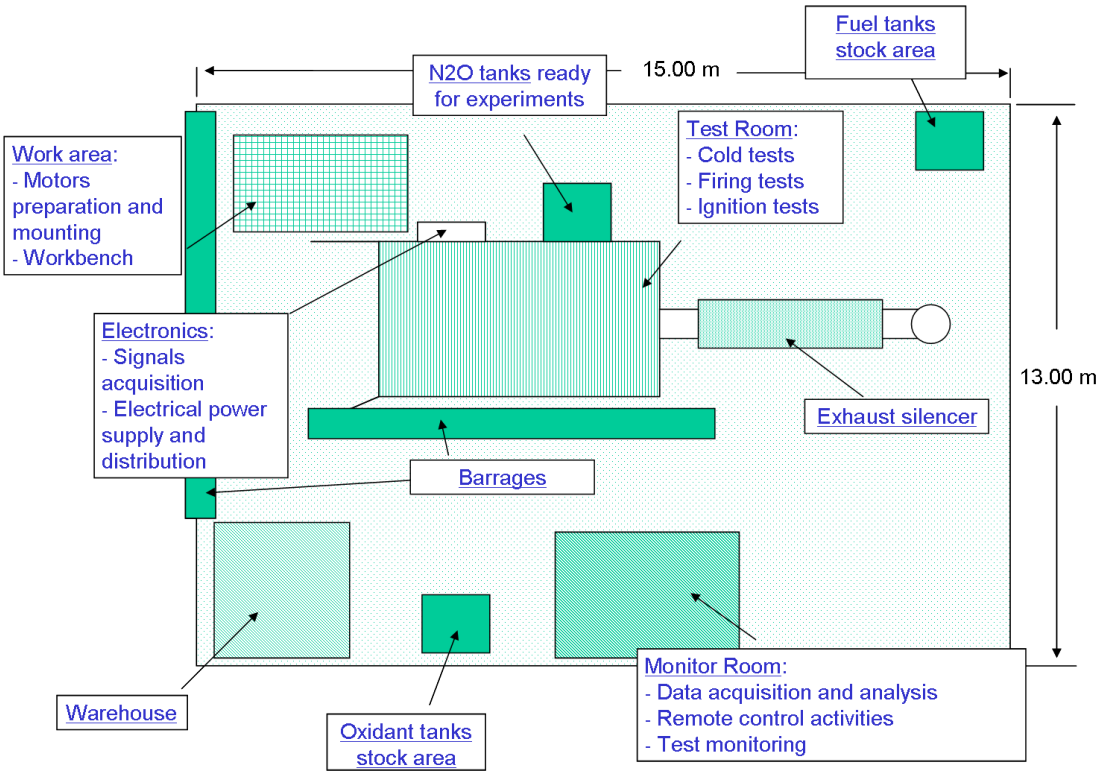

Figure 3.1: Test facility layout.

The different versions of oxidizer tank and combustion chamber have been installed on a fixed structure, which was able to absorb and resist to the high stresses coming from high developed thrust and high vibration condition, assuring in the meantime a great safety factor and structural rigidity. Since many different motor configurations were expected to be tested, it was made the choice for a modular structure for the test bench, in order to simplify and quicken the manipulation and mounting work when changing from a motor version to the other: a fixed structure is used to distribute the stresses and loads to the ground surface, while the interfaces specific for every combustion chamber and/or tank are then fixed to the first one. In this way, when switching from a motor configuration to another, it has been sufficient to dismount the previous interfaces from the basic structure, and mount the following.

The main test bench is made by a truss of square steel pipes, designed for the stresses and loads, that are developed by the full scale version of the hybrid motor: the maximum tolerable thrust is 60 kN, which means a safety factor of 3 with respect to the maximum foreseen thrust of the rocket. The basic structure has been permanently fixed to the ground in the test room of the facility, while the other dedicated interfaces with the motors have been consequently mounted on it.

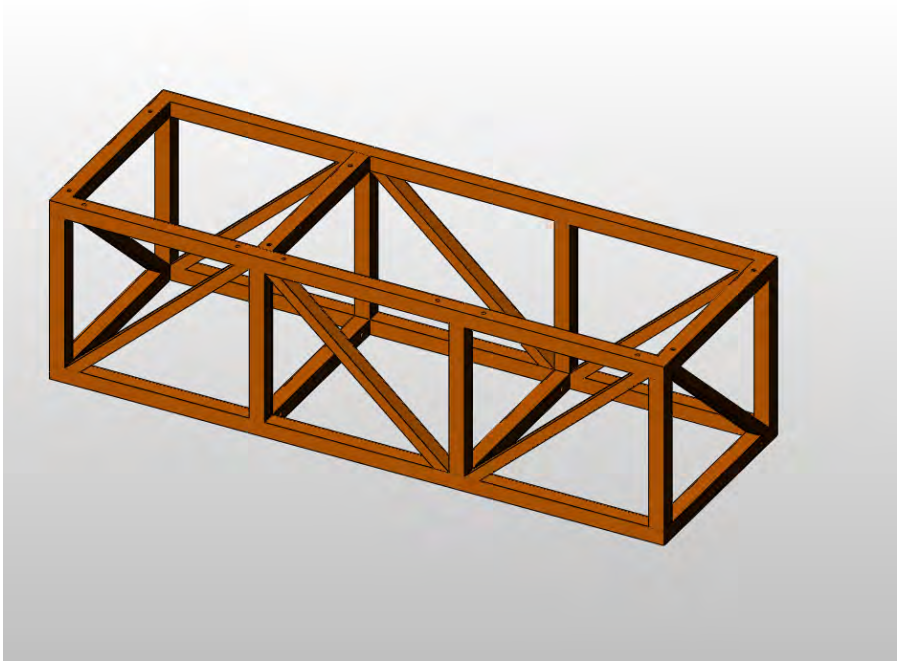

Figure 3.2: Schematic of the basic structure of the test bench.

Figure 3.2 illustrates a 3D schematic of the basic bench.

Small scale test bench

The various small scale versions of the hybrid motor have been installed on a specific removable test bench, which allowed the mounting of the oxidizer tank, the hydraulic circuit and the combustion chamber on the same structure. It consisted in a truss of square steel pipes, as for the described basic bench, and it was attached to it by use of bolts. The maximum allowable thrust of the small scale bench is 15 kN, which greatly overestimates the real developed thrust: this has been done thinking on the possibility to install the small scale bench also on incoherent terrains, in case of open air tests. To get a general investigation of the developed thrust (also for a checking of the bench safety factor), the combustion chambers of the motors have been installed on a ball rail system (made by linear guides and ball runner blocks), to permit the measure of thrust by a load cell (note that the test bench has not been designed for accurate thrust measurements, see par. 3.1.3). The connection to the oxidizer tank is then grant by a flexible pipe. Figures 3.3 and 3.4 illustrate the small scale test bench as a 3D schematic, and as photo in the final installed position on the fixed structure.

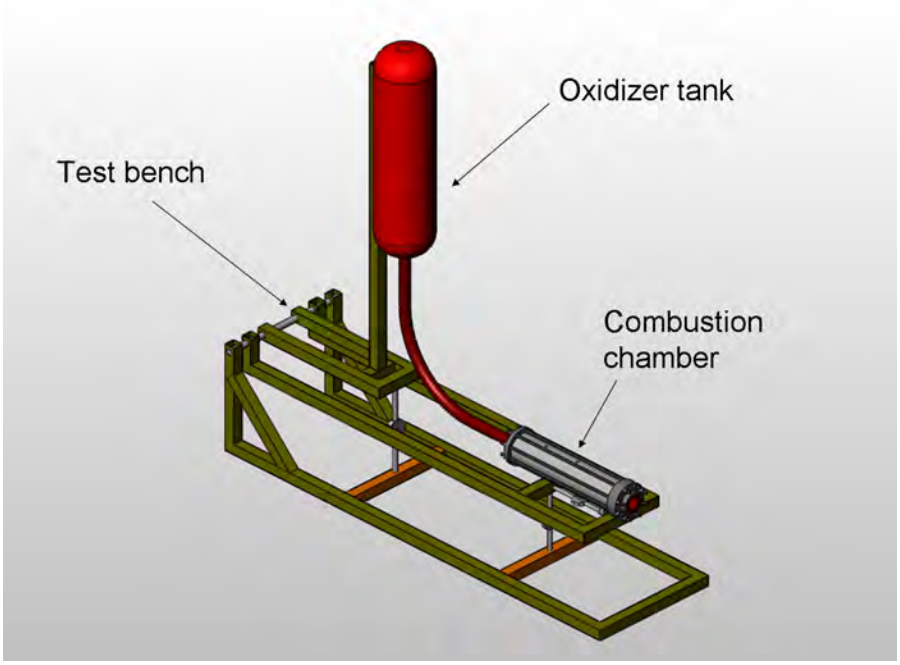

Figure 3.3: Small scale test bench, 3D schematic.

Figure 3.4: Small scale test bench installed on the fixed basic structure, with combustion chamber and tank.

Full scale test bench

The supporting structures of the full scale motor version were more complicate, because of the overall dimension of the system and the acting loads. The twin commercial tanks solution for the oxidizer, and the necessity to weight them to calculate the discharged amount, required to design a specific support system, in which each reservoir transmitted its weight on a load cell. Tanks and weighting systems have been installed on a column made by a truss of square steel pipes, fixed on ground in a very rigid solution: this is illustrated by the 3D schematic of Figure 3.5. For the complete description of the weighting system functioning, please refer to the diagnostic paragraph, 3.1.3. On the combustion chamber side,

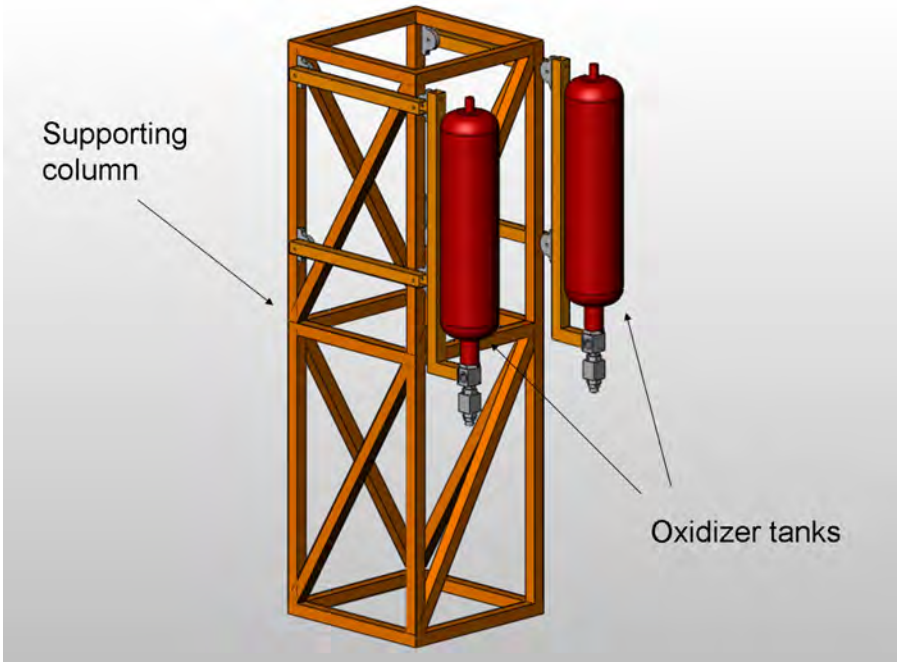

Figure 3.5: Schematic of the column supporting the twin full scale oxidizer tanks.

the solution has foreseen to separate into two distinct sections the cc base and the thrust support, both then mounted on the fixed structure with bolts. As shown in Figure 3.6, the combustion chamber simply leaned on a sort of "V cradle", covered by Teflon to reduce the sliding friction, while the thrust is charged on a square steel pipes structure, specifically designed up to 60 kN force. As for the small scale motors, load cells give a macroscopic measurement of the developed thrust (see par. 3.1.3): to permit this measurement, and not to interfere with the tank weighting, the hydraulic connections have been performed with a couple of flexible pipes. Figure 3.7 reports a photo of the full scale test bench during the assembly

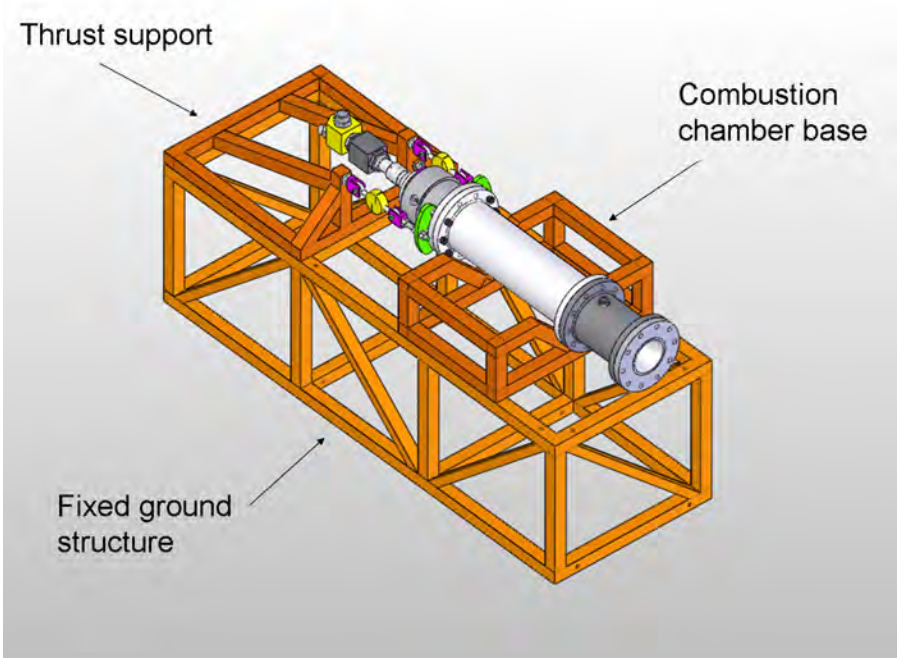

Figure 3.6: Schematic of the full scale version test bench.

phases.

Figure 3.7: Full scale test bench during assembly.

3.1.3 Diagnostic System

The hybrid rocket engine test facility has been designed to be flexible and to allow mounting of a complete array of sensors. Characteristic parameters in a hybrid rocket motor are as follows:

Oxidant pressure The pressure in the tank has been monitored to check the initial oxidizer condition and its behavior during the motor functioning (which is very important, especially with auto-pressurized oxidants, like N_2O).

Combustion chamber pressure Pressure in the combustion chamber has to be monitored for the entire rocket performance reconstruction, as developed thrust, nozzle efficiency, injectors functioning. Measuring pressure in different section helps in the verification of particular devices (different grain length/shape, different post-combustion chamber, mixing plates, diaphragms, etc.), and is also important for the combustion instabilities characterization.

Thrust A load cell has been mounted for verifying the general performances of the rocket: its data are useful in the comparison with the analytical computing of combustion chamber pressure, and to give a macroscopic verification of the propulsive performances of the thruster.

Oxidant temperature In an auto-pressurized oxidant concept, temperature of the oxidizer is important to check the eventual stratification of the liquid in the tank, in order to grant a stable condition prior the ignition of the motor.

Combustion chamber temperature Different sections of the combustion chamber can suffer from critical working conditions: the internal combustion develops high temperature gases (up to 3000°C), which can damage some components, e.g. the nozzle throat and divergent section, the post-combustion chamber section and eventually the pre-combustion chamber section. Usually the central part of the chamber is protected by the ablative the fuel grain during combustion. For these reasons, temperature sensors have been installed during hot firing tests on possible critical points of the motor: their intent was to check that maximum temperature ranges of components and sensors were not exceeded.

Acoustic investigation The acoustic emission of the motor during its functioning can be used for an additional investigation of combustion instabilities: pressure oscillations in the combustion chamber cause oscillations also in the

developed thrust (with possible mechanical issues to the entire vehicle), and this can be observed from the motor sound as well. These data have not been used during the present research program.

Other measurements can help in a more deep investigation of specific characteristic parameters, that involve the functioning of hybrid rockets. These are the values of *fuel average regression rate* in combustion chamber and the *oxidizer mass flow rate*. Due to the physics of the phenomena, the extreme conditions and technological issues affects the availability of these measurements. In fact, real time regression rate monitoring comes up with the high temperatures and pressures of the internal combustion chamber, whereas measuring the mass flow rate of oxidizer can be very difficult in case of biphasic flow, due to its not constant properties in the hydraulic circuit (i.e. the rate between the gas and the liquid in the flow). This arguments will be more deeply discussed in further chapters.

The sensor array comprehends different types of measurement devices:

- sensor pressures, which are mounted on the oxidizer tank (both in liquid and gas section), at the oxidizer injection (both pre and post-injection plate, i.e. in pre-combustion chamber), on the combustion chamber (in different sections along the grain length or in post-combustion chamber);

- temperature sensors, which are mounted on the oxidizer tank and injection (same sections as the corresponding pressure sensors, to monitor the physical conditions of the oxidizer and to check that the working temperatures of the pressure sensors are not overcome), and in different position of the external surface of the combustion chamber, to check eventual failure points due to temperature stress;

- load cells, to monitor the oxidizer weight prior and after each test, and to get a macroscopic monitoring of the motor thrust (see par. 3.1.3).

More details of the sensors mounting position are reported in paragraph 3.3.

The performance of the measurement chain have been deeply analyzed, to evaluate the uncertainty of the data collected during the experimental campaigns. In particular, some quantities have necessitated the development of specific techniques of investigation, due to technical issues, that are intrinsic in the nature of the measures to be carried out (combined effect of high temperatures and high pressures, or very low temperatures acting on the pressure gauges, etc.). For this reason, each

physical quantity have been measured with a different technique, depending on the boundary conditions of the physical phenomenon to be investigated.

Pressure

In the present work were basically used pressure data, and each measuring section has determined a specific measuring technique. In fact, measuring a pressure value in the combustion chamber are quite different from the same physical quantity in the oxidizer hydraulic circuit, because of the different conditions of the measuring subject.

The pressure data, relative to the gases developed by combustion process in combustion chamber, are fundamental in the motor performance evaluation and design. However, due to the physico-chemical phenomenon, the temperature of the gases, that are generated in the combustion chamber, can raise up to 3000° C: it is clearly an issue for the pressure measurement device choice. To get over the problem, for pressure measurement in combustion chamber a specific interface has been developed: the sensors have been installed using a pipe as an extension of the pressure outlet. The air in the pipe will act as an air cushion during the motor functioning, avoiding hot gases reaching the sensor inlet as a thermal insulator. Many calibration tests have been performed to establish the correct length of the pipe, avoid the introduction of uncertainty sources on the measure. As the dynamic behavior is concerned, also the eventual damping effect has been numerically modeled. Figures 3.8(a) and 3.8(b) illustrate the mounting schematic and the realistic view of a pressure transducer mounted on the combustion chamber (the sensor is for full scale cc version, but the solution is the same used also in small scale motor). From the typical pressure oscillations of a hybrid rocket, the maximum frequency of interest has been set to 500 Hz. Using the theory reported in [4], it is possible to calculate that the fluid inside a pipe of 200 mm length and 5 mm diameter has a natural frequency higher than 8500 Hz ±1%, with a very low damping coefficient ($\propto 10^{-3}\ N\,s/m$, ±1%). Furthermore, such dimensional characteristics for the pipe interface have demonstrated a very good thermal insulation effect, with a maximum reached temperature of 40° C (pressure transducers have a maximum operating temperature of 80° C). After these analyzes and some experimental investigation on this solution, pressure gauges in the combustion chamber have been installed as described.

The measurement performance of the installed sensors are described in Table 3.1.

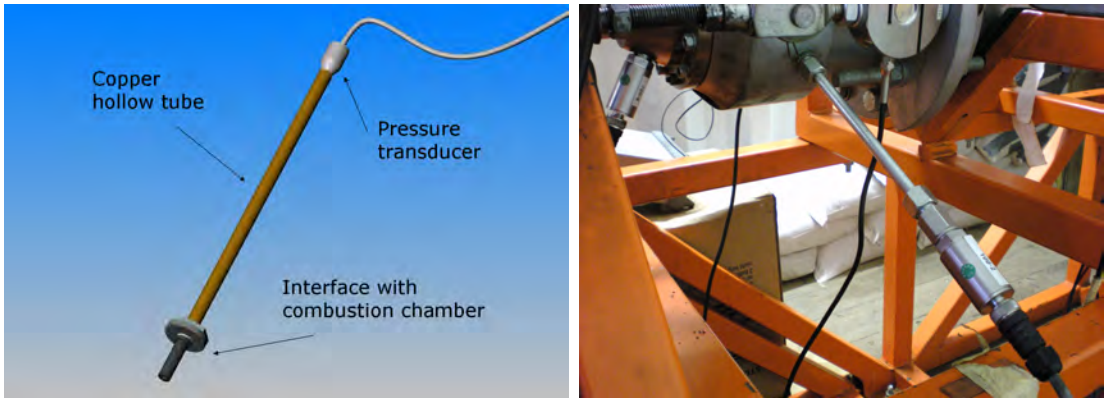

(a) (b)

Figure 3.8: Schematic and photo of pressure sensor mounting on the combustion chamber.

Temperature

Temperature measurements are important in the physical behavior diagnostic of the oxidizer and to check if the pressure sensors are in contact with fluids out of their operating thermal range. It is not required high accuracy for the foreseen applications, and the measurements could be intended to be stable, so thermocouples have been considered well-adapted for the scope (the accuracy of $\pm 0.5^{\circ}$ C was enough, and time constants of 3 seconds were adapted to the slow temperature variations). The major issue was to grant a measurement directly in contact with the fluid (N_2O in liquid/vapor phase or cc gases), in a pressurized working condition. The solution has been the use of mineral insulated J thermocouples, with stainless steel outer sheaths: in this way, they were suitable for high pressure and high vibration applications, and the maximum tolerable temperature was enough high. For more information on the measurement performance, please refer to Table 3.1. Usually, thermocouples have been installed in correspondence to a pressure sensor and in both liquid and vapor phase in the oxidizer tank.

Load cells

Besides physical status of the operating fluids in the motor, there are other macroscopic values that are important for the performance evaluation, as the net mass of burned propellants, and the developed thrust. To achieve these information, as a preliminary solution only mean values have been acquired, because a precise evaluation of real-time mass flow rate is difficult both for the oxidizer and the fuel: N_2O is in biphasic condition in the hydraulic circuit, and the liquid/vapor rate is not

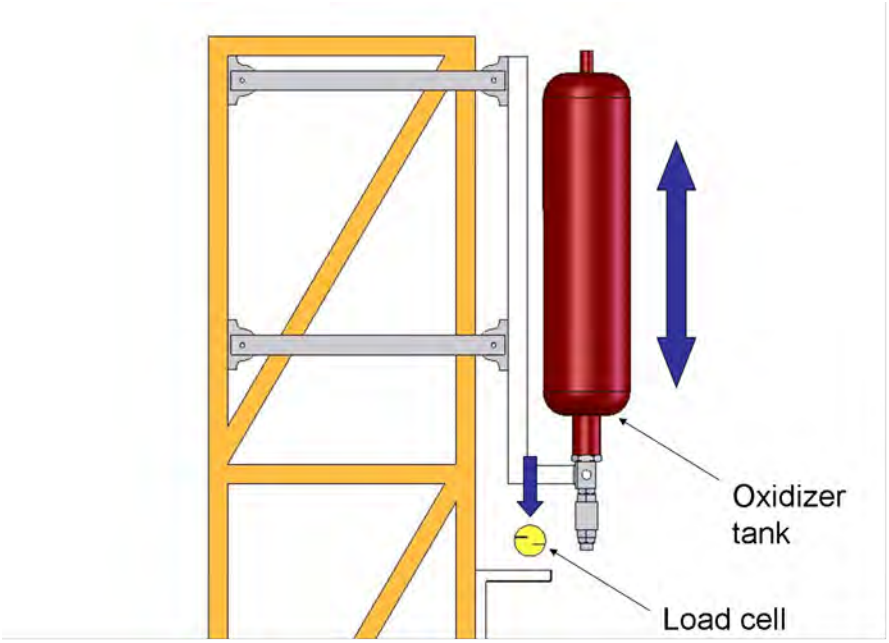

Figure 3.9: Functioning scheme of the full scale tanks weight measurement solution.

known *a priori*, due to the auto-pressurization condition used in the experimental campaigns. Besides, the regression rate of the fuel in combustion chamber is of difficult measurement, especially during the burning time. Numerical models for its evaluation exist, but they are highly dependent on experimental data, and they change on the basis of the propellants (differences in the fuel/oxidizer composition bring to different regression rate values). For these reasons, during small scale tests the tank has been weight before and after each test, hanging it on a load cell, working in traction condition: the differential measure has given the oxidizer amount discharged during the motor functioning, and the measure uncertainty has not been affected by mounting mistakes: it has been sufficient to wait until a stable indication by acquisition device, in order to provide a measurement with the only uncertainty of the load cell, and to grant its reproducibility.

During full scale tests, instead, the large size and weight of the tanks did not allow a simple handling, so a specific apparatus has been developed: the functioning is described by Figure 3.9. Each tank has been fixed to a mounting structure, which allowed it only to move vertically. In this way, leaning the structure on a compression load cell, it has been possible to measure the tank weight. An accurate static calibration of this weighting system, through the application of calibrated weights, have set the *uncertainty* of the collected data to 4% of the measure. method.

Measure	Sensor	Measurement Performance
Pressure	25 MPa (250 bar)	Accuracy: 0.25% FS, thermal error: 1.5% FS, compensated temperatures: −20° to 80° C
	10 MPa (100 bar)	Accuracy: 0.25% FS, compensated temperatures: −10° to 85° C, temperature effect in compensated range: 0.02% FS
	6 MPa (60 bar)	Accuracy: ±1%, temperature error: <1% (over any 80° C temp range)
Temperature	type J thermocouple	±0.5° C, max temperature: 760° C, suitable for high pressure, high vacuum and high vibration applications
Load Cell	25000 N	Combined error: < ±0,03%
	3000 N	Combined error: < ±0,03%
	1000 N	Combined error: < ±0,03%
Balance	2.2 kg FS	Linearity: ±0.002 kg, reproducibility: 0.001 kg, digit division: 0.001 kg

Table 3.1: Performance of diagnostics used in experimental set-up.

For the average evaluation of the consumed fuel grain, both in small and full scale tests a balance has been used to weight it before and after each test. Regarding the macroscopic investigation of the developed thrust, a load cell has been mounted to the sliding table, on which is installed the combustion chamber. Since this measure is not part of the primary objective of this work, but just as a collateral information and support for a macroscopic comparison with other data, it has not been given a specific analysis of the system used to evaluate it, and its value has been considered with low reliability.

3.2 Hybrid Motor

The motors tested by CISAS are ground demonstrators of a booster rocket for aeronautical applications, both in small and full scale version. The first tests have been carried out using the small scale motor, so in this way it has been more easy to keep low development costs, to take confidence with rocketry activities, to set up and calibrate the design numerical model and the diagnostics, to permit many different motor configuration tests with small changes in the hardware. After the small scale tests, a full motor version has been designed and produced. This

permitted to verify the performance of the complete motor and any eventual scale effect.

Every hybrid rocket has been modeled and sized using the Hybrid Thruster Model (HTM) developed at CISAS . This model describes the engine functioning and provides an estimate of its structure (mass and volume): the results come from an optimization process and are the best trade-off between performance and total mass, for the selected hybrid technology. However, the model is simple and does not provide information about complex physical behaviors of fuel/oxidizer and of their interaction. For these reasons, the code can assess the real performance of thrusters only after a detailed experimental campaign, aimed at validating the model and providing its uncertainty.

3.2.1 Small Scale Motor

The aim of the experiments is to validate the HTM and provide an estimate of all the physical behaviors that are not described by the model. To accomplish this task, the thruster has been simplified, adopting a single port grain and adjusting the other parameters (i.e. oxidizer mass flow rate) accordingly.

The design guidelines are summarized as follows:

- simple and versatile combustion chamber, to reduce manual operations among tests;
- simple oxidizer hydraulic circuit, with commercial available components.

Theoretical design performances for the small scale motor are summarized in Table 3.2.

Performance	**Value**
Total Impulse	2000 Ns
Mean Thrust	400 N
Mean Specific Impulse	200 s
Mean combustion chamber pressure	3 MPa
Oxidizer initial pressure	5.6 MPa
Initial port diameter	32 mm
Grain length	145 mm

Table 3.2: Theoretical design performances for the small scale hybrid rocket.

Combustion Chamber

The design of the combustion chamber has taken into account the versatility and safety requirements for these types of tests. The chosen solution is a cylinder closed by flanges and rods, to allow a quick access to the internal parts of the motor during the components substitution between the tests, and the possibility of mounting different grains (in length and diameter) changing only the external cylinder. All mechanical parts are designed for an internal pressure of 10 MPa, adopting a safety factor of 3.

The fuel grain is installed inside a tube made of Nylon 6.6, which works as a thermal insulator and allows an easier mounting and removing. The combustion chamber can take many different motor configurations: pre- and post-combustion chambers with different L/D ratios, different dimension grains, different injectors types. The front flange is also thermally protected by a graphite disc and the pre-combustion chamber is made of steel, so to keep its dimensions unchanged and to avoid maintenance during the tests. The post-combustion chamber and the nozzle are manufactured from a single piece of graphite.

For a schematic of the combustion chamber and all its components, refer to Fig. 3.10, 3.11 and 3.8.

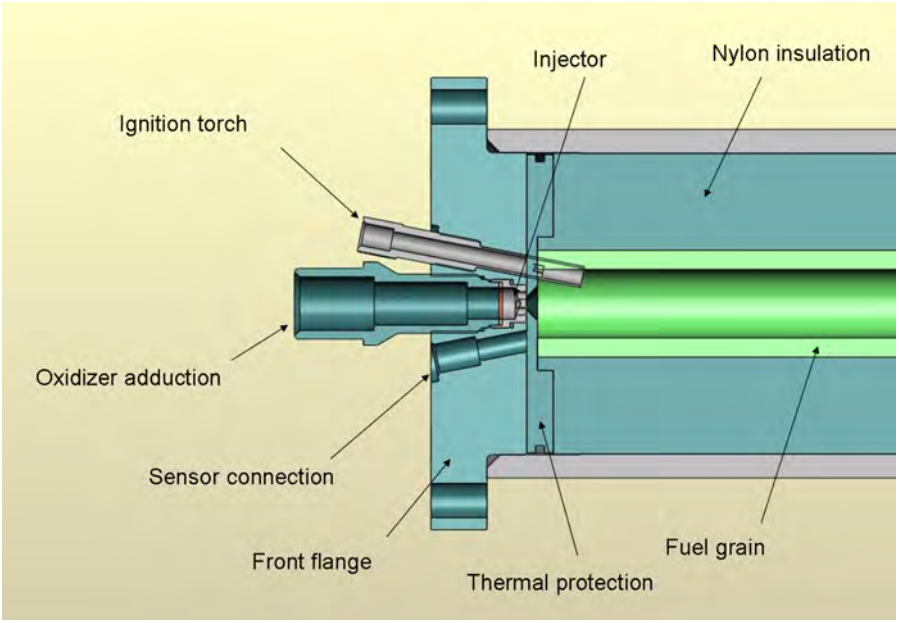

Figure 3.10: Schematic of small scale hybrid motor (front side, here in torch ignition configuration).

Nozzle & Post-Combustion Chamber

The nozzle and the post-combustion chamber of the rocket constitute a single component made of graphite (see Fig. 3.10). This solution reduces the mounting and disassembly operations between the tests, and avoid also the sealing issues, because there are no interfaces between them. Thanks to versatility of combustion chamber, the post-chamber can be adapted to many different L/D ratios motors.

The nozzle can be of different types, like de Laval or bell nozzles.

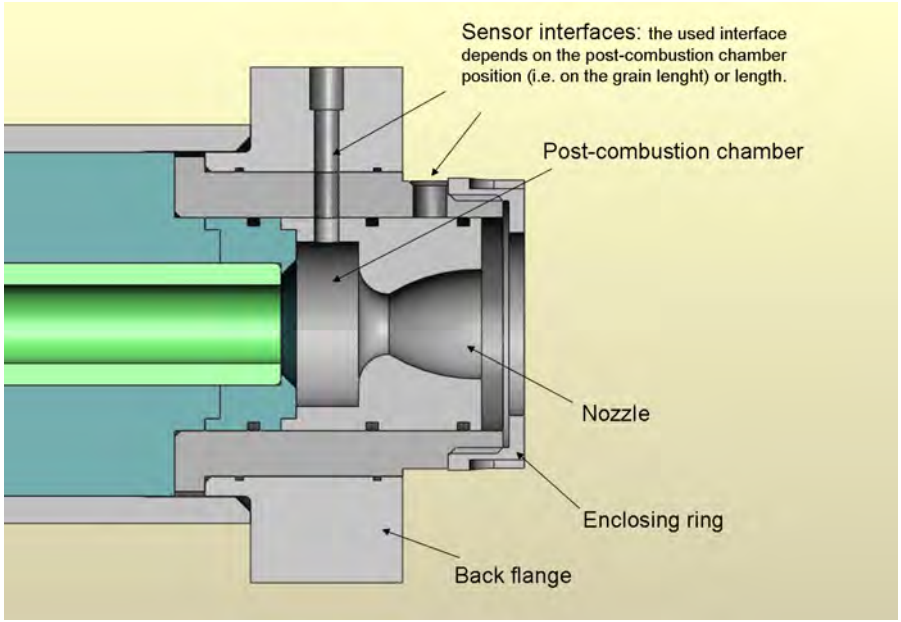

Figure 3.11: Back side of small scale hybrid rocket. A bell nozzle with integrated post-combustion chamber is visible.

Oxidizer Adduction Circuit

In Fig. 3.10 the schematic illustrates how the injector can be mounted in the dedicated seat, which is produced in the front flange, and how the rest of the hydraulic circuit can be connected. With this technical solution, many different injectors can be mounted, so evaluate how a different injector determines different performances of the rocket (Fig. 3.12).

The oxidant tank for the tests is a commercial steel reservoir, which has high values of work and burst pressures and grant high safety factors. It is connected to the main valve by a 1" flexible pipe.

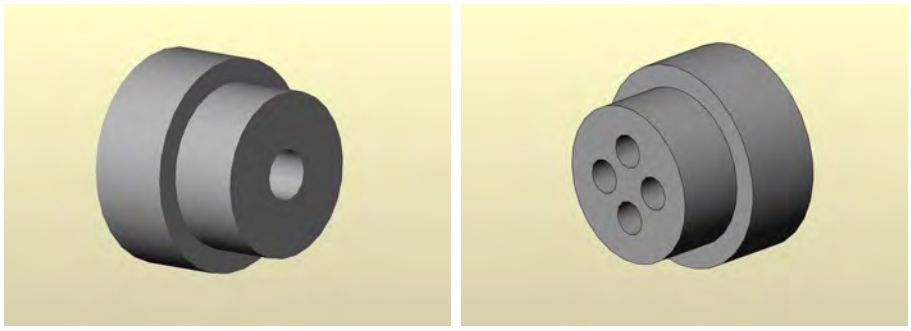

(a) Single hole injector (b) Four holes injector

Figure 3.12: Schematic of different injectors, that can be mounted on the small scale motor.

Ignition System

Two different ignition techniques have been adopted and successfully tested for the small scale motor:

- torch ignition
- ignition with pyrotechnic device

The first technology consists in a bi-propellant torch, which is mounted directly in the front flange (as shown in Fig. 3.10). The oxidizer ignition is obtained by a flame with is lighted just before the main valve opening. This technology, even if not suitable in a flight configuration, has been used to identify the ignition requirements of the hybrid rocket, which are of fundamental importance in the pyrotechnic devices design. In effect, the thermal flux can be modulated both in the given energy and in the opening valve delay.

The second technology adopts a small solid pyrotechnic tablet, which is inserted in a dedicated small housing attached to the combustion chamber: hot gases generated from the pyrotechnic combustion are introduced in the chamber just before the oxidizer main valve opening (for more details concerning this technology, see paragraph 3.2.2 in the full scale ignition section). Figures 3.13(a) and 3.13(b) report two photos of the described ignition systems during calibration and functioning.

3.2.2 Full Scale Motor

The design of the full scale version of the motor has taken place after the conclusion of the small scale experimental campaign, to apply all the verified improvements. The objectives and requirements to be satisfied were as follows:

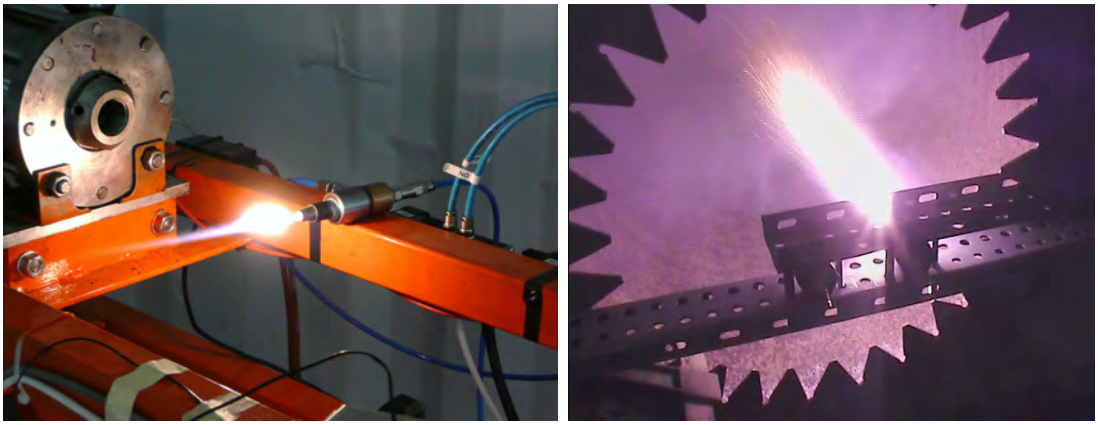

(a) Torch (b) Pyrotechnic igniter

Figure 3.13: Ignition systems for small scale motor.

Obj1: versatility of the system, which means the possibility to adapt the combustion chamber to grain of different length, and to "non-standard" pre/post-chambers.

Obj2: quick mounting, to reduce assembly and test preparation time.

Obj3: safety, which has to be granted also for non-stardard working conditions.

Obj4: performance requirements fulfillment, related to the final version of the motor (i.e. final grain dimension, propellants mass flow rate, subsystems configuration).

Design choices have been finalized after the experience reached with the small scale version. Some restraints, as for example the maximum dimension of the raw graphite for the nozzle, have influenced the final layout of the full scale motor. In the following paragraphs the design details of the motor parts are reported, and in particular:

- Combustion chamber design
- Nozzle design
- Oxidizer injection system design
- Ignition system design

Theoretical design performances for the full scale motor are summarized in Table 3.3.

Performance	Value
Total Impulse	50 kNs
Peak Thrust	12 kN
Burning time	5 s
Mean oxidizer mass flow rate	5 kg/s
Initial oxidizer mass	26 kg
Mean combustion chamber pressure	3 MPa

Table 3.3: Theoretical design performances for the full scale hybrid rocket.

Combustion Chamber

From the small scale tests, the selected fuel for the full scale version is the paraffin wax. The grain length defines the ratio between the fuel and the oxidizer quantities, that take part in the combustion (known as O/F ratio). The ideal value is an O/F ratio of 7, but the small scale tests have demonstrated that it cannot be achieved, due to the low combustion efficiency obtained during the test campaign. Experimental investigations have pointed out that an eventual shorter grain (which would be necessary to reach the O/F ratio of 7) determines a reduction in the efficiency of the propellant reaction, which means lower final performances.

To keep the combustion efficiency on acceptable values (>80%), the O/F ratio has been set to a value of 4, adopting a longer grain, then a greater amount of fuel mass.

The modular configuration of the combustion chamber permits the housing of different types of pre/post-combustion chambers, as well as different length grains.

In Fig. 3.14 the configuration of the full scale combustion chamber is reported: it consists of a central case for the fuel grain, connected to the front and back enclosures, that house the pre-chamber on one side, and the post-chamber and nozzle on the other side respectively. The connection is obtained by use of welded flanges: this solution grants both a quick connection of the parts and a high level of safety during the experimental activities.

Fuel grain external case The fuel grain external case can be of different lengths, depending on the grain dimension; in the full scale performed tests the 800mm grain case has been used, which is the one foreseen for a hybrid rocket functioning with O/F ratio of 4.

The case thickness and the weldings for the flanges have been designed for an

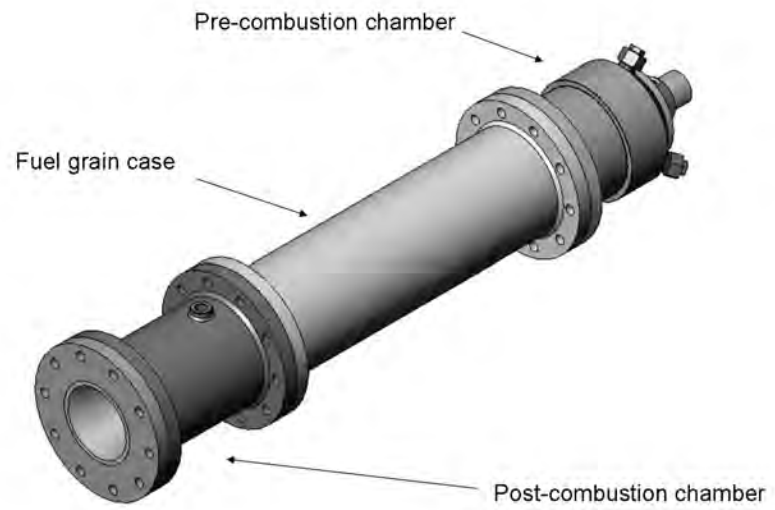

Figure 3.14: Full scale hybrid motor, schematic.

internal pressure of 10 MPa, with a safety factor of 2. The material for the case (Fe 360) has been chosen accordingly to its mechanical properties, weld capacity and market availability.

Pre-chamber case The case of the pre-combustion chamber has many different functionalities:

- It houses the pre-combustion chamber and the first portion of the fuel grain;
- It gives interface with the oxidizer adduction pipe and the dedicated flow diffuser;
- It allows the correct position for igniters mounting, in order to grant an effective ignition of the motor;
- It houses the sensors for the motor diagnostics.

Design criteria and materials are the same as the ones adopted for the fuel grain external case. In Figure 3.15 a schematic of the case is reported. The pre-combustion chamber is a Nylon 6.6 cylinder, design with a L/D rate (length on internal diameter) of 0.3. The choice of the material has been performed thanks to its easiness in manufacturing and procurement, and thanks to its lightness. Furthermore, its ablative effect during the functioning phases of the motor assures a good thermal insulation and also a small contribution in the total propellant mass flow rate

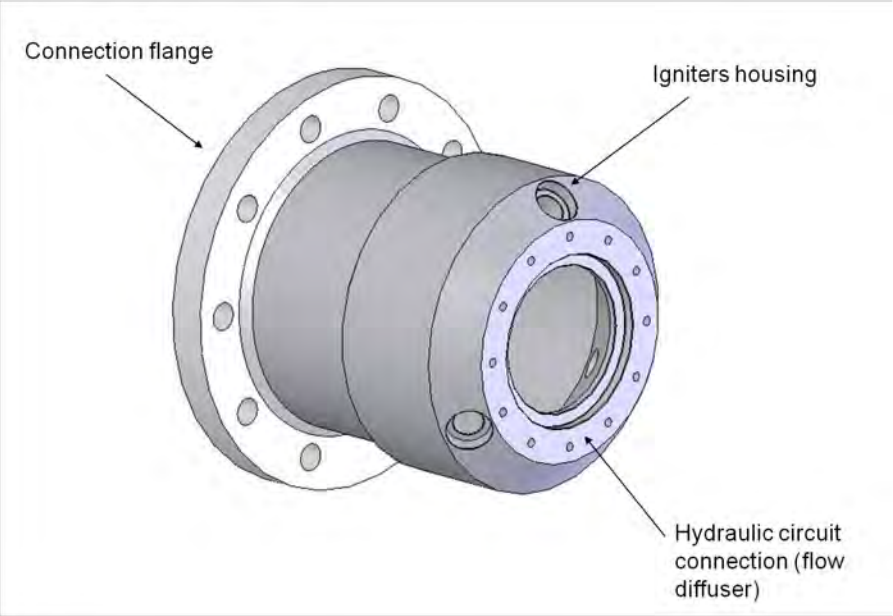

Figure 3.15: Pre-combustion chamber external case.

through the nozzle (nylon has a regression rate value which is definitely lower than wax). From this considerations, it is clear that this component has to be changed at every test.

Post-chamber case The post-combustion chamber external case has been designed with the same safety factors and mounting easiness as the other components, previously described. So are the materials and the design concepts. The tasks of this case are as follows:

- It houses the post-combustion chamber and the final section of the fuel grain;
- It houses all the nozzle parts;
- It allows the mounting of the sensors for the flow diagnostics in the aft combustion chamber, just upstream the nozzle (pressure sensor and/or temperature probe).

In Figure 3.16 a schematic of the design solution is reported. The post-combustion chamber has been designed with the same criteria as adopted for the pre-cc, with the only difference in the L/D rate, which is of 0.7. The interface with the nozzle is in turn the first convergent section of the nozzle, and it fits with the correspondent graphite component. This choice has permitted a smaller raw graphite block for the throat section of the nozzle.

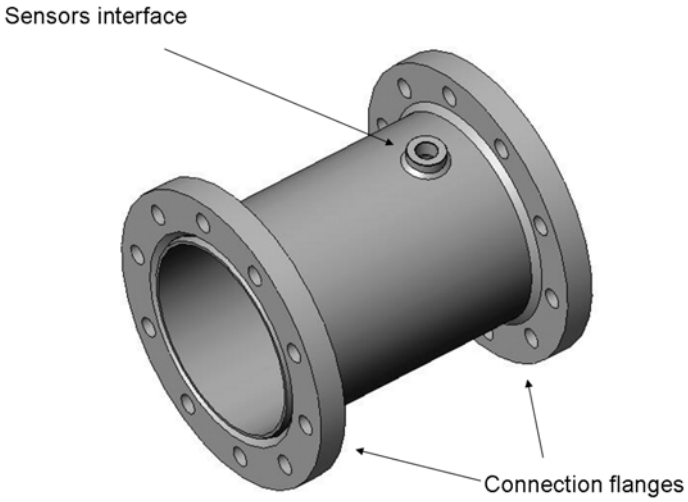

Figure 3.16: Post-combustion chamber external case.

Nozzle

During the designing phases, a very pressing factor have been the dimensions of the raw graphite blocks, that have been used for the throat sections of the nozzle. An Isomolded Graphite has been used, thanks to its good thermal/mechanical properties.

The concept is a De Laval convergent–divergent truncated conical nozzle, to take advantage from its easy manufacturing, with a negligible decrement in the expansion performances. In Fig. 3.17 a schematic illustrates the structure of the nozzle and its housing, which comprehends:

- Convergent section made of graphite, which is interfaced with the post-combustion chamber;
- Divergent first section made of graphite, because it supports the highest temperatures;
- Nozzle external case, made of C40 steel, which performs two main purposes: on one side it houses the graphite components and keep them in the correct position during the motor functioning, on the other side it completes the divergent section of the nozzle. Experimental tests on small scale motors have demonstrated that in this section the temperature values are well tolerated by the material, thanks also to the reduced exposition time to the hot gases

(maximum burning time of 5 seconds).

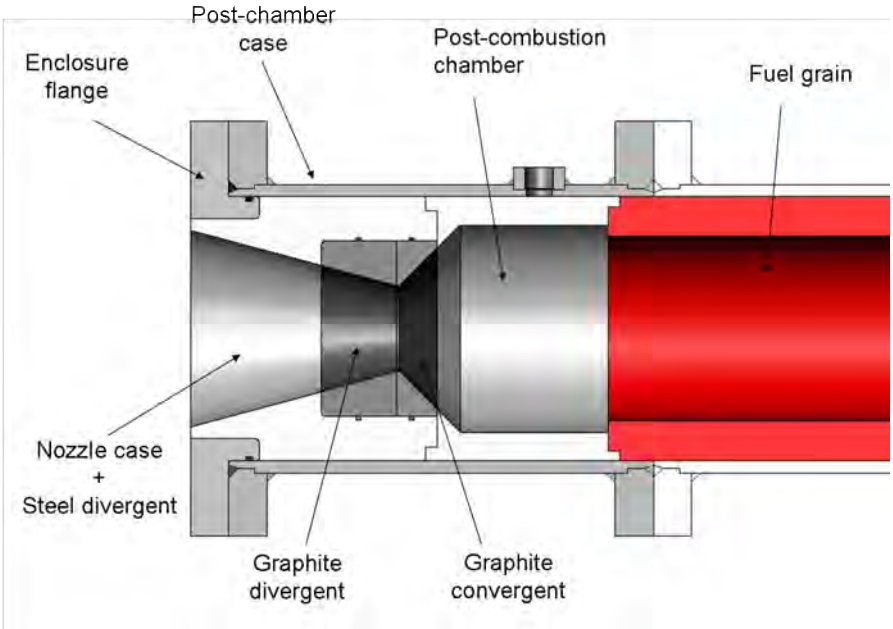

Figure 3.17: Nozzle components and schematic assembly.

Oxidizer Adduction

The oxidizer is stored in two separated tanks, due to the impossibility to procure a single reservoir of bigger dimension and to the handling difficulties that would occur.The two fluxes are piped together and then connected to the combustion chamber with a specifically designed flange interface. The design parameters of the entire hydraulic circuit are a maximum pressure of 10 MPa and a safety factor of 2 on the Yield stress of the material (Fe360 steel).

The following figures give a schematic of the components: the circuit is connected to the external case of the pre-chamber by use of a flow diffuser, to distribute the liquid flow to the entire injection plate dowstream.

Injection system The injection sub-system is mainly composed by elements: the flow diffuser and the injection plate. The **flow diffuser** performs two main functions: it joins the adducting oxidizer pipe to the injection plate, and it permits the mounting of the diagnostics of the flow in the pre-injection section. These measurements are of fundamental importance to monitor the nitrous oxide behavior in the pipes. The **injection plate** is made by AISI 430 steel: it modulates the oxidizer mass flow rate (on the basis of the holes number and their diameter), and

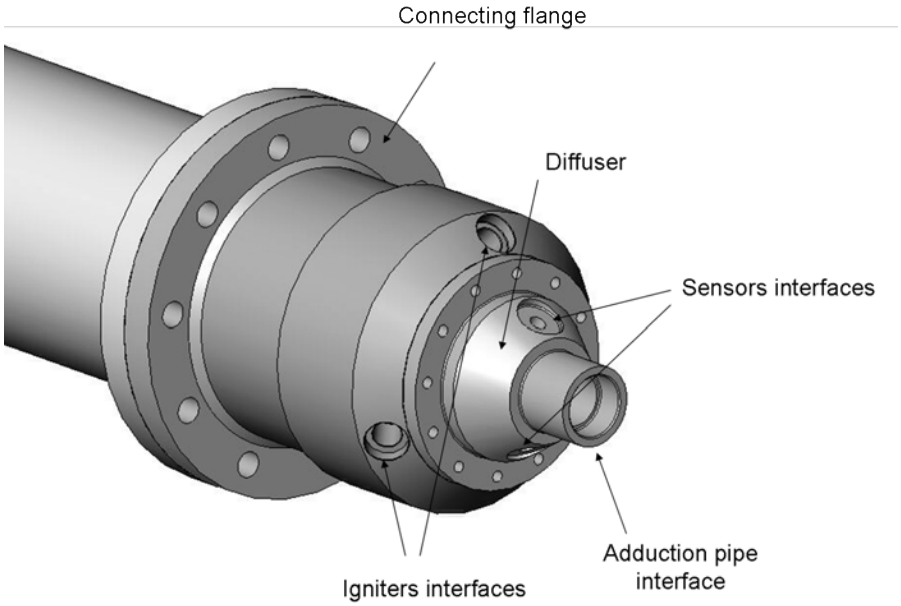

Figure 3.18: Hydraulic circuit connection to the combustion chamber.

on the same time it grants an effective atomization of the oxidizer. Such material has been chosen considering the operating conditions of this component: N_2O is a high oxidant fluid, and the holes geometry needs to be protected, not to change the atomization performances of the plate. There are 121 holes in total, each with a diameter of 1.4mm.

Oxidant Tanks Nitrous oxide is stored in two separated tanks, to simulate the flight requirement just on the ground configuration. As a first ground version of the motor, two commercial alloy steel reservoirs have been used (industrial accumulators, specifically modified by design), to grant a high safety factor (assured by the commercial standards guaranteed by law) and high maximum pressure (38 MPa), and to reduce the costs and the procurement time. The two tanks weight has been measured by two load cells, which have been mounted on dedicated supports (see par. 3.1.3). The connection of each tank to the rest of the hydraulic circuit has been performed by use of flexible PTFE 1" pipes, reinforced with steel (commercial pipes for hydraulic applications).

Ignition Sub-System

To ignite the motor, some small pyrotechnic gas generators have been used: they are able to produce the oxidizer decomposition at the main valve opening, to start

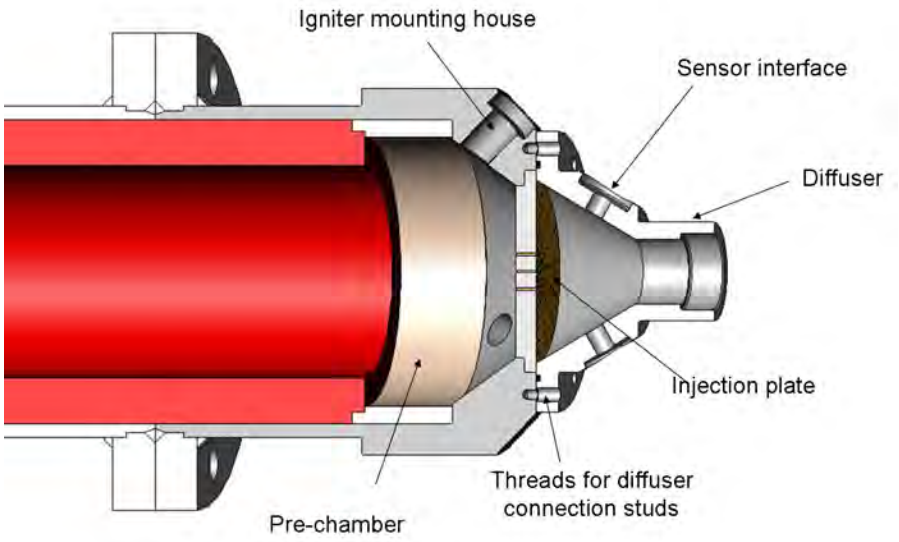

Figure 3.19: Oxidizer injection sub-system parts.

the combustion reaction with the fuel. At the valve activation, the igniters are still functioning (and the fuel grain is in a "pre-heated" condition), so their hot exhaust gases hit the oxidizer flow, they heat it up and decompose it with a temperature rising of almost 1000°C (a schematic of the process is reported in Figure 3.20). The procedure have been deeply studied and calibrate. To maintain a high efficiency

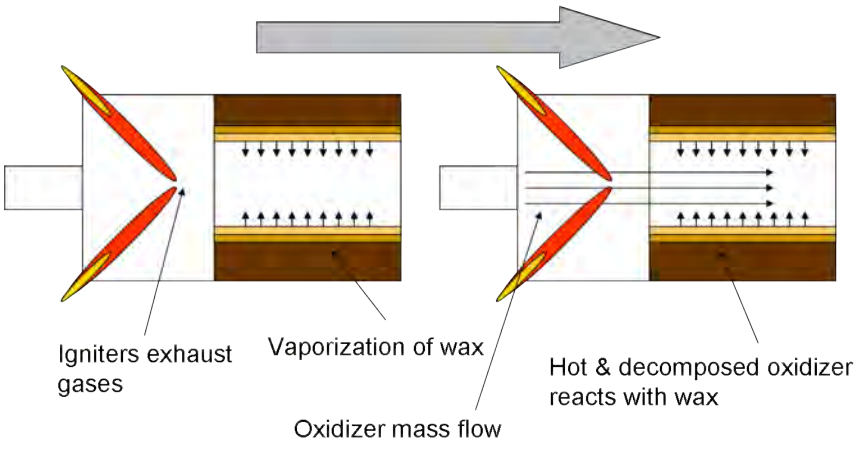

Figure 3.20: Schematic of the motor ignition procedure.

in the ignition process of the motor, three igniters in a 120° configuration have been used, and their mounting is visualized in Figure 3.21: they are tilt at an

angle of 45° with respect to the combustion chamber axis. The calibration of the

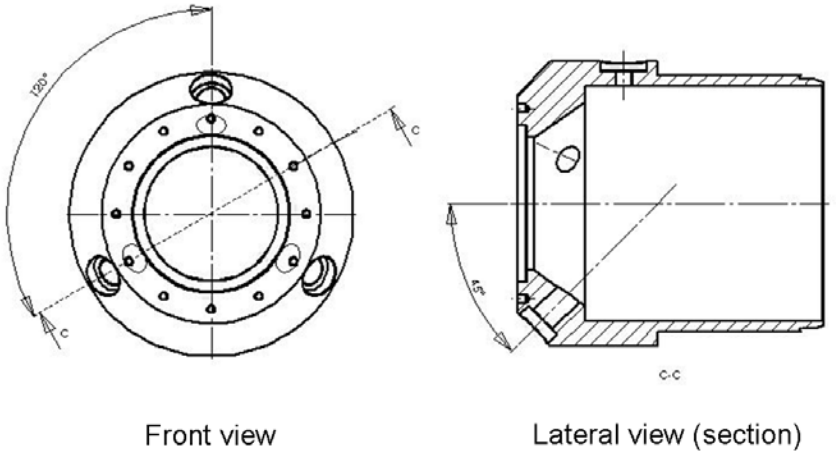

Figure 3.21: Igniters mounting configuration on the front section of the combustion chamber.

ignition procedure has been very useful to evaluate the thermal energy need by the rocket to be correctly ignited. Considering the melting temperature of the wax (about 70°C), the igniters effect produces a layer of liquid wax on the fuel grain surface: at the main valve opening, the oxidizer flux is very high, due to the high pressure difference between the combustion chamber and the hydraulic circuit. If the amount of liquid wax is too high, it will be ejected from the nozzle before starting the combustion reaction, with a notable decrease in performance. The oxidizer instead should enter the combustion chamber while the igniters are still functioning, to be correctly decomposed. In Figure 3.22 two photos of the mounted igniters and a phase of their functioning are reported. The schematic set-up of a single igniter is reported in Figure 3.23. Every single igniter has been designed for a maximum pressure of 10 MPa, with a safety factor of 4. The solid pyrotechnic grain burns inside a small steel cylinder with a progressive combustion (due to the internal geometry), thus producing an increasing exhaust gas flow from the nozzle. The motor ignition procedure follows the steps, that are reported in Table 3.4. Pressure inside each igniter increases to a maximum value just before the end of its combustion process, and the total exhaust gases mass flow rate has been accurately evaluated to effectively decompose the oxidizer. The required energy to be provided by the igniters has been studied and estimated from literature and from experimental tests (see paragraph 3.2.1).

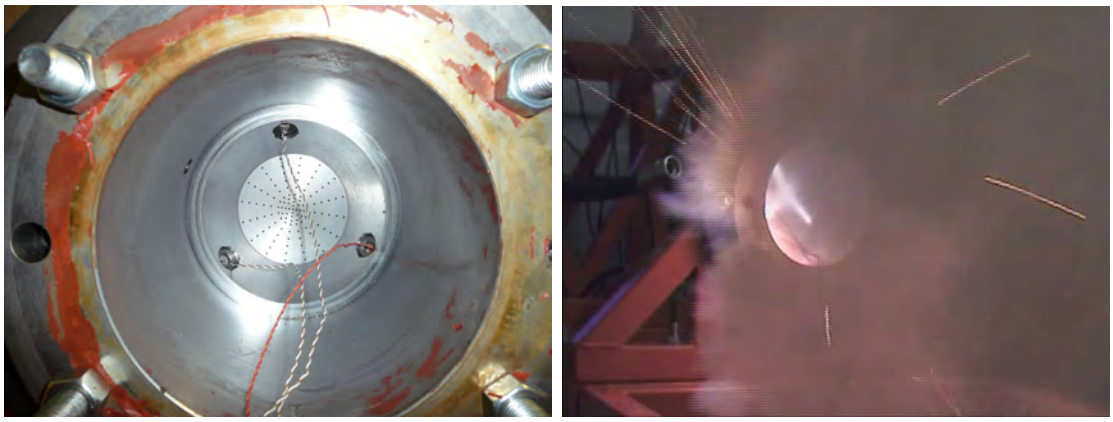

(a) Mounted igniters (b) Functioning phase

Figure 3.22: Full scale motor igniters mounting and functioning.

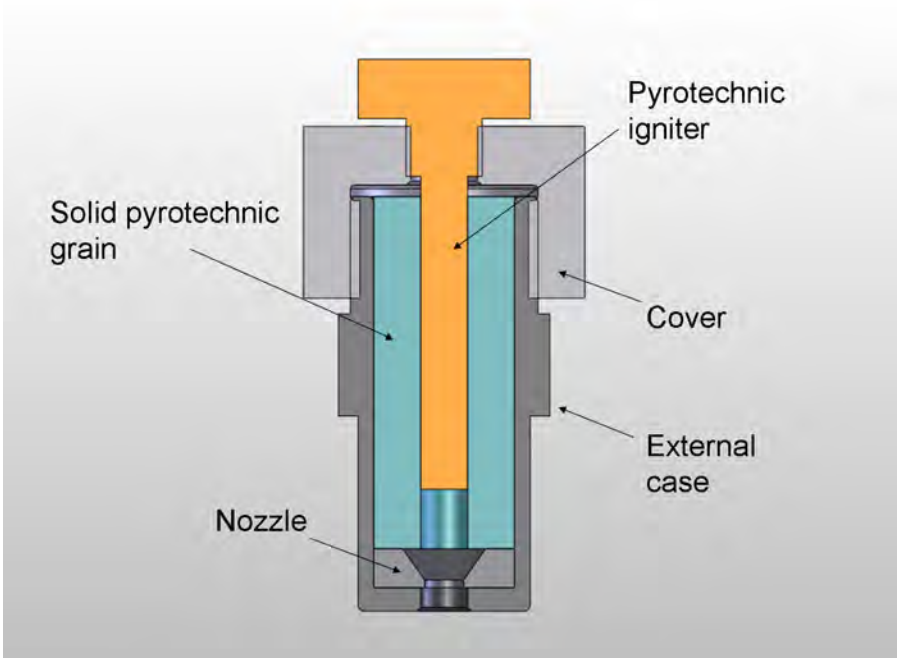

Figure 3.23: Mounting of a single igniter (schematic).

3.3 Fixed Thrust Small and Full Scale Tests

The preparatory phase, in which each set-up was accurately designed and procured, has been followed by an experimental campaign, in which the motor functioning was deeply investigated and all the innovative technical improvements were tested.

In the following sections the small scale and full scale experimental test campaigns are reported together, but it has to be noted that they are consequent: the small scale tests have "prepared" for the full scale motor design.

Time step	Operation	Notes
T0	Solid igniters activation.	
T1	Oxidizer main valve opening	The effective opening time of the valve (ball valve with pneumatic actuator) is of 500 ms. The wax grain is pre-heated.
T2	Mixing of the oxidizer flow with the exhaust gases of the igniters.	Oxidant decomposition produces nitrogen and reactive oxygen (hot gases).
T3	End of igniters combustion.	Hybrid motor combustion already active.

Table 3.4: Full scale motor ignition procedure.

3.3.1 Small Scale Tests

The small scale hybrid motor configuration is described in paragraph 3.2.1. The monitoring of the rocket functioning has been performed with a complete array of sensors, which is briefly described by the schematic in Fig. 3.24. The mounting position of each sensor is summarized in Table 3.5. The thrust load cell has been installed in order to have a macroscopic evaluation of the thruster functioning, as a further parameter to analytically compare the combustion chamber pressure value.

The weight of the oxidizer tank has been performed using a dedicated balance set-up, hanging the reservoir directly to the load cell prior and after each test. This solution has demonstrated to assure reliability and reproducibility of the measurement procedure.

As the regression rate is concerned, its average value has been measured comparing the port diameter and the grain weight prior the test, with the correspondent values after the burning.

Test results - 1st phase

This section details the "cold" and "hot" experimental campaign conducted with the small scale version of the motor: "cold" tests refer to N_2O simple discharges, which have been useful for the hydraulic circuit functioning assessment; "hot" tests refer to complete burning of oxidizer and fuel in the combustion chamber, with the entire array of sensors. As a very preparatory phase of the experimental activity,

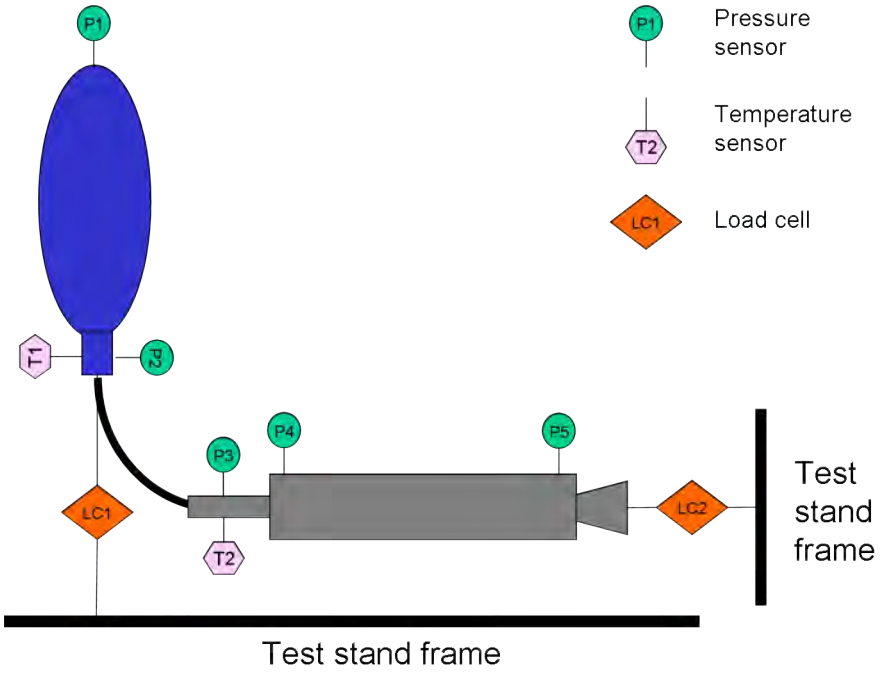

Figure 3.24: Diagnostics installation layout in hybrid rocket test bench.

the first discharge tests are not reported in this work, postponing the oxidizer behavior description with the hot tests results.

Test no. 1, 2 and 3 have been done to initially assess the facility performance and to tune the measurement and data acquisition systems: they have been carried out without pressure sensors on the combustion chamber, and with total oxidizer mass discharge, till its complete depletion. The pressure sensors have been replaced with thermocouples to assess if the environment was compatible with the maximum allowed temperature of the pressure gauges. The maximum temperature measured in the post-combustion chamber section (most severe position) did not exceed 40° C.

Experiments starting from test no. 4 are valid for the data acquisition. Table 3.6 summarizes the main results for each experiment, while results and further information are given in the next paragraphs.

Symbol	Sensor & installation	Notes
P1	Vapor phase N_2O pressure.	25 MPa
P2	Liquid phase N_2O pressure.	25 MPa
P3	Injection pressure (prior injection plate).	6 MPa
P4	Pre-combustion chamber pressure (after injection plate).	6 MPa
P5	Post-combustion chamber pressure.	6 MPa
T1	Liquid phase N_2O temperature.	Type J thermocouple
T2	Pre-injection N_2O temperature.	Type J thermocouple
LC1	Oxidizer tank weight load cell.	1000 N load cell
LC3	Thrust load cell	1000 N load cell, replaced by a 3000 N from test # 33.

Table 3.5: Sensors placement legend (reference to Fig. 3.24).

Test n°	**Description**	**Fuel**	**Configuration**	**Igniter**	**Nozzle**	**Notes**	**Mean Isp (s)**	**Burning Time (s ± 0,001s)**	**Burned Propellant (kg ± 0,5%)**	**Total Impulse (Ns ± 2,60%)**
4	Performance test	Nylon	Nominal	EU	Nominal		161,2 ± 3,11%	5,499	1,73	2733 ± 4,50%
5 - 6 - 12	Performance test	PE Wax	Nominal	EU wax	Nominal	3 tests				
7	Performance test check	Nylon	Nominal	EU	Nominal		173,6 ± 3,10%	5,613	1,84	3132
8	Post-cc off	Nylon	Nominal	EU	Nominal		139,4 ± 3,15%	5,661	1,71	2338
9	O/F change	Nylon	L+100	EU	L+100		173,0 ± 3,03%	5,656	1,96	3320
10	Post-cc off check	Nylon	Nominal	EU	Nominal		161,2 ± 3,13%	5,656	1,82	2873
11	O/F chance check	Nylon	L+100	EU	L+100	Incorrect injection				

Continued on next page

Test n°	**Description**	**Fuel**	**Configuration**	**Igniter**	**Nozzle**	**Notes**	**Mean Isp (s)**	**Burning Time (s ± 0,001s)**	**Burned Propellant (kg ± 0,5%)**	**Total Impulse (Ns ± 2,60%)**
13	Gox change	Nylon	Gox/2	EU Gox/2	Nominal		136,2 ± 3,17%	5,752	1,82	2433
14	Gox change	Nylon	Gox/2	EU Gox/2	Nominal	Igniter failure				
15	Burn: 20 s	PE wax	Nominal	EU wax	Wax long	Very low Gox	159,0 ± 7,00%	21,628	1,68	2617
16	Gox change	Nylon	2 Gox	EU 2 Gox	Nominal		178,5 ± 3,05%	5,564	1,77	3099
17	Gox change check	Nylon	2 Gox	EU 2 Gox	Nominal	2 Gox (selected)	185,1 ± 3,08%	5,745	1,80	3269
18	Performance test	PE	Nominal	EU wax	Nominal		156,6 ± 3,21%	5,575	1,78	2726
19	Performance test check	PE	Nominal	EU wax	Nominal		152,4 ± 3,25%	5,578	1,87	2789

Continued on next page

Test n°	Description	Fuel	Configuration	Igniter	Nozzle	Notes	Mean Isp (s)	Burning Time (s ± 0,001s)	Burned Propellant (kg ± 0,5%)	Total Impulse (Ns ± 2,60%)
20	O/F check	Nylon	L+100	EU	L+100	Data acquisition failure				
21	O/F check	Nylon	L+100	EU	L+100		163,6 ± 3,06%	5,813	1,94	3116
22	Pre-cc variation, no fuel mass measurement	Nylon	Nominal	EU	Nominal			5,717		2927
23	N_2O supercritical	Nylon	Nominal	EU	Nominal		143,7 ± 3,11%	5,553	2,00	2821
24	One-way valve	Nylon	Nominal	EU	Nominal	Injector 4.3 mm	177,4 ± 3,12%	5,526	1,71	2973
25	One-way valve	Nylon	Nominal	EU	Nominal	Injector 3.75 mm	181,5 ± 3,07%	5,398	1,65	2942
26	4x PE wax	PE wax	Nominal	EU wax	Nominal		196,4 ± 3,10%	5,503	1,65	3170

Continued on next page

Test n°	**Description**	**Fuel**	**Configuration**	**Igniter**	**Nozzle**	**Notes**	**Mean Isp (s)**	**Burning Time (s ± 0,001s)**	**Burned Propellant (kg ± 0,5%)**	**Total Impulse (Ns ± 2,60%)**
27	4 cylindrical multiport	Nylon	Multiport	EU Gox/2	Nominal	Igniter failure				
28	4 cylindrical multiport	Nylon	Multiport	EU Gox/2	Nominal	Failure (electrical connection error)				
29	4 cylindrical multiport	Nylon	Multiport	4x EU 2 Gox	Nominal		128,5 ± 3,01%	5,588	2,04	2576
30	4x PE wax - high Gox	PE wax	Nominal	EU 2 Gox	PE Wax long	Injector 4.9 mm	152,0 ± 3,04%	5,471	2,26	3370
31	3 port helical	Nylon	Multiport	3x EU Gox/2	Nominal		147,6 ± 2,92%	5,653	1,93	2798
32	4 cylindrical port 2 Gox	Nylon	Multiport	2x EU 2 Gox	Nominal		126,7 ± 3,05%	5,602	1,89	2353
33	Igniter test	Nylon	Nominal	DTM	Nominal		152,9 ± 3,13%	5,517	1,74	2615

Continued on next page

Test n°	Description	Fuel	Configuration	Igniter	Nozzle	Notes	Mean Isp (s)	Burning Time (s ± 0,001s)	Burned Propellant (kg ± 0,5%)	Total Impulse (Ns ± 2,60%)
34	Igniter test	Nylon	DTM	Nominal	Full port diameter igniter		140,0 ± 3,16%	5,495	1,82	2500
35	Igniter test	PE	Nominal	DTM	Nominal		108 ± 3,14%	5,603	1,82	1933

Table 3.6: Summary of results of first small scale test campaign.

Symbols and abbreviations used in Table 3.6 are described as it follows:

Symbols	Description
PE	Polyethylene grain. It is a material similar to nylon, but with a greater optimal O/F ratio (8 instead of 3.5 as for nylon) and a lower density (890 kg/m^3, respect to 1150 kg/m^3 of PA nylon 6.6).
PE wax	Polyethylene wax. This material has been tested to verify the performance of a an advanced, high regressing fuel. It was supposed to provide the highest regression rates, characteristic of the "liquefying" fuels like paraffin wax, together with and enhanced structural resistance.
EU	Igniter type. The symbol comes from the supplying company of the pyrotechnic tablets used for this motor version ignition.
DTM	Igniter type. It represents another supplier for the motor igniters.

A total of 35 small scale motor tests were successfully completed at CISAS. Nylon 6.6, polyethylene and polyethylene wax have been tested, together with different grain configurations, hydraulic circuit set-up and igniters. Table 3.7 summarized the performance of all the tests. For each experiment typology (double *Gox*, nominal, etc.) the medium value for Isp have been used for the comparison. It has to be remarked that the uncertainty in the total burned oxidizer mass measurement was high for many experiments (around 10%), due to initial set-up problems in the weighting system of the tank.

Test Type	Test #	Average Isp (s)
Nominal	4-7-24	168
Double Gox	16-17	178
Half Gox	13	137
O/F ratio	9-21	168
Without post-cc	8-10	146
Only liquid discharge	25	181
PE	18-19	170
DTM igniters	33-34	146

Table 3.7: Small scale tests results.

The injection dynamic and the igniter performance showed to be the key parameters affecting the hybrid engine:

- The oxidizer mass flow rate must be carefully sized because:

  1. too high oxidizer mass flow rates (respect to the designed value) do not provide an efficient combustion
  2. the early depletion of liquid phase dramatically decreases the thrust level, since the injector is sized for liquid phase and does not work well with vapor.

  For the same reasons, it is fundamental to measure this parameter directly during experimental verification, because of its criticality to code validation, engine performance and Isp calculation.

  As example, the thrust and pressures time histories for test no. 4 and 7 (nominal nylon) are provided in the Figures 3.25 and 3.26. It is shown how the time of the end of liquid phase in the oxidizer adduction causes a dramatic decrease in the developed thrust. Also the initial condition of the liquid phase in the tank influences the motor performance: due to biphasic properties of N_2O, the initial temperature determines the initial pressure, so the liquid/vapor ratio in the tank. To summarize, a certain amount of oxidizer charged in the tank will assure as much liquid flow in the combustion chamber as the lower stock temperature (i.e. higher liquid/vapor ratio). On the other hand, the lower pressure of the oxidizer, the lower will be the combustion chamber pressure, to assure an efficient ΔP to the injector.

- The specific oxidizer mass flow rate demonstrated its high influence on most performance parameters of the motor. Figure 3.27 reports the thrust signal comparison between tests no. 13, 16 and 17, in which the value of Gox has been changed from nominal value. Double Gox configuration performance is high (test no. 16 and 17). High peak thrust (1000 N), high total impulse (>3000 Ns) and high average regression rate (0.73 mm/s). These good results can be due to different effects, or a combination of them:

  – Grain geometric L/D ratio. The internal flame ballistic efficiency is strictly connected to this ratio. If the port diameter is large compare to the grain length, the diffusion flame may be too far from the grain surface, and thus reduce its heating performance (see Figure 3.28). Moreover, if the grain is short, a substantial oxidizer portion could not be mixed before entering the post-combustion chamber. The double Gox L/D ratio is 30, while the nominal test L/D is 21. Half Gox L/D is 15.

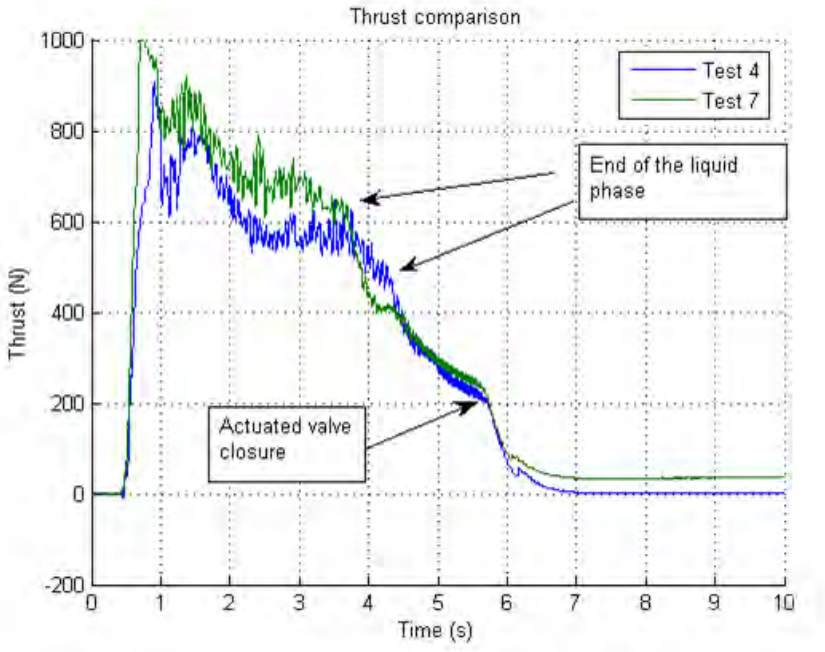

Figure 3.25: Thrust time history for tests n° 4 and 7 (both nominal nylon). The time of liquid phase end and closure of the actuated valve are shown.

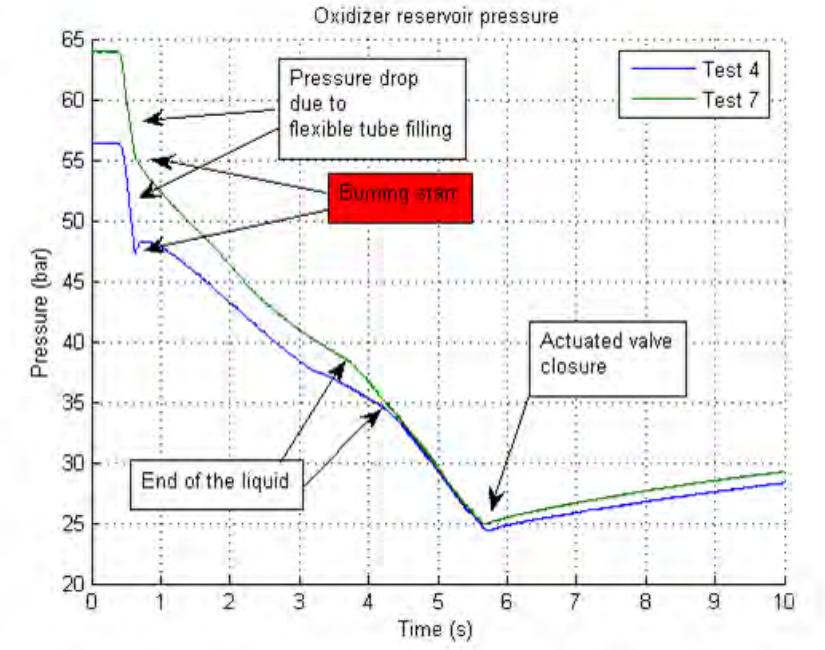

Figure 3.26: Vapor phase pressure signals for tests no.4 and 7 (both nominal nylon). The different engine functioning steps are shown: circuit tube filling, engine start, liquid end and valve closure.

Humble [1] reports typical L/D between 20 and 30 for polymeric hybrid engine grains.

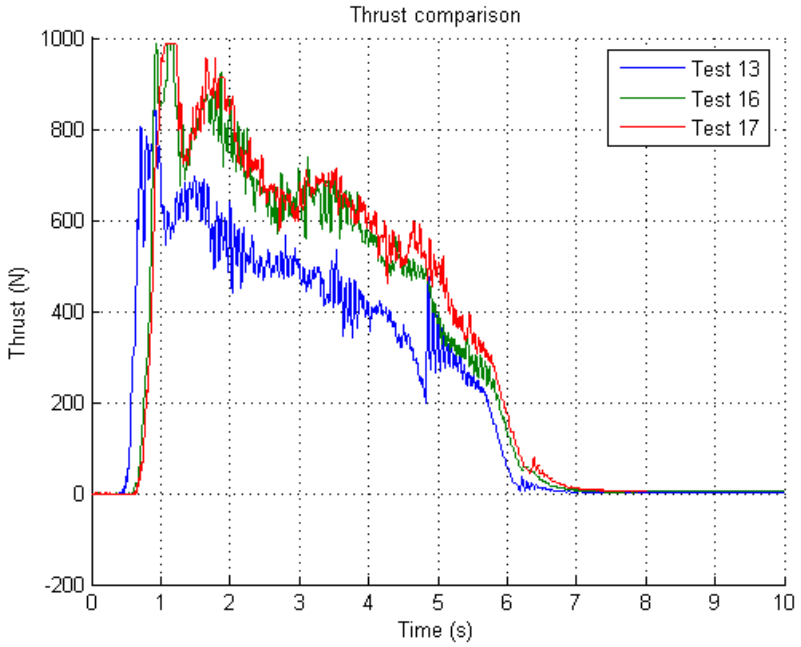

Figure 3.27: Thrust comparison between test no. 13 (half *Gox*), no. 16 and 17 (both double *Gox*). Test 13 shows a lower thrust respect to double *Gox* experiments.

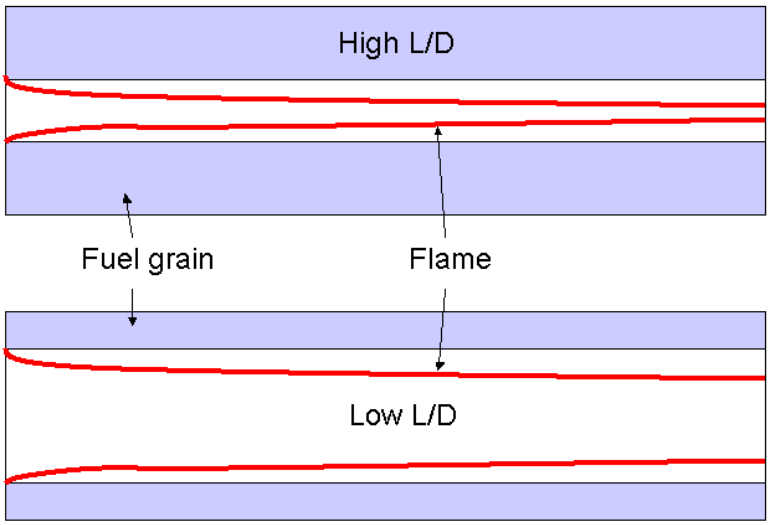

Figure 3.28: The effect of the L/D ratio on the flame and on the regression rate. With high L/D the flame is nearer to the solid fuel surface, on the contrary, with low L/D the flame is far from the surface. The heat flux to the grain in the second case is smaller.

  - The fuel regression rate is function of the instantaneous Gox (see par. 3.1.3). The optimum nylon O/F is 3.5, while the designed value for a nominal test is 7.5. The double Gox configuration lowers the O/F value towards its optimum ($O/F = 6.5$ for double Gox experiments, $O/F = 8.5$ for half Gox). For this reason the thrust is expected to increase: about 3% on the Isp. The average regression rate for test no. 16 and 17 is 0,73 mm/s, for test no. 13 only 0.41 mm/s.
  - Internal flow and flame stability: from literature, the suggested maximum Gox (per port) is of 700 $kg/s\,m^2$. Greater values could bring to flame instabilities and premature combustion end [1]. The fact is that tests with double Gox show only a little more instability at the beginning of the thrust (it accounted for an initial $Gox > 1200$ $kg/s\,m^2$). Perhaps the increase in performance due to the high L/D ratio shadows the instability of the increased Gox. To be notable, also Isp values result to be enhanced with higher specific oxidizer flux.

- The sizing of the injector has to be done for liquid phase flow, and cavitation before injection has to be avoided. The mixed phase behavior is difficult to predict and to analyse with data post-processing. Moreover, concerning safety constrictions, N_2O vapor phase is more subjected to endothermic decomposition, due to its compressibility.

- Ignition affects directly the combustion stability and efficiency. Differences in thrust between identical configurations (i.e. test no. 4 and 7, nominal nylon; no. 8 and 10, without post-combustion chamber) are probably due to bad ignition.

- Ignition and injection optimization is of fundamental importance, especially in multi-port experiments and in combustion stability. Tests demonstrates that the multi-port configuration gave lower performance than the single-port motors, and these bad results depend on differential ignition between ports (especially test no. 32), on bad oxidizer injection behavior and on small (both diameter and length) post-combustion chamber dimensions. It should also be stretched that injectors have not been specifically designed for these tests: these were only preliminary tests on multi-port grains, made to verify their general behavior and the mechanical issues to be solved in their production.

- PE and PE wax grains have given roughly the same performance as nylon.

Figure 3.29: 3 ports helical grain after burning.

PE grants a quite higher regression rate, but it suffers of a lower density, which penalizes the obtainable fuel mass flow rate. PE wax demonstrated a certain increment in the average regression rate value, but it was not worth to select this material, due to its high cost and difficulties in its manufacturing. Resulting mean values are as follows: 0.6 mm/s for PA nylon, 0.65 mm/s for PE, and 0.72 for PE wax.

Test results - 2nd phase

The second part of small scale hybrid tests deserves a special mention, because it has been completely dedicated to the paraffin wax, used as fuel grain. The intent is to verify the performance of a high regressing material, in order to do the final choice for the full scale version of the motor: a high regressing fuel would simplify and save the overall dimension of the entire grain, thus of the combustion chamber. The main verified characteristics are as follows: ignition-ability, average regression rate, grain structural strength and combustion efficiency. Subsequently, a further objective was to increase the efficiency up to 90% of the theoretical value (simulated in frozen equilibrium hypothesis). These parameters have been verified and all of them could be assessed to be satisfactory: the ignition of paraffin wax is feasible, the average regression rate value is similar to the theoretical value (4 times higher with respect to polymeric materials), high efficiency ($> 80\%$) and the grain is able to tolerate thermal and mechanical stresses, without breaks or melting: wax has an ablative behavior in the combustion chamber.

In this tests the same hydraulic circuit as the ones with polymeric materials

has been used.

Tests no. 1, 2 and 3 have served to calibrate the exact dimensions of the pyrotechnic tablets to correctly ignite the motor: if the ignition is too much powerful, that would mean a high detonation in the combustion chamber at the main oxidizer valve opening, and this was caused by a high concentration of fuel rich gases, which were produced by the vaporization of wax. This phenomenon has been called "hard start", and should be avoided.

During tests 6 and 7 a mixer plate have been inserted in the post-combustion chamber, just prior to the nozzle convergent section. This element would increase the overall efficiency off the motor, mixing together the fuel and the oxidizer, that would otherwise enter the nozzle without burning.

Tests no. 10, 11 and 13 served to perform a second ignition strategy: a bipropellant torch. The scope was to identify the consumed mass of fuel during the motor ignition transitory phase, just switching off it at the end of the pre-heating phase. This fuel amount has been measured in test 14, using for the torch the same functioning of test 13. The resulting consumed mass was the 2-3% of the inizial grain mass (about 10 grams on 380 g total mass). Typical delayed ignitions were due to the reduced thermal power, which a propane/oxygen torch was able to provide, but the conducted tests have been very useful in the ignition dynamic comprehension and development.

Table 3.8 summarizes the data of all the successful tests conducted with paraffin wax (mean thrust data obtained from total impulse and burning time).

Test n°	Scope	Ignition	Burned Propellant (kg ± 0,1%)	Port Diameter (m ± 0,001m)	Post-cc: length and type (mm ± 0,1mm)	Throat Diameter (m ± 0,0001m)	Burning Time (s ± 0,001s)	Mean O/F	Total Impulse (Ns ± 2,6%)	Mean Thrust (N ± 2,6%)	Mean Isp (s ± 2,7%)	Notes
3	Motor ignition verification	Cosolo pyro igniter	1,23	0,032	62 - single ring	0,0151	5,127	4,4 ± 0,47%	1949,7	380	162	
4	Long post-cc	Cosolo pyro igniter	1,24	0,032	92 - double ring	0,0151	4,862	4,3 ± 0,46%	1935,8	398	160	Delayed ignition (0.2 sec). No higher efficiency.
5	Higher cc pressure	Cosolo pyro igniter	1,30	0,032	42 - Single perforated ring	0,0125	5,143	4,0 ± 0,41%	2238,5	435	176	Higher performance thanks to higher cc pressure.
6	Higher GOX	Cosolo pyro igniter	1,23	0,03	42 - tungsten mixer	0,0125	4,755	3,3 ± 0,38%	1973,49	415	164	Delayed ignition (0.5 sec). High efficiency.
7	Repetition	Cosolo pyro igniter	1,16	0,03	42 - tungsten mixer	0,0125	4,42	3,9 ± 0,46%	1831,7	414	162	Delayed ignition (0.7 sec). Breaking of tungsten mixer.
8	Repetition of test 5	Cosolo pyro igniter	1,19	0,032	51 - Single perforated ring	0,0125	5,184	4,0 ± 0,45%	2019,7	390	173	Results as test 5.

Continued on next page

Test n°	**Scope**	**Ignition**	**Burned Propellant (kg ± 0,1%)**	**Port Diameter (m ± 0,001m)**	**Post-cc: length and type (mm ± 0,1mm)**	**Throat Diameter (m ± 0,0001m)**	**Burning Time (s ± 0,001s)**	**Mean O/F**	**Total Impulse (Ns ± 2,6%)**	**Mean Thrust (N ± 2,6%)**	**Mean Isp (s ± 2,7%)**	**Notes**
9	Shorter grain, lower OF	Cosolo pyro igniter	1,03	0,032	51 - Single perforated ring	0,0125	3,856	7,2 ± 0,83%	1465,7	380	146	High delay in ignition (1.4 sec).
10	Torch ignition	Propane/oxygen torch	1,29	0,032	51 - Single perforated ring	0,0113	5,302	3,5 ± 0,38%	2183,08	412	173	Delayed ignition (0.15 sec). Results as test 8, no influence of torch on ignition.
11	Lowering ignition delay	Propane/oxygen torch	1,47	0,032	51 - Single perforated ring	0,0125	5,315	4,5 ± 0,41%	2525,5	475	176	Delayed ignition (0.25 sec). Delayed ignition causes low efficiency and Isp.
13	Lowering ignition delay	Propane/oxygen torch	1,26	0,033	51 - Single perforated ring	0,0125	5,006	3,8 ± 0,41%	2112,8	422	171	Delayed ignition (0.1 sec). Results as test 10.

Table 3.8: Summary of results of the second small scale test campaign.

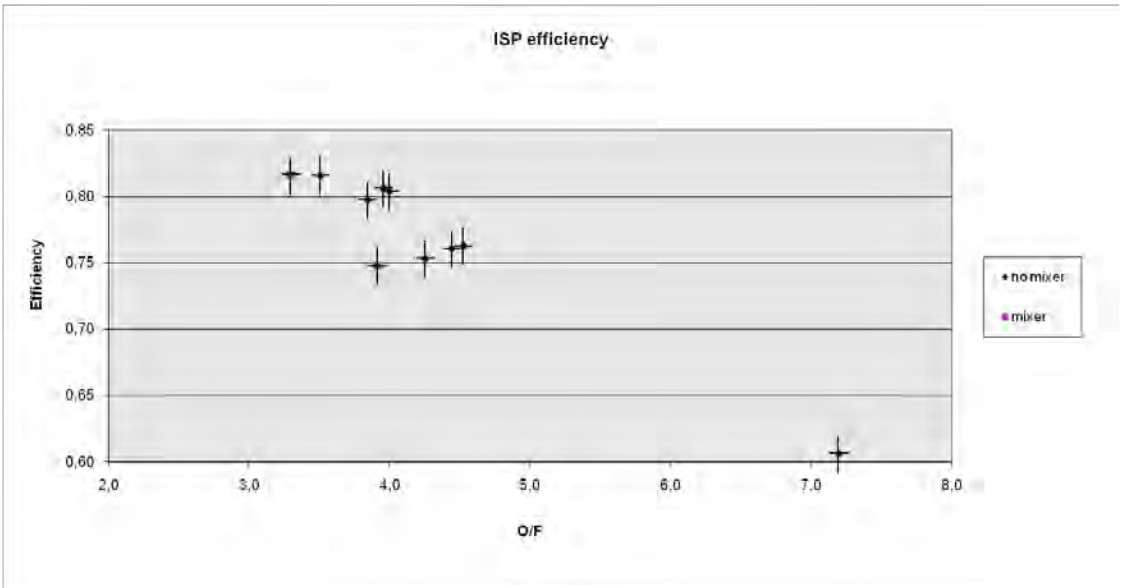

Figure 3.30: Motor efficiency with respect to O/F ratio.

The motor had correct functioning only in three tests (# 3, 5 and 8). During other tests (both with pyrotechnic igniter and bi-propellant torch) a "cold" oxidizer discharge has been followed by a delayed *ignition*: from 0.1 s to 1.4 s (test # 9). This initial oxidizer discharge contributed to a lower efficiency of the motor. This phenomenon can be related to the physical behavior of nitrous oxide: its exothermic decomposition at ambient pressure occurs when its temperature exceeds 600° C; the higher the temperature, the faster is the decomposition. Higher pressures permit the decomposition even at lower temperatures. For these reasons, the delayed ignition of the motor can be related to an insufficient thermal power given to the combustion chamber, prior the main valve opening.

As the *motor efficiency* is concerned, Figure 3.30 illustrates the results for the conducted hot firing tests, in terms of O/F ratio and motor efficiency. For the efficiency uncertainty bounds, the propagation method has been applied to the formula: $\varepsilon = \frac{c^*}{c^*_{th}}$, where ε is the efficiency value, c^* is the empirical value of the characteristic exhaust velocity (described by equation (2.6) in chapter 2) and c^*_{th} is the correspondence theoretical value, calculated with equation (2.5). Test no. 9 had the worst ignition performance (with 1.4 s delay), and this seemed to be the reason for such low efficiency (= 0.6). Test with mixer installed in the post-cc, which had low efficiency, is test no. 7: during this test the mixer was broken during the motor functioning, and this seemed to be the reason for such a low performance (in addition to the delayed ignition). This can be justified also from results of

test no. 6 (with mixer and high delayed ignition of about 0.5 s): in this case the measured efficiency is the higher of the entire test campaign, even if compared with regular-ignition tests. This facts conduct to the following considerations:

- In case of paraffin wax hybrid rockets, the efficiency is generally high (> 0.8). This is also connected with the small scale of the motor, in which the oxidizer and fuel are better mixed together than in higher scale motors.
- The installation of a mixer in the combustion chamber seemed to have positive influence on the efficiency value. Tungsten is not adapt as building material.
- There are no considerable differences on the motor performance when using pyro-igniters or a bi-propellant torch.

The *regression rate* measurement has been conducted only on average values, dividing the weighted burned paraffin by the burning time. For the regression rate value uncertainty, the propagation method has been applied to the formula: $\dot{r} = M_f/t_b$, where $\dot{r}$ is the average regression rate value, M_f is the burned fuel mass and t_b is the burning time. Tests no. 6, 7 and 9 have not been considered, due to their high delay on ignition. Figure 3.31 gives a comparison between the measured average regression rate and the theoretical value, with respect to the specific oxidizer flow, as in the equation:

$$\dot{r} = a \cdot G_{ox}^{n} \tag{3.1}$$

Empirical parameters a and n have been assumed from literature ([7]). The Gox mean value has been determined from initial and final port grain diameter (mean values A_{in} and A_{fin}) and mean value of oxidizer mass flow rate, with the equation:

$$\overline{Gox} = \frac{\overline{\dot{m}_{ox}}}{\left(\frac{A_{in}+A_{fin}}{2}\right)} \tag{3.2}$$

The measured values have been higher than the expected from literature values. This is an important result: paraffin wax has average regression rate values much higher than Nylon and Polyethylene, and in the meantime it grants high structural performance. The high measured values can be justified by some different factors, as the small scale of the motor (initial port diameter of 32 mm) and the high obtained efficiency. Furthermore, the theoretical equations, which have been used to calculate the theoretical values, are highly approximated and they don't take

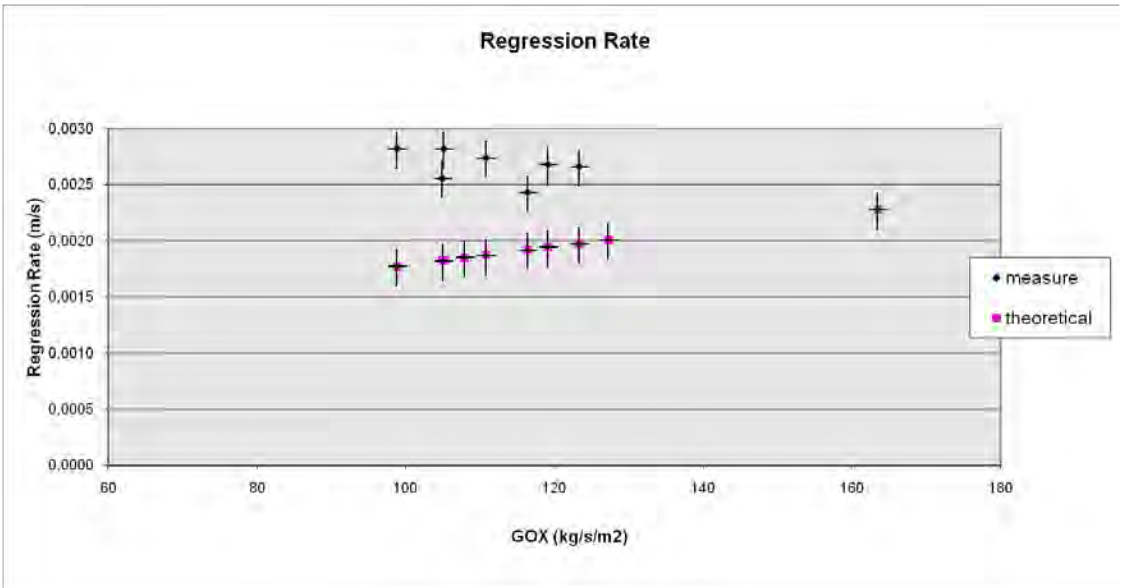

Figure 3.31: Average regression rate with respect to Gox.

into account many parameters (as, for example, the motor scale and the efficiency themselves). For these reasons, the calculated coefficients are valid only for the same motor configuration, with the same efficiency, fuel composition and internal fluid dynamics.

To conclude, small scale paraffin wax tests had the expected results. In particular:

- Paraffin (in addition with EVA glue) can be used as fuel for hybrid rockets, without any restraints on its mechanical performance.

- The higher combustion efficiency (82%) has been achieved with a mixing plate installed in the combustion chamber. This leads to consider the importance of the combustion chamber in the hybrid rocket peformance increasing.

- Transitory ignition phases are of fundamental importance in the overall performance of the motor. The process should be well analyzed, in order to grant also its repeatability.

- Thanks to its regression rate, paraffin wax permits a more simple motor design, with a single-port configuration (instead of multi-port, as with polymeric fuel version). This also reflects in a more simple design and cost reduction for the injection and the combustion chamber.

Uncertainty Analysis The same measurement diagnostics equipment has been used both during the first and second small scale test campaign: the performance of the adopted sensors have been described in Table 3.1. The resulting uncertainty on calculated quantities are reported in Table 3.9, with specific reference to the variables, which have been evaluated by means of the following expressions:

- Propellant mass: $M_{prop} = M_{ox} + M_f$
- Mean thrust: $\overline{T}$
- Total impulse: $I_{tot} = \int_0^{t_b} \overline{T}\, dt$, where t_b is the burning time
- Specific impulse: $I_{sp} = \frac{I_{tot}}{M_{prop} \cdot g_0}$, where g_0 is the gravitational acceleration constant
- Mean O/F: $O/F = M_{ox}/M_f$, where M_{ox} and M_f are the weighted masses of the burned oxidizer and fuel, respectively.

Variable	**Value (%)**
Propellant mass	0.1
Mean thrust	2.6
Total impulse	2.6
Specific impulse	2.7

Table 3.9: Uncertainty analysis for calculated performance values of small scale tests.

Figure 3.32: Wax test # 4 during burning phase.

3.3.2 Full Scale Tests - 1st phase

The monitoring of the full scale rocket functioning has been performed with the array of sensors described by the schematic in Fig. 3.33. The mounting position of each sensor is summarized in Table 3.10. The double thrust load cell solution has been imposed by the mechanical mounting of the motor on the test bench, and they have been installed in order to have a macroscopic evaluation of the thruster functioning. The weighting system for the oxidizer tanks has already been described by Figure 3.9.

Experimental tests on full scale hybrid motor have been arranged to produce a complete test (5 seconds of burning time) with limited preliminary activities. They have been divided into four phases:

1. ignition phase definition
2. oxidizer injection set-up
3. reduced burning time tests, for safety reason during initial experimental activities
4. nominal burning time tests (5 or 3.5 seconds)

Symbol	Sensor & installation	Notes
Gas1 & Gas2	Vapor phase N_2O pressure of tank 1 and 2.	Upstream the tanks.
Liq1 & Liq2	Liquid phase N_2O pressure of tank1 and 2.	Downstream the tanks.
Diff1 & Diff2	Injection pressure (diffuser prior injection plate).	Double pressure outlet for redundancy.
Precc1	Pre-combustion chamber pressure (after injection plate).	
Postcc1	Post-combustion chamber pressure.	
Lc1 & Lc2	Developed thrust.	
Lc3 & Lc4	Tanks 1 and 2.	Tanks weight measurement sensors.

Table 3.10: Sensors placement legend (reference to Fig. 3.33).

The test campaign have comprehended the following activities: "cold" oxidizer discharge tests, ignition tests (with and without oxidizer discharge, no grain in combustion chamber) and "hot" firing tests (ignition and oxidizer discharge, with grain in combustion chamber). The discharge, ignition and first firing tests have been useful in the measurement diagnostics and total oxidizer mass flow rate calibration, in order to avoid any possible risks with such scale propulsion system. Table 3.11 summarizes the objectives of the conducted tests:

Discharge Tests

Oxidizer cold discharge tests had the following objectives:

- Correct diagnostics functioning on hydraulic circuit.
- Data acquisition for verification and calibration of the theoretical model, used for mass flow rate indirect measurement.
- Set-up of oxidizer tanks weighting system and charging procedures.
- Injection plate mechanical design verification.

During the first tests, some measurement issues have been identified, and they are summarized in the following paragraphs:

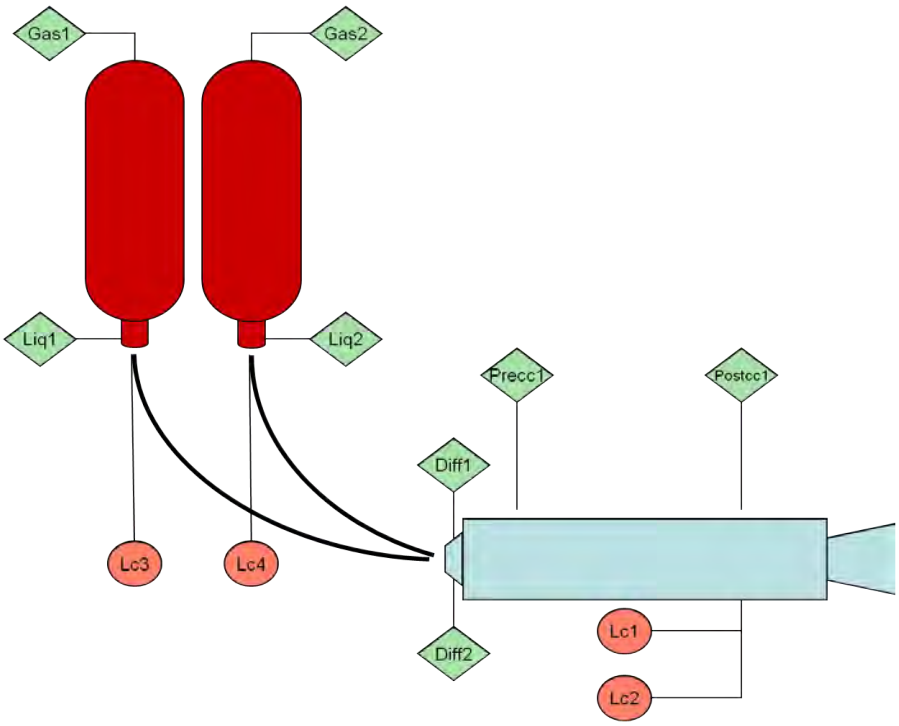

Figure 3.33: Diagnostics installation layout in full scale hybrid rocket test bench.

- pressure measured on oxidizer tanks (vapor side) is lower than the measured pressure downstream, on the injection section (see Figure 3.34). The kinetic pressure term does not explain this considerable difference;
- same problem as in DT1, but in this occasion it affected only one tank (see Figure 3.35);
- different measurement between different pressure sensors (25 and 10 MPa sensors), when mounted upstream the injection plate (see Figure 3.36).

The measurement anomalies were due to different causes:

1. 25MPa sensors have high temperature sensitivity (1.5% of full scale, even in compensated range), which bring to measurement errors as high as 0.375 MPa (3.75 bar). Since N_2O grows cold during its discharge, the tests have highlighted that these sensors can not be used for the present purposes. Measurement anomalies happen after approximately 2 seconds after the beginning of the discharge, so probably when the N_2O temperature goes beyond the compensated thermal range of the sensors.
2. The measurement section on the vapor side of the tanks have been analyzed: it presented a sort of restriction, which could have influenced the correct

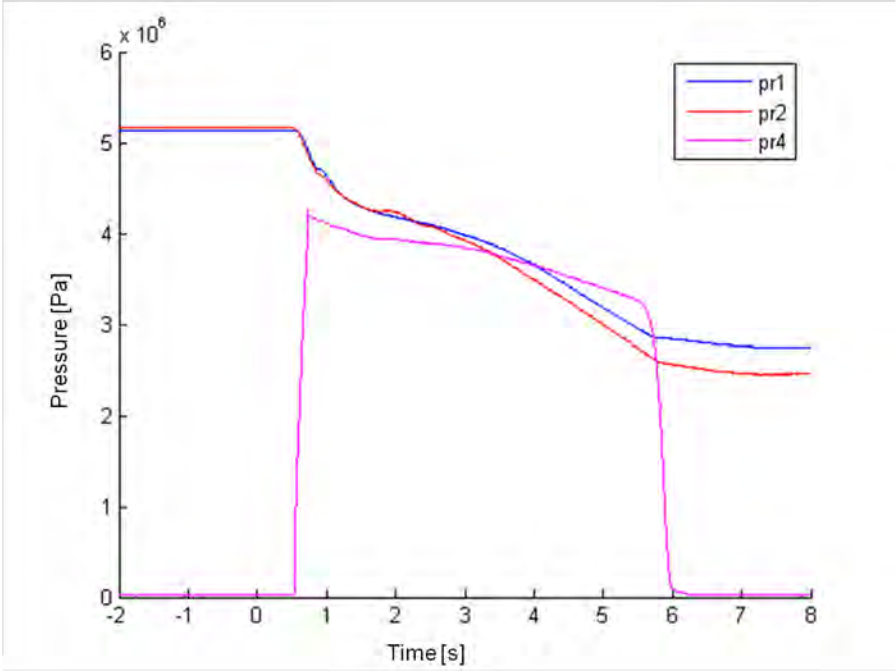

Figure 3.34: Pressure data for discharge test # 1 (DT1): pr1 and pr2 25MPa sensors on vapor side of the tanks, pr4 is a 10MPa sensor mounted upstream the injection plate.

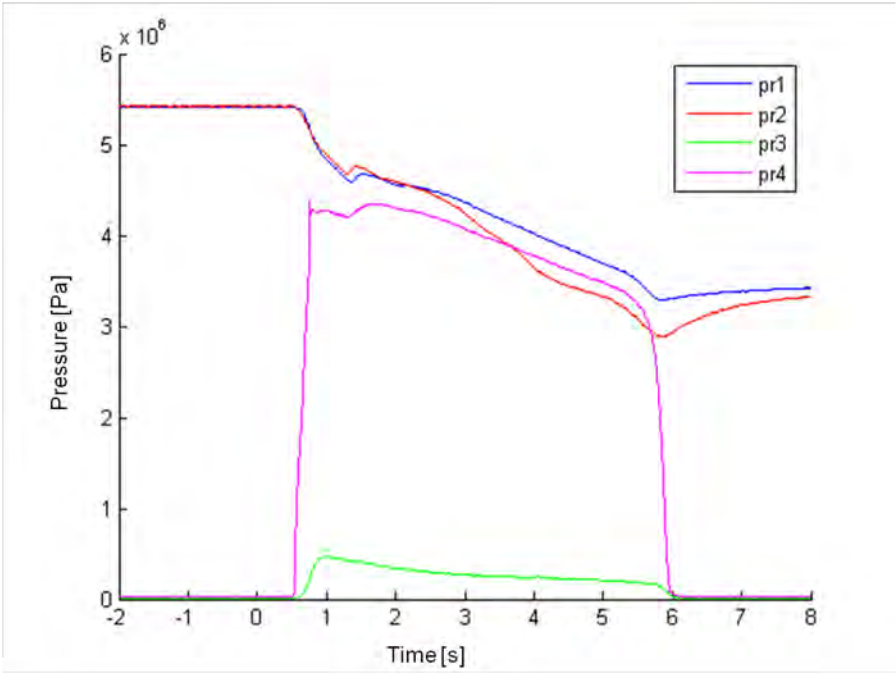

Figure 3.35: Pressure data for discharge test # 4 (DT4): pr1 and pr2 10MPa sensors on vapor side of the tanks, pr4 and pr3 are 10MPa sensors mounted upstream the injection plate and in combustion chamber respectively.

Test type	Description	Scope
Discharge test (DT)	Motor installation without fuel grain and nozzle. Hydraulic circuit, injection plate and combustion chamber are set as for complete tests.	• mean oxidizer mass flow rate measurement • injection plate calibration • hydraulic circuit functioning verification • measurement diagnostics calibration
Ignition tests (IT)	Pyrotechnic igniters are mounted to the combustion chamber and activated simultaneously. One test has foreseen also the oxidizer discharge, to check the effects on its dissociation.	• measurement of igniters functioning time • main valve opening delay set-up • N_2O decomposition verification at the beginning of the discharge
Firing tests (FT)	Ignition, oxidizer discharge and combustion with different burning time. Motor configuration is described in section 3.2.2.	Functioning parameters measurement.

Table 3.11: Full scale test types description.

measure of the tanks pressure. In fact, the described problems appeared both with 25MPa and 10MPa sensors.

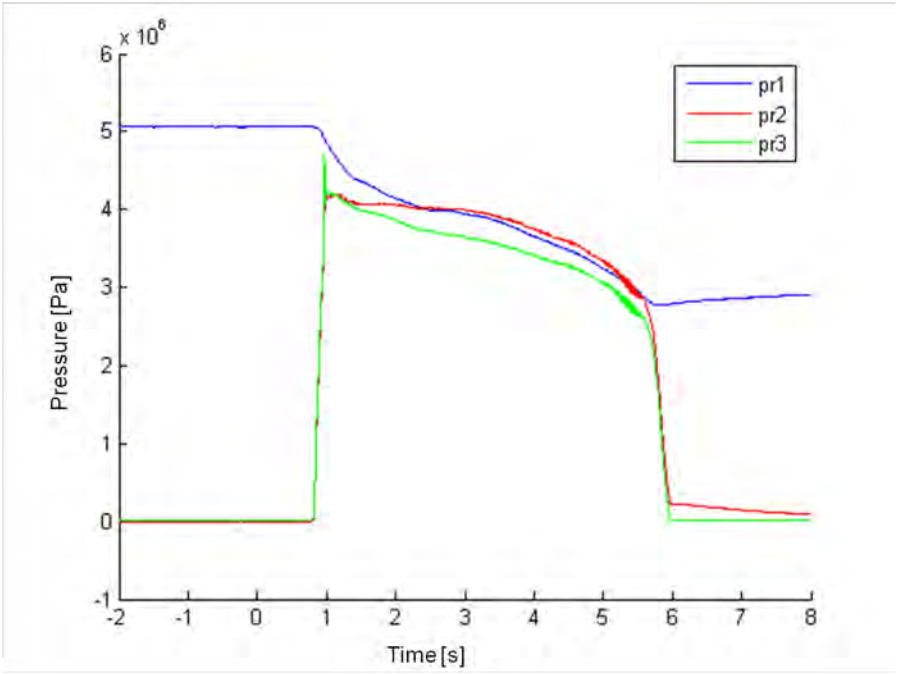

Figure 3.36: Pressure data for discharge test # 3 (DT3): pr1 is a 25MPa sensor mounted on vapor side of the tank no. 1, pr3 and pr2 are 10MPa and 25MPa sensors respectively, mounted upstream the injection plate.

3. As the hydraulic circuit is concerned, a consistent difference on the check valves has been found. This discrepancy could have been the cause for different discharge performance, that have been verified between the two adducting pipes: Figure 3.37 illustrates this phenomenon, in which pr1 shows an early end of the liquid phase (at about 5 seconds, indicated by change in the gradient of the pressure).

In summary, measurement anomalies were due to the sensors placement and to their thermal sensitivity. To solve these issues, the following solutions have been adopted:

- 25MPa sensors have been substituted by 10MPa sensors, with lower sensitivity to temperature variations;
- the measurement sections for the tanks pressure have been set to the liquid side (see Figure 3.33). The kinetic error have been evaluated, and was proportional to 0.01 MPa, thus negligible;
- one way valves have been substituted with other two identical valves, with the same performance.

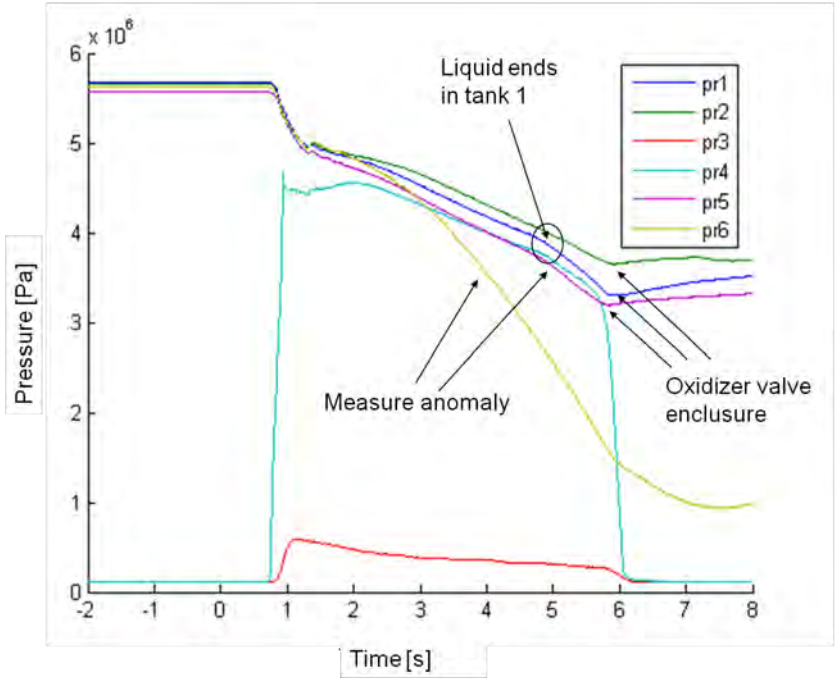

Figure 3.37: Pressure data of a complete discharge test: pr1 and pr2 are 25MPa sensors mounted on liquid side of the tanks, pr5 and pr6 show the anomaly of 25MPa sensors mounted on vapor side of the tank, pr4 is a 10MPa sensor, mounted upstream the injection plate and pr3 is a 10MPa sensor, mounted on combustion chamber.

The adopted modifications have solved the verified measurement issues from DT5 and from FT3.

Ignition System

The ignition system of the hybrid motor foresees three pyrotechnic igniters, that are activated by electrical signal from the controlling electronics (Fig. 3.39). As described in section 3.2.2, each igniter is composed by two different parts: a high sensitivity pyrotechnic igniter with electrical activation, and a solid tablet with lower thermal sensitivity. In this way, the complete ignition device can be activated only when correctly mounted.

The power supply provided to each igniter have been accurately calibrated: too high and too low currents are unable to ignite the device. Tests on single injectors were useful for the functioning time definition, in order to calibrate the entire motor ignition procedure. From the conducted tests, igniters start the burning after approximately 2 seconds after the START command, and burn for about 4 s with an almost constant mass flow rate (visual experimental investigation of all the parameters).

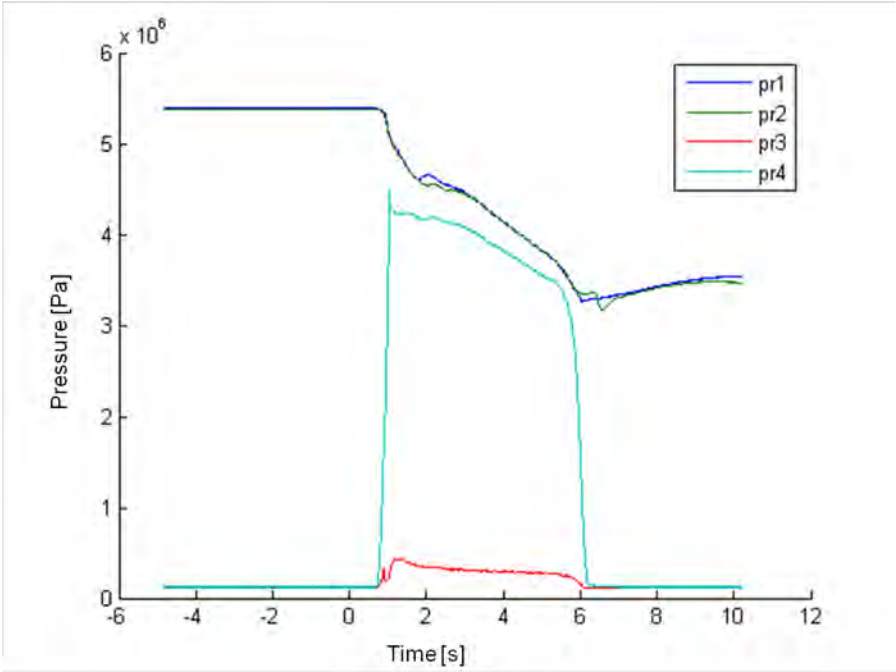

Figure 3.38: Pressure data for discharge test # 7 (DT7): pr1 and pr2 are mounted on liquid side of the tanks, pr4 is mounted upstream the injection plate and pr3 is mounted downstream the injection plate, on the combustion chamber.

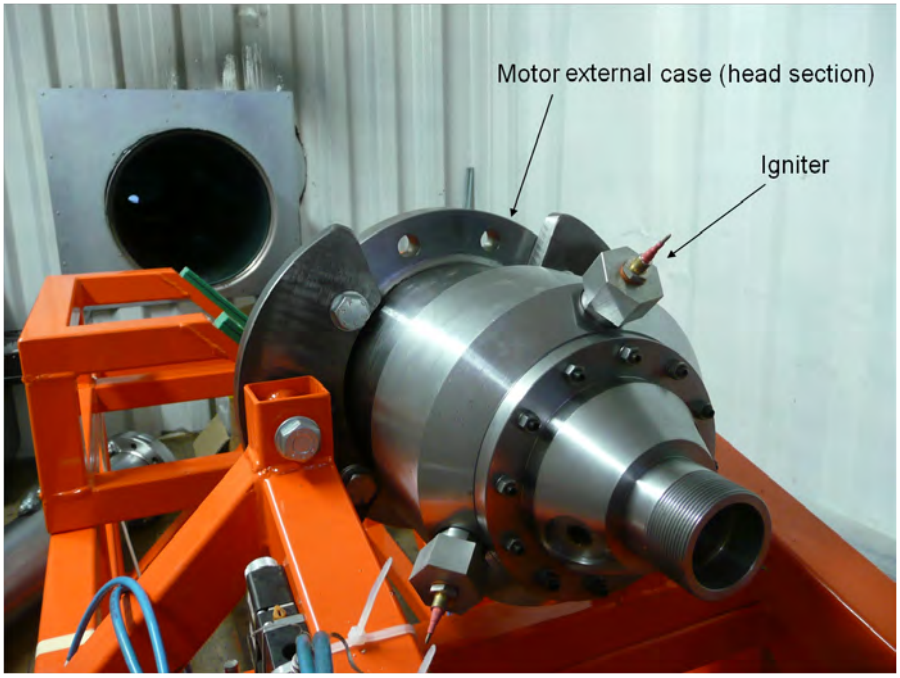

Figure 3.39: Pyrotechnic igniters mounted on the full scale motor external case.

Firing tests

Among the conducted hot firing tests, only the ones from FT4 have been considered for the motor performance evaluation. Tests FT1, FT2 and FT3 were performed to verify the correct ignition of the motor and its safe functioning during the first and most critical phases.

Table 3.12 summarizes the developed motor performance in terms of the measurements and evaluated data. The requirements of the motor to be satisfied were 87.7% of overall efficiency (divided into 90% of combustion efficiency and 97.5% of nozzle efficiency) and 50 kNs of total impulse. Column *Notes* summarizes the configuration variations made to the motor throughout the test campaign, with respect the described configuration in section 3.2.2, which have been:

- installation of convergent pre-combustion chamber instead of the cylindrical type, in two different materials: nylon and aluminum;
- vapor fraction reduction in the oxidizer tanks, which have been charged with more mass than necessary (22 liters of liquid N_2O instead of 18 liters used during nominal tests);
- different L/D rate of the injection plate holes;
- different post-cc configurations: double ring and mixer;
- burning time reduction from 5 to 3.5 seconds (last test: FT20).

Test n°	**Scope**	**Mox (kg ± 4,06%)**	**Mf (kg)**	**Port Diameter (m ± 1mm)**	**Cc mean press. (MPa)**	**T burn (s ± 0,001s)**	**Mean fuel mass flow rate (kg/s)**	**Mean ox mass flow rate (kg/s)**	**Mean O/F**	**Total impulse (Ns)**	**Mean Isp (s)**	**Efficiency**	**Notes**
FT4	nominal	20,62	3,493 ± 0,14%	0,12	2,21 ± 1,13%	5,325	4,53 ± 0,16%	3,87 ± 4,08%	5,9 ± 4,20%	41402,19 ± 1,37%	175 ± 5,57%	0,78 ± 6,53%	Undamaged grain
FT6	nominal	19,62	3,352 ± 0,15%	0,12	2,16 ± 1,16%	5,171	4,44 ± 0,17%	3,79 ± 4,08%	5,9 ± 4,21%	38885,62 ± 1,39%	173 ± 5,60%	0,77 ± 6,56%	Small holes on grain surface, due to initial small cracks
FT8	nominal	20,82	3,406 ± 0,15%	0,12	2,42 ± 1,03%	5,091	4,76 ± 0,17%	4,09 ± 4,08%	6,1 ± 4,21%	41620,32 ± 5,61%	175 ± 5,61%	0,76 ± 6,44%	Big longitudinal crack on grain
FT10	USA solid igniters	20,32	3,471 ± 0,14%	0,12	2,40 ± 1,04%	5,378	4,42 ± 0,16%	3,78 ± 4,08%	5,9 ± 4,20%	41926,10 ± 1,36%	180 ± 5,57%	0,79 ± 6,44%	Undamaged grain
FT11	USA solid igniters	20,72	3,011 ± 0,17%	0,12	2,43 ± 1,03%	5,205	4,56 ± 0,19%	3,98 ± 4,08%	6,9 ± 4,23%	41612,80 ± 1,39%	179 ± 5,61%	0,78 ± 6,45%	Undamaged grain
FT12	USA solid igniters, convergent pre-cc	20,32	3,395 ± 0,15%	0,12	2,45 ± 1,02%	5,087	4,66 ± 0,17%	3,99 ± 4,08%	6,0 ± 4,21%	39447,00 ± 1,40%	170 ± 5,61%	0,74 ± 6,43%	Big longitudinal crack on mean grain section
FT13	Convergent Al pre-cc, full tanks	18,02	3,935 ± 0,13%	0,12	2,48 ± 1,01%	5,16	4,25 ± 0,15%	3,49 ± 4,08%	4,6 ± 4,19%	39613,00 ± 1,39%	184 ± 5,58%	0,83 ± 6,39%	Totally broken grain during dismounting, remaining fuel mass not reliable

Continued on next page

Test n°	Scope	Mox (kg ± 4,06%))	Mf (kg)	Port Diam-eter (m ± 1mm)	Cc mean press. (MPa)	T burn (s ± 0,001s)	Mean fuel mass flow rate (kg/s)	Mean ox mass flow rate (kg/s)	Mean O/F	Total impulse (Ns)	Mean Isp (s)	Efficiency	Notes
FT14	Full tanks	17,62	3,193 ± 0,16%	0,12	2,13 ± 1,18%	5,002	4,16 ± 0,18%	3,52 ± 4,08%	5,5 ± 4,22%	33875,70 ± 1,41%	166 ± 6,63%	0,74 ± 6,59%	Undamaged grain
FT15	Full tanks, double ring post-cc	18,52	3,141 ± 0,16%	0,12	2,09 ± 1,20%	5,202	4,16 ± 0,18%	3,56 ± 4,08%	5,9 ± 4,22%	34953,00 ± 1,39%	164 ± 5,61%	0,74 ± 6,53% ± 6,61%	Undamaged grain, post-cc good final conditions
FT16	Full tanks, injection plate holes L/D = 4	21,42	3,761 ± 0,13%	0,12	2,54 ± 0,98%	5,025	5,01 ± 0,15%	4,26 ± 4,08%	5,7 ± 4,19%	41334,00 ± 1,41%	167 ± 5,60%	0,73 ± 6,38%	Undamaged grain, post-cc good final conditions
FT17	Mixing plate, injection plate holes L/D = 4	7,77	1,789 ± 0,28%	0,12	3,10 ± 0,81%	2,1	4,55 ± 0,33%	3,70 ± 4,11%	4,3 ± 4,34%	19615,00 ± 2,18%	209 ± 6,52%	0,93 ± 6,37%	Undamaged grain, post-cc good final conditions
FT18	Mixing plate, injection plate holes L/D = 4	19,05	3,984 ± 0,13%	0,12	3,03 ± 0,82%	5,16	4,46 ± 0,14%	3,69 ± 4,08%	4,8 ± 4,19%	47829,70 ± 1,39%	212 ± 5,58%	0,92 ± 6,21%	Undamaged grain, post-cc good final conditions
FT19	Mixing plate, injection plate holes L/D = 4	19,15	4,254 ± 0,12%	0,12	3,18 ± 0,79%	5,063	4,62 ± 0,14%	3,78 ± 4,08%	4,5 ± 4,18%	47379,90 ± 1,41%	206 ± 5,58%	0,90 ± 6,16%	Undamaged grain, post-cc good final conditions

Continued on next page

Test n°	**Scope**	**Mox (kg ± 4,06%))**	**Mf (kg)**	**Port Diameter (m ± 1mm)**	**Cc mean press. (MPa)**	**T burn (s ± 0,001s)**	**Mean fuel mass flow rate (kg/s)**	**Mean ox mass flow rate (kg/s)**	**Mean O/F**	**Total impulse (Ns)**	**Mean Isp (s)**	**Efficiency**	**Notes**
FT20	Reduced burning time, mixing plate, injection plate holes L/D = 4	15,572	3,345 ± 0,15%	0,12	2,80 ± 0,89%	2,968	6,37 ± 0,18%	5,25 ± 4,09%	4,7 ± 4,21%	36036,00 ± 1,84%	194 ± 6,05%	0,85 ± 6,29%	Undamaged grain, post-cc good final conditions

Table 3.12: Results of the first full scale test campaign.

The *uncertainty analysis* on calculated values (total impulse and specific impulse) has been conducted through the uncertainty propagation method, which has been applied to the equations (2.8) and (2.10), described in chapter 2. The uncertainty on the mean O/F values has been evaluated through the propagation method on the mean O/F ratio formula: $O/F = M_{ox}/M_f$, where M_{ox} and M_f are the weighted masses of the burned oxidizer and fuel, respectively. The uncertainty on the mean mass flow rates values has been calculated using the propagation method, applied to the mean mass flow rate formula: $\overline{\dot{m}} = \frac{M}{t_b}$, where $\overline{\dot{m}}$ is the mass flow rate relative to the initial mass M, and t_b is the burning time. The uncertainty on mean thrust data have been evaluated from a static calibration of the full scale measurement scheme, and it is $\pm$ 1% of the measured data. For the efficiency uncertainty bounds, the propagation method has been applied to the formula: $\varepsilon = \frac{c^*}{c^*_{th}}$, where ε is the efficiency value, c^* is the empirical value of the characteristic exhaust velocity (described by equation (2.6) in chapter 2) and c^*_{th} is the correspondence theoretical value, calculated with equation (2.5).

Main results of the test campaign are reported in the following paragraphs, and they are divided into different sections:

- ignition
- motor efficiency
- regression rate

Ignition To obtain an instantaneous ignition of the motor at the main oxidizer vale opening, the use of a nozzle cap has been necessary. In fact, during FT1, FT2, FT7 and DT2 the cap has not been used, and an initial oxidizer discharge verified prior the ignition of the combustion reaction (Figure 3.40). Even adopting a longer pre-heating time (changing the time sequence of the igniter activation and valve opening), the problem was not solved. With the mounting of a specific cap to the nozzle, and the calibration of its opening at a pre-determined chamber pressure, the ideal combustion chamber conditions for a correct ignition have been reached. The function of the cap is to increase the combustion chamber temperature prior the opening valve (hot gases are kept within the chamber), thus to permit the decomposition of nitrous oxide with the same thermal power given by igniters (Figure 3.41.

To conclude:

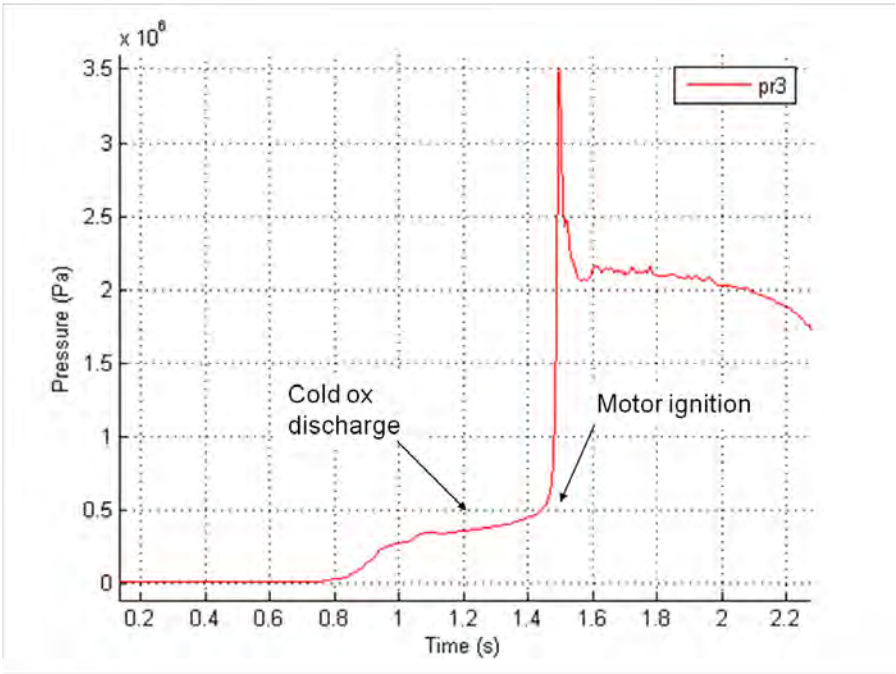

Figure 3.40: Delayed ignition in FT2: pr3 is the pressure signal in combustion chamber.

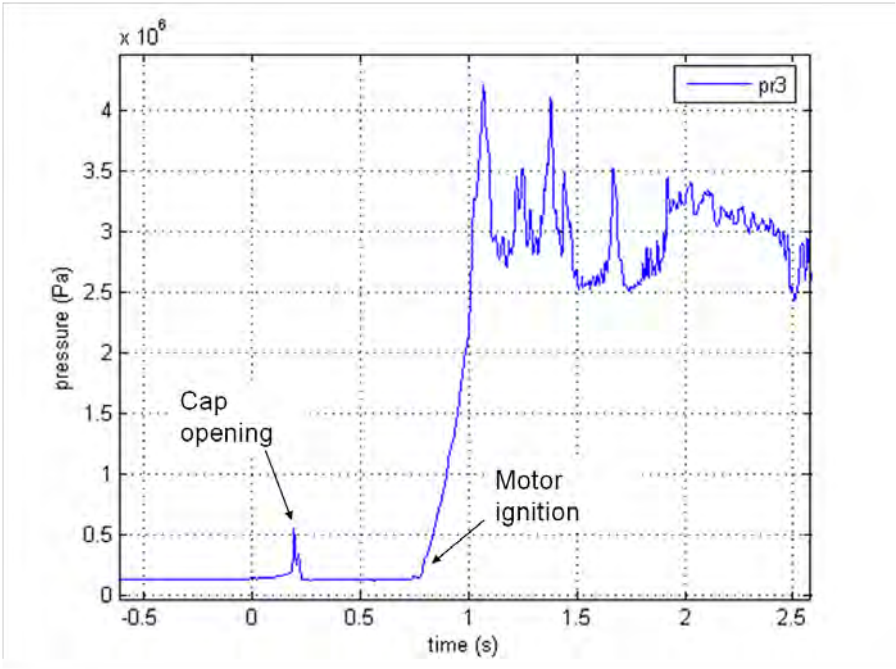

Figure 3.41: Combustion chamber pressure signal in FT6: initial pressure peak indicates the opening of the nozzle cap, then motor ignites instantaneously.

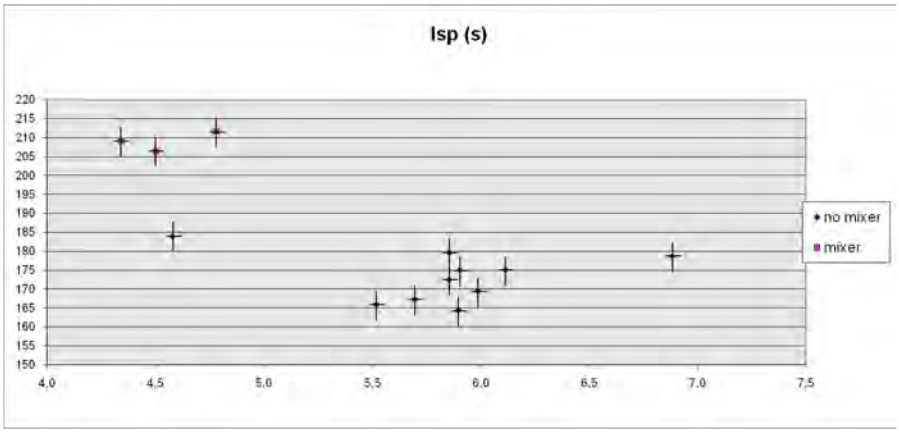

Figure 3.42: Isp values with respect to O/F ratio.

- Ignition phase does not seem to influence the motor efficiency, evenf if too short pre-heating times are not able to ignite the motor. After the combustion reaction has started, however, performance are not influenced by the ignition technique.

- Nozzle cap is important for an instantaneous ignition; a possible alternative could be the use of more powerful igniters.

- Combustion instabilities may be determined by ignition technique, especially during the initial burning phases. Influencing parameters are: *a*) uniformity in grain pre-heating, *b*) equal functioning time for the igniters during oxidizer discharge, *c*) equal ignition time of the igniters.

Motor efficiency Figure 3.42 illustrates the Isp values calculated for the conducted firing tests, with respect to the O/F ratio: during tests with Isp higher than 200 s, a mixing plate on the post-cc section has been used.

From the obtained data, the following considerations can be done:

- High efficiency has been reached only with the use of a mixing plate in post-cc section: this solution permits the mixing of oxidizer and fuel fluxes prior entering the exhaust nozzle.

- Global motor efficiency is not influenced by ignition technique and pre-combustion chamber type (cylindrical or convergent pre-cc).

- Oxidizer injection dynamics influence both on combustion stability and efficiency. As described in section 3.4, during tests from FT4 to FT15 the efficiency changes between two different "stability" conditions: high efficiency

with instabilities and low efficiency with less instabilities. Reduction of L/D rate of the injection plate holes has solved this problem, stabilizing the motor to a unique injection regime.

- Full scale motor, with respect to small scale version, has given general lower efficiency for the correspondant configurations (from 5% to 10%, without mixer). Two parameters seem to determined the verified differences: *a*) small scale motor had mean Gox values equal to 100-150 kg/m^2s, while full scale motor functioned with 200-300 kg/m^2s; the increasing of the Gox value determines a decrease in the obtainable efficiency, due to lower mixing of oxidizer and fuel and to reduction of the residence time in combustion chamber. *b*) Scale effect.

Regression rate The average regression rate value of the firing tests has been calculated from the differential fuel mass, prior and after each test. The hypothesis was of a uniform grain consumption along its longitudinal dimension, conserving its initial cylindrical internal shape. Experimental investigation have however highlighted that a greater consumption happens at the beginning of the fuel grain, with some non homogeneous patterns.

Figure 3.43 summarizes the results of the calculated average regression rate values (with an uncertainty of 0,17%) with respect to the mean Gox, evaluated with the equation $\overline{G_{ox}} = \frac{\overline{\dot{m}_{ox}}}{\overline{A_p}}$, where A_p is the mean port area of the fuel grain, evaluated from the initial and final port area of the burned grains (final diameter has been calculated from the burned grain mass, uncertainty: $\pm$ 2%). It is clearly notable how the mixing plate in the post-cc has improved also the behavior of the fuel in the combustion chamber.

The most evident results are:

- Measured average regression rate is between 70% and 80% of the same theoretical value, foreseen for paraffin wax and N_2O. This discrepancy can be caused by several effects, which comprehend the scale effect on the motor (theoretical values have been calculated on the basis of small scale tests) and the fuel composition: to improve mechanical properties of wax, it has been added with EVA glue and carbon. This fuel additives have not been taken into account in the theoretical regression rate prediction.

- The combustion efficiency seems to well influence also the performed regression rate of the fuel: more efficient motors burn more grain mass.

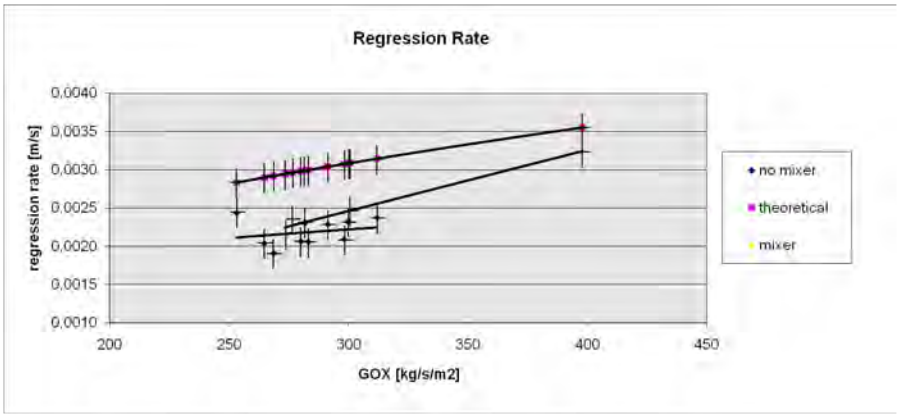

Figure 3.43: Average regression rate values for conducted firing tests: comparison between measured and theoretical values.

In conclusions, a total amount of 20 firing tests have been conducted on a first version full scale motor, together with oxidizer discharge tests and ignition tests. The measurement diagnostics have been optimized to allow the availability of measures when dealing with biphasic fluids, in high time-varying conditions. The overall efficiency has been higher than 90% (inital requirement: 87%), and total impulse has been higher than 47 kNs with 5 s of motor functioning time (requirement: 50 kNs). This different result from the required value is due to lower discharged oxidizer mass with respect the foreseen calculations (19 kg instead of 20 kg, during the maximum total impulse tests). To reach the performance requirement, a higher oxidizer mass flow rate is necessary, and this can be achieved with some additional holes on the injection plate. This minimal modification can not have negative influence on the motor performance.

From the obtained performances, and the specific tests on single hole injectors (see section 4.2.1), the injection plate has been re-designed with lower L/D ratio holes, in order to give more stability to the combustion reaction.

Figure 3.44: Test FT10 during burning phase.

3.4 Instabilities Identification

The motor stability is one of the most studied problems in the development and testing of hybrid propulsion systems. The low frequency instabilities frequently observed in hybrids can be broadly categorized into two groups:

1. pressure oscillations inherent to the turbulent boundary layer combustion and other fluid dynamic behavior in the chamber,

2. feed system coupled instabilities.

During CISAS tests the latter are often present. Successful diagnostics is essential for formulating a working strategy to eliminate the combustion instabilities in combustion systems. Therefore it is imperative to be able to distinguish the feed coupled instabilities from the other kinds of chamber pressure oscillations. In general, the following characteristics of the feed coupled instabilities can be used in the identification process:

- Pressure oscillations are typically quite regular, spectra show narrow peaks, and the higher modes (at multiples of the fundamental frequency) are typically also evident in the spectra.

- The following two coupling mechanism are essential in driving the feed system instabilities:

  - Oxidizer flow rate that depends on the chamber pressure.
  - Combustion delay (vaporization delay) is needed for positive feedback.

- Note that even systems with flow isolation elements are vulnerable to this kind of coupling through the finite compressibility of the fluid in the feed lines (particularly if vapor bubbles are present).

More details on feed couple instabilities can be found in [17].

In a hybrid motor, the liquid (or gaseous) oxidizer needs to be fed into the combustion chamber through the feed system. In reality, the feed system response time is finite due to the inherent dynamics of the components in the system. Accurate response depends on the details of the systems, which is likely to be significantly different for every motor design. During this project the design of the motor changed several times (as it will be discussed later, in chapter 5). Isolating elements decoupling the motor from the feed system (for example: cavitating venturi, sonic orifice, etc.) are widely used, but unfortunately such solutions are difficult to apply with saturated nitrous oxide: isolating elements tends to produce too much bubbles and pressure drop in the feed lines. The pressure drop through the injectors is limited by the required chamber pressure and the saturation pressure of the nitrous oxide. With such pressure drop, choking of the injectors does not occur, and therefore all the tests ran in blowdown mode without isolation elements.

As described during the injection characterization, complete vaporization of the oxidizer droplets in the combustion chamber requires a certain characteristic time depending on parameters, such as the droplet size and the thermal/flow environment of the zone, in which droplets vaporization takes place. Note that this subsystem, too, depends on the design parameters of the motor, such as injector design, oxidizer initial conditions and pre-combustion chamber heating mechanism (ignition). The existence of a coupling between the feed system and the motor is necessary but not sufficient for the feed system coupled instability. A reasonably long vaporization delay for the oxidizer is also needed to produce pressure oscillations.

Another important phenomenon that can occur is the spontaneous shifting in motor operation. Dynamic behavior in a hybrid rocket motor is established by a number of complicated nonlinear physical and chemical processes, which could potentially lead to multiple equilibrium points for the motor operation. Depending on the stability of the equilibrium points, switching from one mode to the other, during the motor functioning, is a highly possible outcome. Spontaneous shifting

of the operational point during the motor burning is commonly observed in hybrid rockets using liquid oxidizers. The shifting behavior is typically random and results in low efficiency operation and undesirable thrust time performance. Thus they shall be eliminated.

It is important to note that the shifting of equilibrium points which is the subject of this section is quite different from the classical "DC-Shift" observed in solid and hybrid rockets. It is well established that the "DC-Shift" is an upward movement in the mean chamber pressure caused by large amplitude combustion oscillations. The overall performance of a hybrid rocket system is established by a set of highly complicated and coupled physical and chemical processes, some of which can be listed as:

- two phase flow in the feed lines and the injector,
- atomization vaporization of the oxidizer,
- thermal transients in the solid fuel,
- fluid dynamics and combustion processes in the chamber.

As a direct result of the coupling between these highly nonlinear phenomena, small configurational or operational variations could lead to drastic changes in the motor operation. Specifically, it has been shown in literature that an inverse dependency between the motor efficiency and the injector pressure drop could lead to multi-modal operation. Such a reverse correlation is physically plausible, since for a system that is already operating at a large injector pressure drop, any additional drop would lead to an increase in the jet break up distance. Under certain conditions hydraulic flipping of the injector orifice is also possible.

This phenomenon is discontinuous in nature. The physical basis for such a discontinuous behavior can be justified by the flipping and unflipping transition of the injector orifice. It is well known that for short nozzles with sharp corners, the cavitation bubble covers the entire length of the nozzle and the liquid never contacts the orifice walls. This phenomenon, which is referred to as the "Hydraulic Flip", changes the injector performance significantly, both in terms of the mass flow rate through the injector and the atomization characteristics of the jet generated by the flipped injector. Specifically, the efficiency of a motor operating with a flipped injector is expected to be low due to the significantly increased break up distance for such a jet, that lacks the disturbances created by the shear flow over the orifice wall.

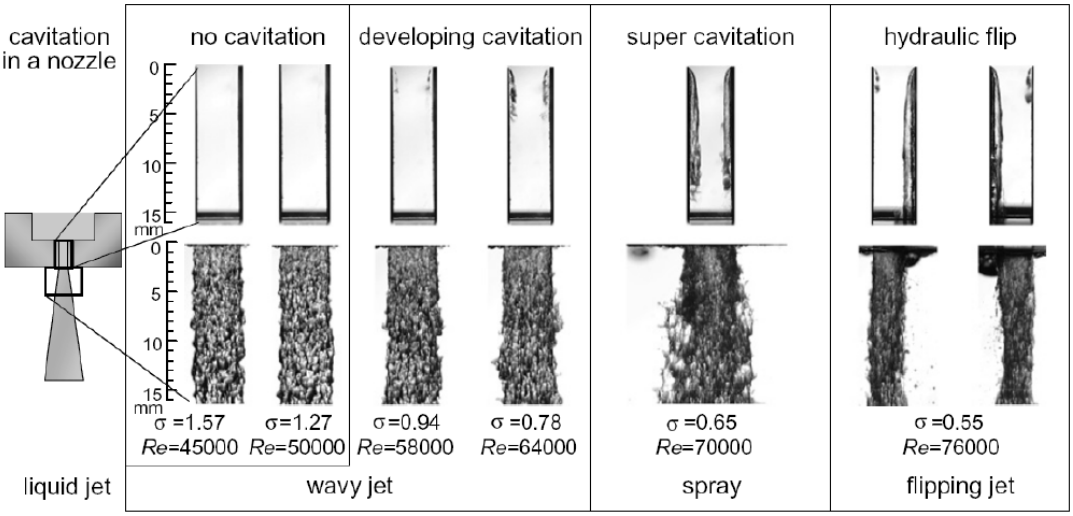

Figure 3.45: Injection behavior in cavitating injector: σ is a pressure ratio which takes into account the saturation condition of the fluid, when $\sigma < 1$ cavitation occurs.

3.4.1 Full Scale Tests - 1st phase

The instability analysis has been conducted only for full scale motors, while small scale tests have been useful to establish the final configuration of the subsystems.

During the first part of the 1st full scale experimental campaign the typical encountered behavior is illustrated in Figure 3.46.

The most significant aspect to be considered is the presence of a switch between two equilibrium points. The first point corresponds to a higher average pressure and strong oscillations while the second point has a smooth behavior around a lower pressure.

The higher pressure condition is unstable due to the lower injector pressure drop.

It is clear from the pressure time signal that these shifting events are spontaneous, rapid and random. The shifts in pressure levels (and so, in the thrust) are substantial and sustained for long durations, for most cases for a large fraction of the total burn period. In order to examine the possible reasons for these shifting events, one has to consider the parameters that could influence the chamber pressure, which can be listed as:

1. Oxidizer flow rate: for most events the oxidizer flow rate did not change significantly (enough to result in such a drastic change in chamber pressure). Even if the oxidizer flow rate changes, it is believed that the change is induced by the injector pressure drop variations for motors that run with no choking

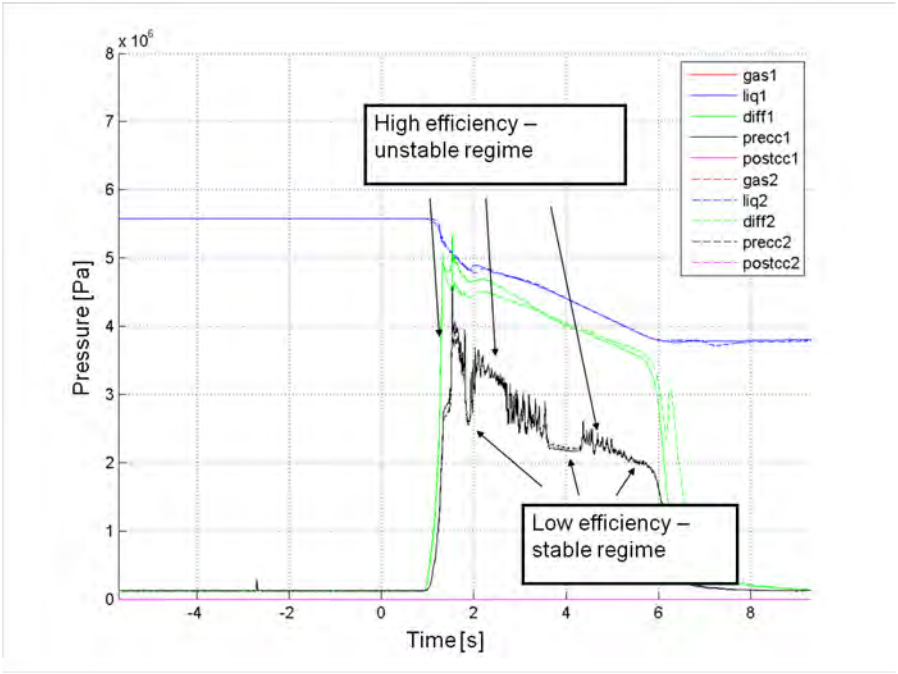

Figure 3.46: Pressure data for FT11: two different efficiency regimes can be noted.

elements in their feed lines.

2. Nozzle throat area: for most tests, the change in the nozzle erosion was low. Moreover the events were too long to be explained by a temporary blockage of the nozzle.

3. Regression rate: small variations in the regression rate cannot explain the substantial changes in the chamber pressure.

4. Motor c^* efficiency.

Based on the observations made on the measured quantities and the overall intensity of these events, it is suspected that a sudden change in the c^* efficiency was responsible for the sudden shift events. The difference between the two different efficiency states has been calculated to be up to 22%. The reason for this is believed to be a sudden shift between an unflipped and flipped condition. It is expected that the low pressure (low c^*) phase corresponds to the flipped case.

The length of the injector plate holes was 12 for the first group of tests, while after FT15 the L/D of the injector plate was changed. For all the successive tests (included 2nd and 3rd campaigns, see chapter 5), the injectors hole length was set to 3.8. This choice was done because this was the L/D of the small scale motor: the small scale motor tests, in fact, were resulted to be substantially stable.

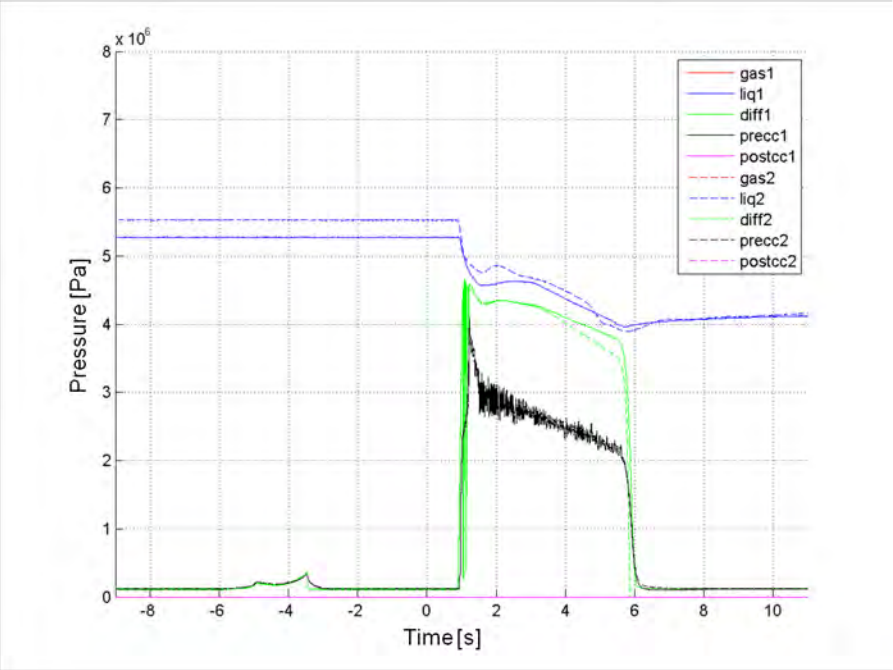

Figure 3.47: Pressure data for FFT16: L/D ratio reduction for the injection plate holes has brought to more stable combustion.

After the change in the injector L/D, the bimodal behavior disappeared: in all the successive test (included again 2nd and 3rd campaigns) some degree of instability is always present, but the average value of the pressure does not shift discontinuously anymore. Only the amplitude of the oscillations can change in time, but not their average value.

To conclude, during the 1st experimental campaign on full scale motor, the following behaviors have been analyzed:

- Pressure oscillations as in Figure 3.46, due to high L/D rate of the injection plate. The oxidizer flux characteristics determined two different combustion regimes: high and low efficiency. This theory is confirmed by the non-oscillating decreasing pressure of the fluid upstream the injection plate, which can be referred to a non-oscillating mass flow rate. Thus, pressure oscillations have been caused only by efficiency variations of the combustion reaction, and this was attributed to flip/unflip motor behavior.

- Stable combustion from FT16, after reducing the L/D ratio of the injection plate (even with convergent nylon pre-cc).

- Unstable combustion in FT13, with an aluminum pre-cc. Reasons have not been explained yet.

- Initial instabilities during tests with mixer in post-cc (higher efficiency tests): they have been noticed only in the first transitory phases of the motor functioning; they can be due to a not completely developed oxidizer mass flow rate, during the first moments after the main valve opening.

Chapter 4

Instabilities Due to Feed System: Injection Characterization

During the performance test verification it has been noted as the main instabilities have raised from the adopted oxidizer injection technique. This is the reason why its behavior have been necessarily studied, developing a specific test facility to validate numerical and fluid dynamics codes. The concept of the study is to test single holes of the injection plates used during complete experimental tests, and check the behavior of N_2O both in the combustion chamber and the tank, in many different discharge conditions. Measurements during experimental activities have been pressures and mass flow rate, for which a dedicated measurement technique has been developed and adopted.

4.1 Test Bench Design

The reproduction of the oxidizer injection for the hybrid motor has needed the same subsystems of the real rocket motor: *a*) a tank to stock the liquid at a controlled pressure/temperature, which would allow weighting even during the discharge phase and eventually the visual monitoring of its behavior; *b*) a chamber in which to discharge the flux, with the possibility of different pressurization levels and monitoring of the morphologic properties of the spray in different conditions; *c*) a hydraulic circuit to connect the two devices. The test bench is also able to mount different injector types.

The discharge chamber has been designed with the purpose of monitoring the spray structure during different condition injections, i.e. with different pressure levels or different mounted injectors. The internal pressure simulates the combus-

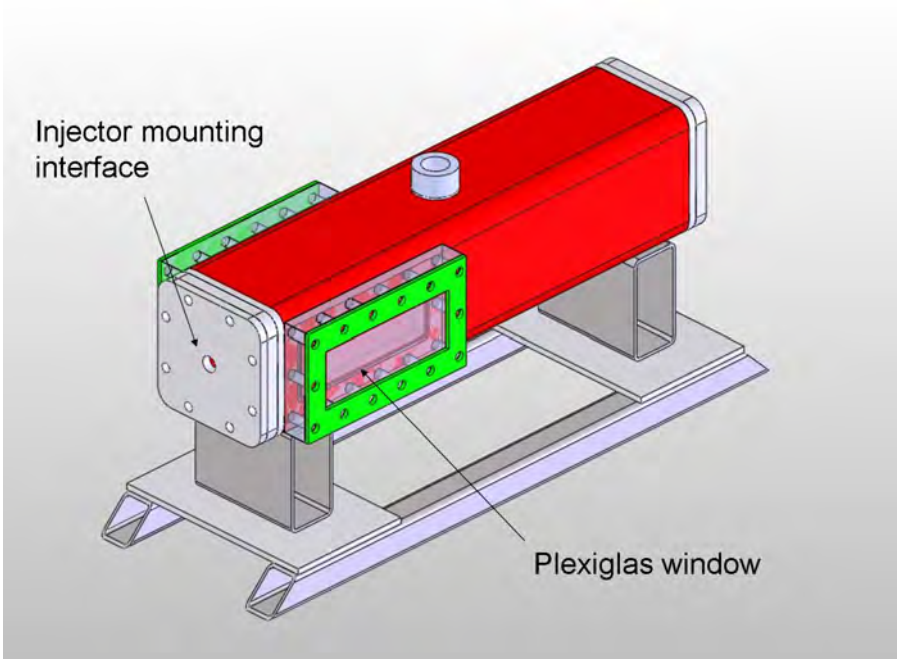

Figure 4.1: Schematic of the discharge chamber.

tion chamber pressure during the functioning of the motor, and it influences the injection cone that develops from the hole, the dispersion of the liquid, so finally the vaporization capacity of the injector. The thermal effect of combustion and the fuel mass flow rate are not simulated, since the test are "cold" by definition. To do this, the conformation of the spray had to be visible, and this has been achieved providing the chamber with two opposite Plexiglas windows. This versitile solution allows for many experimental investigation techniques, both visual and in contact, such as: high-speed cameras, Shadowgraphy, Schlieren Technique, PIV (Particle Image Velocimetry), LDA (Laser Doppler Anemometer), LIF (Laser Induced Fluorescence), pressure mapping with tactile pressure and force measurement systems. For the sake of brevity, please find the description of these techniques in literature. During experimental campaigns in the present work, only visual investigation with high-speed cameras and first attempts of Shadowgraphy have been performed.

The discharge chamber has been designed for a maximum operative pressure of 8 MPa (80 bar), with a safety factor of 4. Plexiglas has been chosen for the windows, thanks to its mechanical and optical properties. Figure 4.1 reports the 3D schematic of the chamber and the mounting solution on its dedicated bench.

In case of high mass flow rate, the chamber is not able to support the entire inflow, thus changing its internal pressure. To avoid this phenomenon, a 24 liters reservoir has been installed downstream the chamber, enlarging in this way the

entire available volume. This solution and the connection between the two volumes have been numerically simulated and accurately analyzed, in order to grant the effectiveness of the the solution: the intent of the designing process was to avoid the chocking phenomenon in the connecting pipe, so its dimension have been specifically studied by means of a time-varying analysis based on the *Darcy-Weisbach* theory for non-compressible fluids. Thanks to this configuration, the discharge chamber (with compensation reservoir) is able to tolerate mass flow rates higher than 100 kg/s.

4.1.1 Mass flow rate instrument design

The oxidizer mass flow rate value is of fundamental importance in a hybrid rocket performance evaluation, but sometimes it reserves some issues in order to have a measurement with an acceptable level of accuracy. Two different approaches can be used in the mass flow rate measurement: *1*) simultaneously measuring of volumetric mass (density) and volumetric flow rate, *2*) direct measuring of the mass flow rate.

When dealing with auto pressurized N_2O, the working conditions are continuously affected by pressure and temperature: the fluid is in saturation condition, with a co-existence of liquid and vapor phase. The difficulty of managing a two-phase system lies in the impossibility of accurately predicting the evolution of the ratio between phases. Between the two phases exists a continuous transfer of mass and energy, and if at the beginning of the discharge the starting conditions are defined by saturation point, during the evolution of the phenomenon the transformation is not ideal anymore, especially with fast outflow. Table 4.1 reports the characteristics of N_2O in terms of vapor tension and density as functions of temperature: please note the wide variability of vapor tension, even with small temperature steps. Furthermore, an additional inconvenient concerns the behavior of nitrous oxide: from the compressibility factors, the liquid phase can not be considered to be incompressible, and the vapor phase may not be assumed as an ideal gas. Please refer to Table 4.2 for the data in case of different propellants.

On the basis of the described physical properties, the first approach is not suitable in case of auto pressurized N_2O: its flow is in biphasic condition, with a variable and not predictable *a priori* vapor fraction, so density and volumetric flow rate can not be considered to be constant in the measuring section. In case of direct measurement instruments (second approach), there are various commercial mass flow rate measurement devices, as for example:

Temperature (° C)	**Vapor Tension (MPa)**	**Liquid Density (kg/m^3)**	**Vapor Density (kg/m^3)**
-20	1.801	995.4	46.82
-15	2.083	975.2	54.47
-10	2.397	953.9	63.21
-5	2.744	931.4	73.26
0	3.127	907.4	84.86
5	3.547	881.6	98.41
10	4.007	853.5	114.5
15	4.510	822.2	133.9
20	5.060	786.6	158.1
25	5.660	743.9	190.0
30	6.315	688.0	236.7
35	7.033	589.4	330.4
36 ($T_{critical}$)	7.251	452.0	452.0

Table 4.1: Thermodynamical properties of nitrous oxide in saturation condition.

Fluid	$\mathbf{Z}^L$	$\mathbf{Z}^V$
Water	0.000023	0.997
Decane	0.000014	0.994
LOX (90K)	0.004	0.97
LH2 (20K)	0.017	0.90
Propane	0.034	0.82
N_2O	0.13	0.53

Table 4.2: Compressibility factor of different propellants (liquid Z^L, vapor Z^V).

- momentum change measurement instruments;
- Coriolis effect measurers;
- thermal measurers.

The last category is used only with gas mass flow rate, so it is not adapt with the application of the present work. For the other types of sensors, the main reasons for which they could not have been used are highlighted below; for their functioning concept, please refer to [4].

Momentum change measurer The working principle of this sensors is based on the transfer of angular momentum between the operative fluid and the inner parts of the instrument. With the hypothesis of incompressible fluid and

low viscosity variations, a precise analytical formulation can give directly the measurement of the flowing mass flow rate. But it is precisely the basic hypothesis, which makes these sensors not suitable for an application with auto pressurized nitrous oxide: within the hydraulic circuit the N_2O vapor fraction can change without any possible prediction, thus refuting the incompressibility and low viscosity variation hypotheses. For these reasons, these types of measurement devices can not be used.

Coriolis effect measurer These sensors usually are able to directly measure the mass flow rate with high accuracy, without density, volumetric flow rate or pressure measurements. Furthermore, they don't suffer from viscosity, pressure or temperature variations. In any case, they are not even suitable to be applied with liquid auto pressurized N_2O for some different reasons: their functioning concept supposes to deal with a uniform mass distribution within the instrument, and this hypothesis can not be acceptable, because it is very likely that liquid nitrous oxide would change its vapor fraction during the flow in the sensor, due to the auto pressurized condition, so the rate between liquid and vapor would not be the same in the entire length. Another wrong consideration in the mass flow rate evaluation made by these sensors is that the velocity V is considered to be constant in the cross section of the instrument pipe. Again, due to biphasic condition of auto pressurized nitrous oxide, liquid and vapor phases would not be necessarily in equilibrium, and so the velocity distribution would not be homogeneous. With reference to [5], the mass flow rate measurement with a Coriolis sensor can cause significant errors in the mean mass flow rate evaluation, as high as 25% to 40% of the same value measured with a differential measure of the oxidizer tank, prior and after the discharge.

It is clear that commercial sensors are not suitable for the described measurement intents, and this has led to the development of a dedicated measurement process, which could finally give an accurate evaluation of the oxidizer behavior.

Scope of the instrument

The scope of the measurement instrument, which is described in the present work, is to permit the evaluation of the mass flow rate of auto pressurized nitrous oxide, during the discharge phase, in order to check eventual oscillations in the flow rate trend.

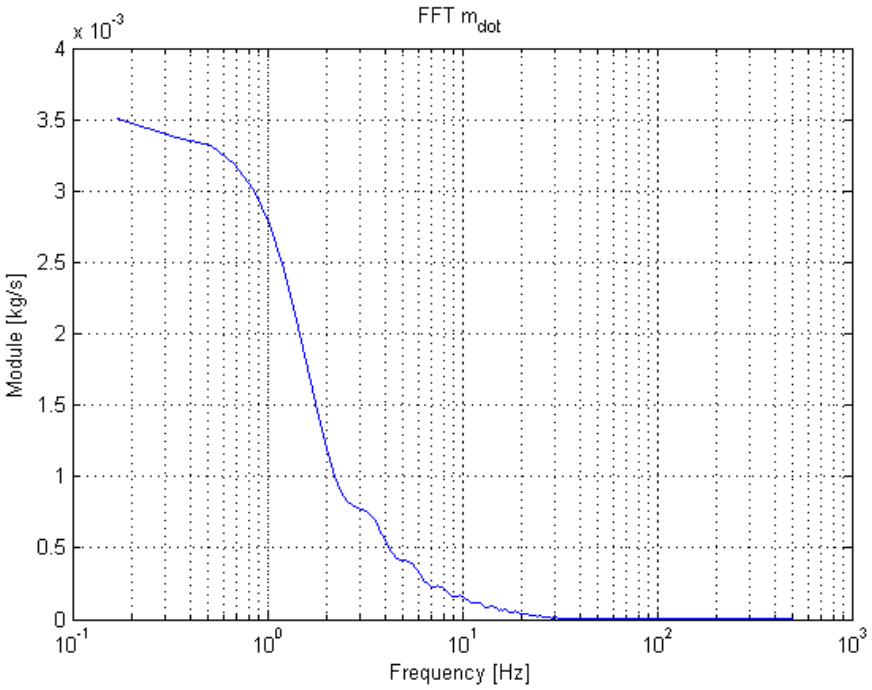

Figure 4.2: Frequency content expected for the mass flow rate measurement instrument.

To determine the performance required to the instrument, data from numerical calculation have been considered, and this data were based on experimental tests results. Using the numerical code described in [6], it has been possible to calculate the real-time mass flow rate of auto pressurized nitrous oxide, from the pressure data of tank, hydraulic circuit and discharge chamber, collected during cold discharge tests similar to the ones the instrument would operate with. These data have been validated with experimental activities, so they have been used in the bandwidth definition for the instrument. Figure 4.2 summarizes the frequency content of the expected mass flow rate signal coming from the measurement device: the calculation has been performed with the code described in [6], adopting one of the most significant discharge tests as source for the data.

From the numerical calculations, and the conducted experimental tests on different types of injectors, the performance requirements for the mass flow rate instrument can be summarized as follows:

Dimension	**Value**
Bandwidth	> 25 Hz -3 dB
Full scale	100 g/s
Accuracy	10%

Measuring instrument design

From the considerations described in the previous sections, it appeared clear that a direct measurement in contact with N_2O in auto pressurized condition was not possible, principally because of its unpredictable vapor fraction value. The chosen concept has derived from the one already used for the mean value evaluation of the mass flow rate, and has implied the weighting of the oxidizer tank and the derivative calculation of the signal. It is evident how the weight signal should be as "smooth" as possible, not to determine overshoots in the derivative calculation.

Many different weighting schemes have been taken into account (load cells, suspension systems with strain gauges, balance support, etc.), but whatever the concept used, every solution suffers of some constraints due to the different weight of the net fluid charged in the tank and the empty weight of the vessel. So adopting traditional commercial steel tanks (as during hot firing experimental campaigns) and weighting the entire system would bring to low levels of resolution for the small expected discharged mass, since a high full scale measurement device is needed. On the other hand, the development of a balance system for weighting only the net charged mass showed some critical issues in its vibrational behavior, with some low natural frequencies, which would affect the measurement (especially after a derivative calculation).

The first, most simple solution was to adopt a pressure vessels, whose empty weight was comparable with the charged liquid mass, and to accurately design the weighting measurement chain to satisfy the required vibrational bandwidth. As container for the liquid nitrous oxide in auto pressurized condition, a small Aluminum alloy cylinder has been adopted: thanks to the reduced dimension and the light-weight material, the empty mass of the container was of approximately 2 kg, with an internal volume of 2 liters (i.e. approx. 1,6 kg of liquid nitrous oxide).

To weight the tank, it has been hanged to a traction load cell, thanks to the simplicity and effectiveness of this solution: in this way, after the calibration of the system, the only uncertainty source is the accuracy of the cell. Finally, the support has been accurately designed and analyzed with Finite Elements modal analyses, to keep the natural frequencies of the structure as high as possible. The output of the design process is summarized in the following Figures 4.3 and 4.4, and in Table 4.3, where the first vibrational modes of the structure are reported.

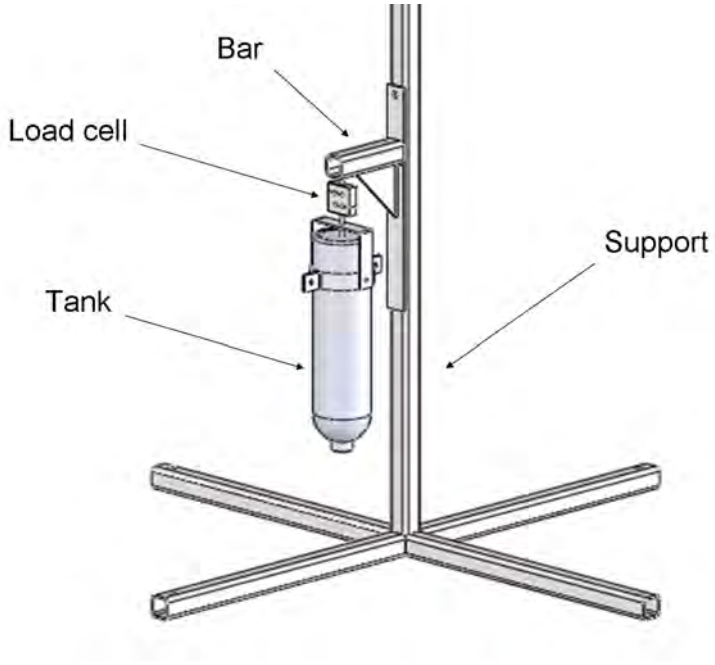

Figure 4.3: Schematic of the cylinder and the weighting solution.

#	**Frequency (Hz)**	**Mode**
1	54.128	Axial, mass-spring system
2	161.9	Flexural, support, x-y plane
3	165.8	Flexural, support, y-z plane
4	515	Torsional, support

Table 4.3: Frequency analysis results for the weighting system.

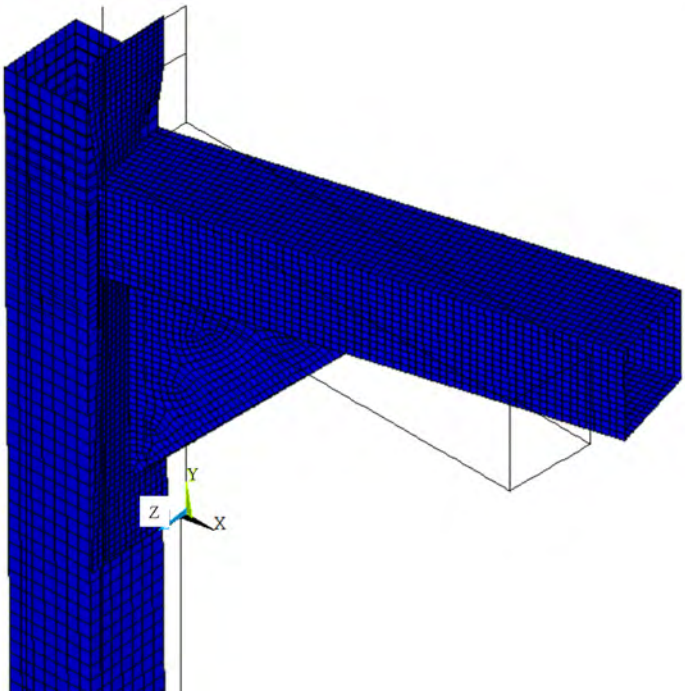

Figure 4.4: F.E.M. modal analysis of the cylinder support: displacement on y-z plane.

With the tank described in previous sections it has not been possible to visually monitor the behavior of the oxidizer during the discharge, and it could not be modified to permit it, since it was a commercial product. The solution has been to split the two main requirements and satisfy them with two different apparatus: the first one, already described, would be useful in the mass flow rate evaluation, the second would serve when the internal tank oxidizer behavior has to be monitored.

Taking into account the same solution adopted for the discharge chamber, a specific tank has been completely designed and produced. Two opposite Plexiglas windows have been mounted to permit the internal inspection of nitrous oxide, and all the system has been designed to a maximum operative pressure of 8 MPa (80 bar), with a safety factor of 4. Figure 4.5 illustrates the schematic of the second version of the oxidant tank, while Figure 4.6 reports the hydraulic circuit scheme of the injection test bench facility.

Measurement Procedure

Preliminary discharge tests have been performed with N_2O, in order to verify the performance of the system in the exact discharge conditions (in terms of the operative fluid, pressures and hydraulic circuit). In Figure 4.7 the raw data acquired during the first discharge test are reported.

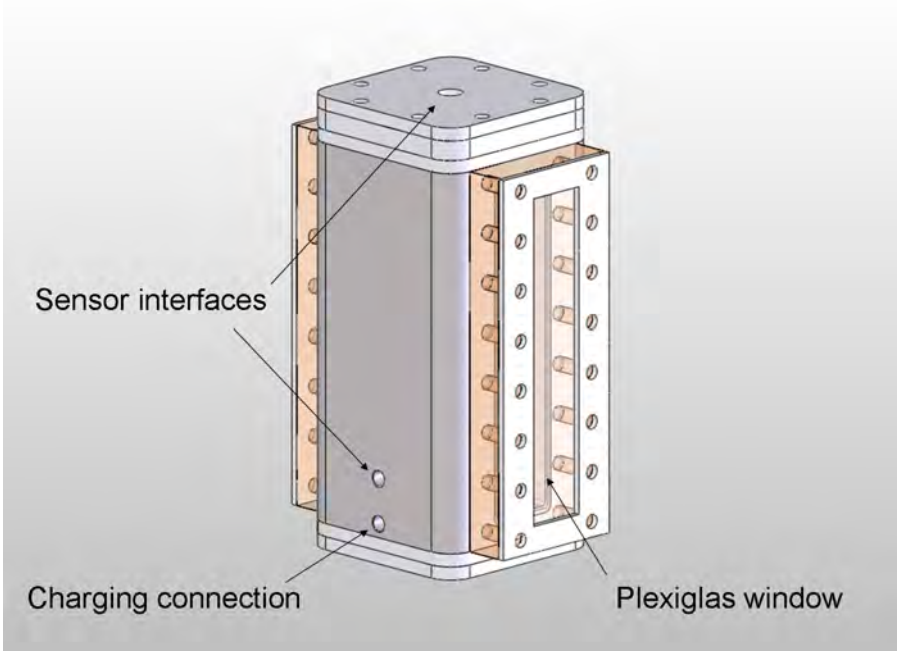

Figure 4.5: Schematic of the tank designed for the internal behavior monitoring during discharge tests.

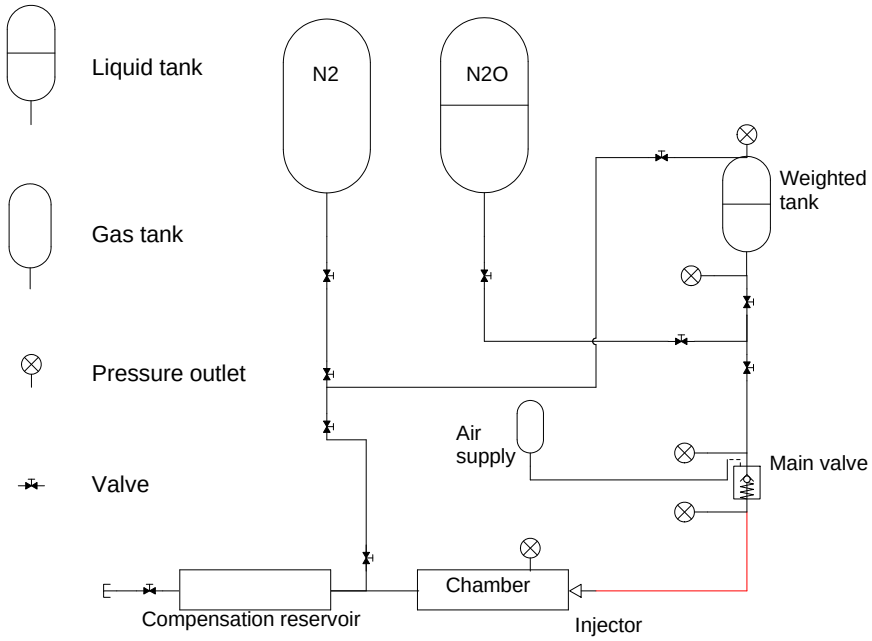

Figure 4.6: Hydraulic circuit scheme for injection test bench.

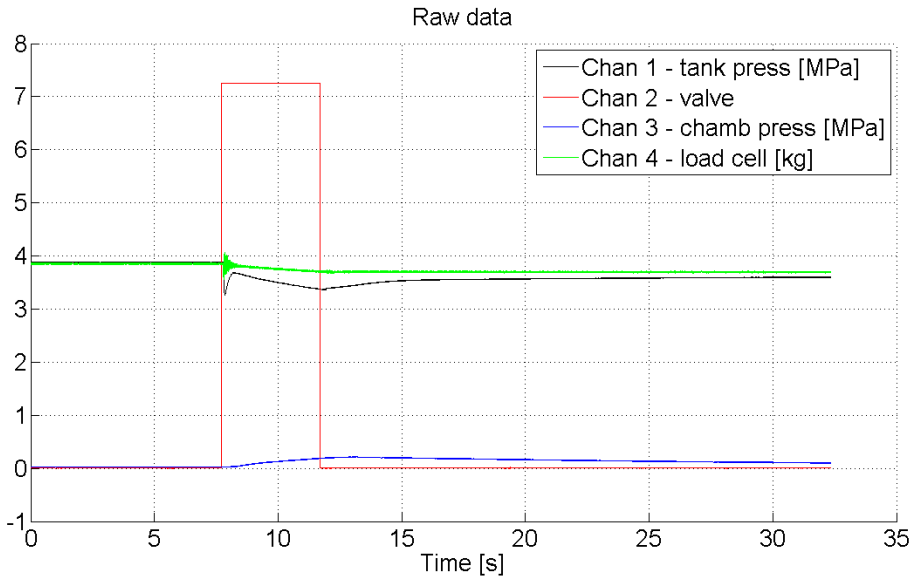

Figure 4.7: Raw data of discharge test # 1.

From the graphic, the following considerations can be done:

- Initial sudden pressure drop in tank pressure: it occurs when the valve is opened, and it is due to the filling of the hydraulic volume between the valve and the injector hole. This phenomenon could not be avoided with the described hardware, and it shall not be taken into account in the final mass flow rate value determination.

- Low pressure increasing in the discharge chamber (approx. 0.02 MPa, which corresponds to 5% difference in the Δp with respect to the tank). The performed evaluation have demonstrated that this behavior does not interfere with the mass flow rate measure, and that the discharge chamber design is correct.

- Initial transitory oscillations in the load cell signal, which are caused by mechanical stress of the opening valve (they physically can not be mass oscillations).

The measurement procedure of the designed instrument starts from load cell data, which are consequently analyzed and numerically processed to obtain the final mass flow rate value. The process steps are described in the following paragraphs:

1- Filtering The load cell raw data are filtered, in order to remove the frequency components higher than 25 Hz (in accordance with the performance requirements, see par. 4.1.1); this operation is necessary also for the following fitting

curve evaluation, in order to keep low interpolation errors. Figure 4.8 reports the signal acquired from the load cell, prior and after filtering operations.

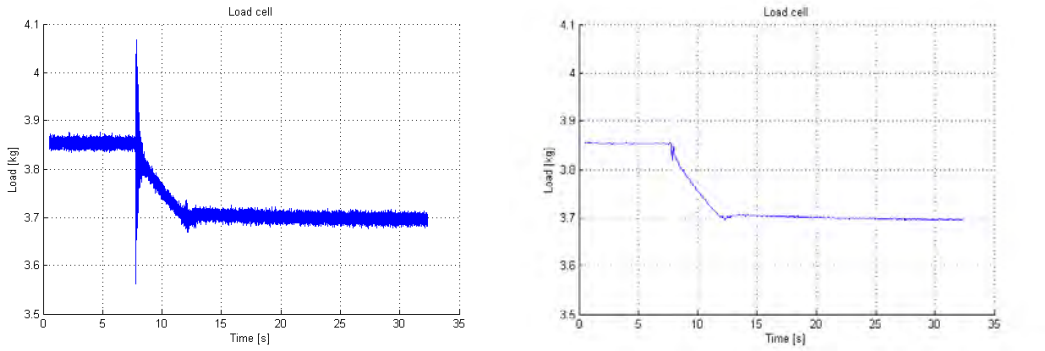

(a) Original data. (b) Filtered data (>25 Hz).

Figure 4.8: Load cell signal of test # 1.

2- Interpolation A numerical derivative operation of the signal (even if filtered) would give spikes and discontinuous results, due to residual discrepancies in the signal trend. For this reason, the filtered data have been analyzed to obtain a fitting polynomial curve, using an interpolation method. To evaluate the uncertainty of this mathematical operation, the root mean square errors between the fitting curve and the original data have been calculated: the curve with minimum fitting error has been chosen, and the resulting best case has been a 4-order polynomial curve. To verify the quality of this calculation, Figure 4.9 reports a comparison between the original filtered data and the fitting curve, while Figure 4.10 compares the frequency content of the original raw data with respect the polynomial curve. Resulting uncertainty bounds of the obtained fitting curves are from 1% to 2%.

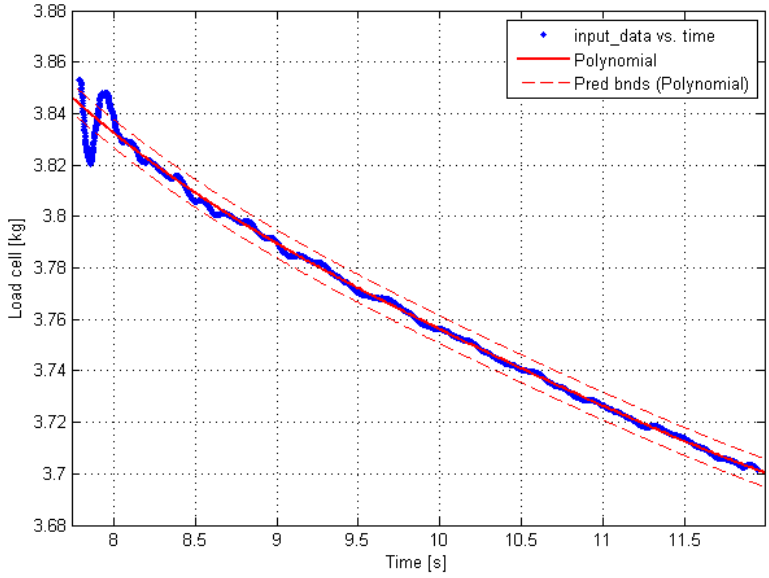

Figure 4.9: Filtered load cell data and reconstructed fitting curve for of test # 1 (reduced to only discharge phase), uncertainty bounds of polynomial are ± 1.5%.

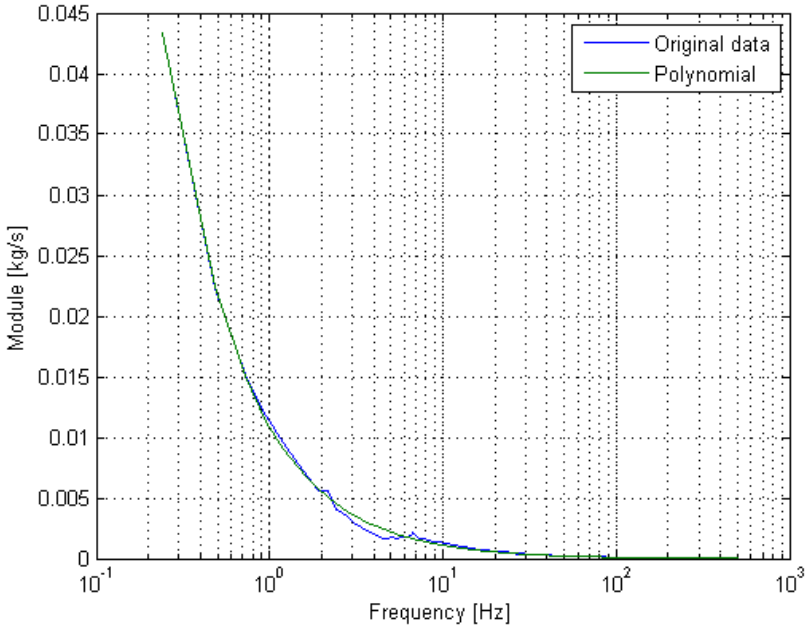

Figure 4.10: FFT of original data and polynomial fitting curve.

3- Derivative Calculation The numerical derivative of the fitting curve has permitted to calculate the mass flow rate of discharge tests: results are shown in the following Figures 4.11, 4.12 and 4.13. For the uncertainty bounds calculation, the propagation of uncertainty method has been used, and it has

been applied to the conducted derivative operations. The results for the first three discharge tests are visible in the reported figures; in general, they have always satisfied the accuracy instrument requirements.

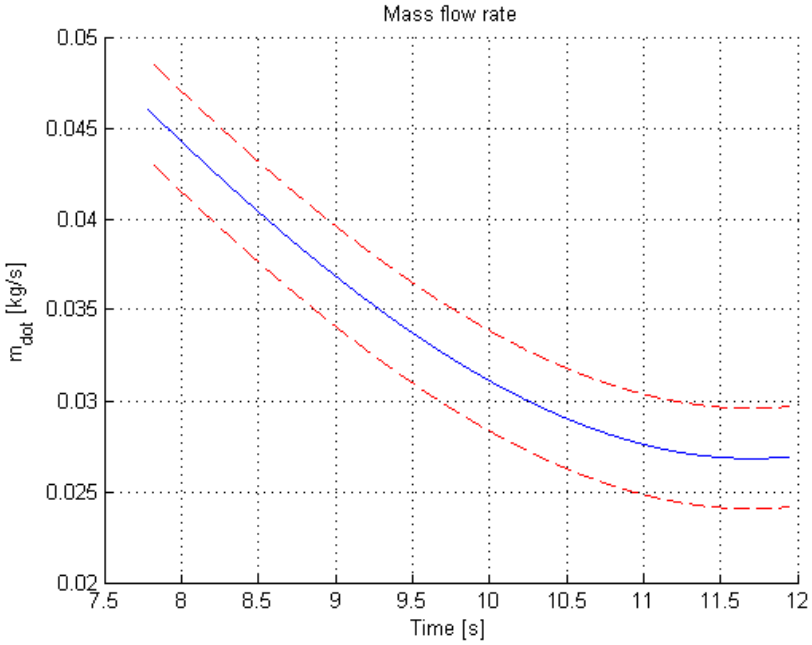

Figure 4.11: Mass flow rate calculated with data of test # 1, uncertainty boundaries: ±9.21%.

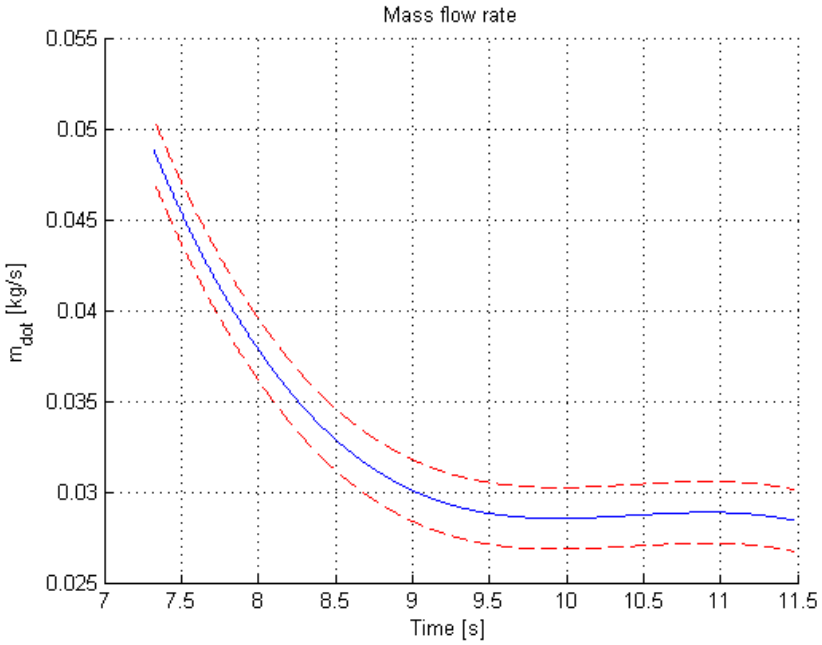

Figure 4.12: Mass flow rate calculated with data of test # 2, uncertainty boundaries: ±5.66%.

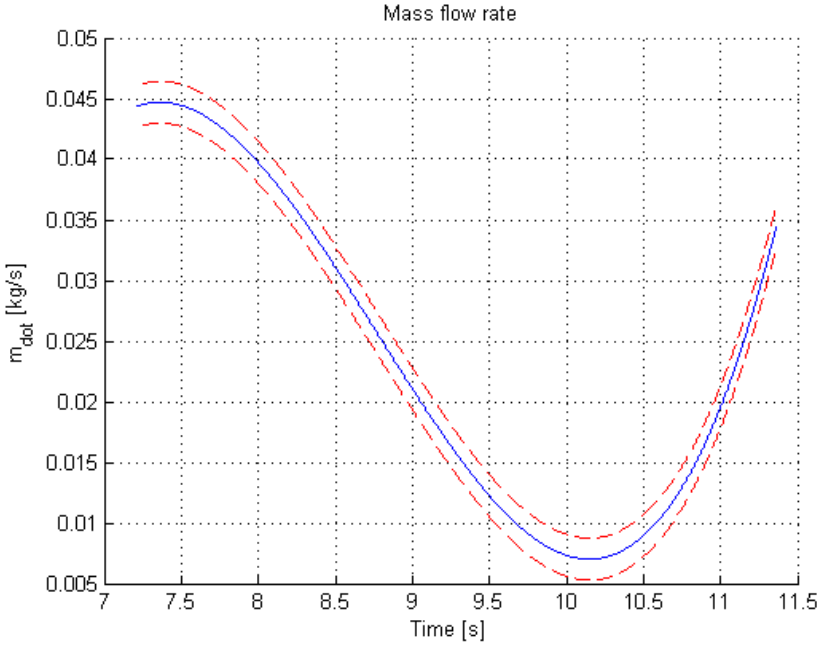

Figure 4.13: Mass flow rate calculated with data of test # 3, uncertainty boundaries: ±5.77%.

Instrument Calibration

The performance of the produced measurement instrument have been verified through two different calibration procedures: static and dynamic.

The static calibration has foreseen the application of calibrated weights to the structure, and the acquisition of the instrument outputs. The process results have highlighted the performance of the balance system, that reflects the same uncertainty compatible values of the used load cell: the demonstrated system uncertainty bounds resulted in ± 0.05% of the output value. The characteristics of the mounted load cell are summarized in the Table 4.4.

Parameter	**Value**
Full scale	150 N
Combined error	0.02%
Temperature effect on span	0.0013%
Compensated temperature range	-10 / +40 °C
Sensitivity	2 mV/V ±10%
Deflection at nominal load	0.2 mm

Table 4.4: Performance parameters of the load cell used in the measurement instrument.

The dynamic calibration of the instrument has been performed through discharge tests in the operative configuration. After the acquisition of the data, and the numerical processing described in section 4.1.1, calibration has been conducted using the numerical integration of the evaluated mass flow rate data, and the comparison of the resulting values with the discharged mass calculated with differential weighting of the tank, prior and after the discharge. The results of the comparison are summarized in the Table 4.5:

Test #	**Integration [kg]**	**Weight [kg]**
1	0.139 ± 2.33%	0.154 ± 8.67%
2	0.134 ± 2.29%	0.143 ± 8.89%
3	0.098 ± 2.59%	0.098 ± 12.49%

Table 4.5: Discharge mass values: comparison between integration of mass flow rate and weighted value.

The propagation of uncertainty has been used to calculate the bounds both in case of the integrative calculation and for the weighted data: relatively high values of these ones come from the small quantity of liquid, that is discharged during the tests (0.25% of relative uncertainty on the values used during the differential weight calculation).

The experiments have been performed without re-filling the tank, i.e. with a unique discharge in three separate steps. This is the reason of the different mass flow rate and discharged mass values among the three tests: the different level of the liquid nitrous oxide in the tank have determined a different behavior during the auto-pressurization phenomenon, because it strictly depends on the vapor volumetric fraction within the tank.

From the comparison table (4.5), it is possible to verify that the measurement methods are compatible to each other, and the developed instrument has satisfied the performance requirements.

4.2 Injection Tests

In this section the geometry of the injector is analyzed to underline its importance in the evolution of the oxidizer within the feed system, in particular in the injector canal, till the outlet in the discharge chamber.

During the flow from the tank to the injector, the fluid is subjected to a decompression, which, in association with the formation of a *vena contracta*, determines the vapor formation inside the pipe. The process is mainly characterized by two conflicting factors: the overheating of saturated liquid (and a higher bubble nucleation) on one side, and a faster outflow (with shorter residence time) on the other side. With its depressurization, the liquid progressively gets under its vaporization pressure and vaporizes: the complicate thermodynamical process, which interests the liquid during this evolution, depends on the rate between the characteristic nucleation time (τ_n) and the residence time (τ_p). These two times can be correlated with the following expressions, where *in* and *out* refer respectively to the upstream and downstream conditions with respect to the injector, and p_v is the vaporization pressure:

$$\tau_n = \sqrt{\frac{2}{3}\frac{\rho_{in}}{p_v - p_{out}}} \tag{4.1}$$

$$\tau_p = \frac{L}{v} = L\frac{\rho_{in}}{\sqrt{2\Delta p}} \tag{4.2}$$

From the rate of these two variables, the *non-equilibrium parameter* can be defined, and it indicates the percentage of verified vaporization:

$$k = \frac{\tau_n}{\tau_p} = \sqrt{\frac{p_{in} - p_{out}}{p_v - p_{out}}} \tag{4.3}$$

When the nucleation time is longer than the residence time, the vaporization has not enough time to occur, so the fluid density can be considered approximately

constant between the upstream and downstream sections, and the mass flow rate can be calculated[1] with:

$$\dot{m}_{ox} = C_d A \sqrt{2\rho\Delta p} \tag{4.4}$$

Instead, when the residence time is longer with respect the nucleation time, vaporization starts and mass flow rate can be calculated with more difficult mathematical relations, which for brevity are not described here and can be found in [12]. From eq. 4.1 it is notable that the time used by bubbles to nucleate decreases with the increasing differential pressure between upstream and downstream; the residence time, instead, is proportional to the injector canal length, and inverse to fluid flow velocity (eq. 4.2), so to the differential pressure. So Δp has a double opposite influence on these two parameters.

4.2.1 Single hole injectors

In the first test phase two types of single hole injectors have been tested, to verify the performance of a single hole of the injection plate used during hot firing tests. The difference between the injectors is the length of the hole, which is $L = 12$mm and $L = 3.8$mm respectively. Both have been tested in many different pressure ranges: from the above considerations, the expected behavior is of lower discharged mass in case of $L = 12$mm injector, due to higher nucleation rate, thus to higher vapor production.

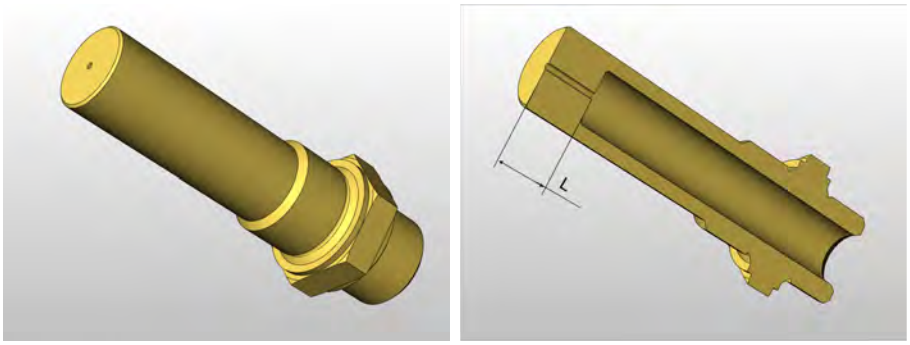

(a) External schematic. (b) Section.

Figure 4.14: Schematic of a single hole injector for the injection test facility.

The discharge tests have been performed using the same diagnostics as during the calibration of the mass flow rate instrument, with an additional pressure sensor

[1]Simplified version of the mass flow rate calculation, which is obtainable from the Bernoulli formula, considering the upstream velocity close to zero.

(same model and performance of the ones already mounted in the oxidizer tank and discharge chamber circuit sections) mounted downstream with respect the main valve, to check eventual pressure loss in the hydraulic circuit. The pressure sensors types are the same gauges, which have been already used during motor tests: for performance evaluation, please refer to 10 MPa pressure sensors of Table 3.1.

	L = 12mm						**L = 3.8mm**					
	$\mathbf{p_t^i}$ [MPa]	$\mathbf{p_{dc}^i}$ [MPa]	$\mathbf{\Delta p}$ [MPa]	$\mathbf{p_t^f}$ [MPa]	$\mathbf{p_{dc}^f}$ [MPa]	$\mathbf{\Delta m}$ [kg]	$\mathbf{p_t^i}$ [MPa]	$\mathbf{p_{dc}^i}$ [MPa]	$\mathbf{\Delta p}$ [MPa]	$\mathbf{p_t^f}$ [MPa]	$\mathbf{p_{dc}^f}$ [MPa]	$\mathbf{\Delta m}$ [kg]
$\mathbf{\Delta p = 4,00}$	4,14	0	4,14 $\pm 1,21\%$	3,97	0,26	0,179 $\pm 2,21\%$	4,13	0	4,13 $\pm 1,21\%$	3,94	0,20	0,202 $\pm 1,98\%$
$\mathbf{\Delta p = 3,00}$	4,19	1,10	3,09 $\pm 1,62\%$	3,95	1,26	0,186 $\pm 2,19\%$	4,24	1,28	2,96 $\pm 1,69\%$	4,03	1,47	0,186 $\pm 2,18\%$
$\mathbf{\Delta p = 2,00}$	4,19	1,93	2,26 $\pm 2,21\%$	4,02	2,06	0,176 $\pm 2,20\%$	4,04	1,94	2,10 $\pm 2,38\%$	3,87	2,06	0,186 $\pm 2,18\%$
$\mathbf{\Delta p = 1,00}$	3,89	2,90	0,99 $\pm 5,05\%$	3,77	3,00	0,168 $\pm 2,26\%$	3,93	3,02	0,91 $\pm 5,49\%$	3,79	3,13	0,170 $\pm 2,27\%$
$\mathbf{\Delta p = 0,5}$	3,97	3,49	0,49 $\pm 10,20\%$	3,76	3,52	0,125 $\pm 2,29\%$	3,94	3,45	0,49 $\pm 10,20\%$	3,83	3,50	0,129 $\pm 2,28\%$
	$\mathbf{p_t}$: *tank pressure (relative)*						$\mathbf{p_{dc}}$: *discharge chamber pressure (relative)*					
	i: *initial, pre-discharge condition*						**f**: *final, post-discharge condition*					
	$\mathbf{\Delta p = p_t - p_{dc}}$: *differential pressure*						$\mathbf{\Delta m}$: *discharged mass (polynomial method)*					

Table 4.6: Single hole injectors tests: results comparison.

Table 4.6 summarizes the data of the injection tests conducted in case of single hole injectors: the table reports only the mean values acquired for the verified configurations (Δp), which have been calculated from the data of a greater number of tests (at least three tests for each configuration). The obtained results have to take into account the behavior of auto-pressurized nitrous oxide, especially in case of small discharged mass: small differences in the pressure levels can cause different discharge performance. Furthermore, there are other unpredictable phenomena, which may occur during the tests:

Ambient and fluid temperature influence The first one can be considered constant during each test, while the fluid experiences an expansion transformation, with vaporization of the liquid phase and variation of the vapor fraction. As a consequence, the instantaneous physical properties (temperature, thus density) of the working fluid are not predictable *a priori*, then its behavior may vary during a discharge test, and this is more evident in case

of the present work, due to such small discharged masses. On the other hand, it has not been possible to have higher mass values, because the discharge chamber would not support them, and the spray behavior would have been influenced.

Pressure influence Pressures in the different hydraulic circuit sections govern the fluid discharge behavior. The acquired measures give only mean values, and this can be an issue, especially for the tank pressure, because of the biphasic condition of the stored fluid: liquid may be stratified in different layers, with small differences in the temperature values. Due to the low thermal conductibility of N_2O, the equilibrium condition would be reached only in a long time, and in any case it could not be verified with a commercial cylinder. This reflects in an unpredictable expansion behavior during discharge.

However, adopting repeatable and controlled conditions during the tests, a macroscopic investigation has been operated, and results reflect what expected.

On equal Δp the injector with hole length of $L = 3.8$mm performs a general higher discharged mass, from 5% to 10% with respect the longer one, and this is consistent with the discussed behavior. This is more evident with greater Δp, as the $L = 12$mm can perform a greater vaporization of the liquid and the overall density of the spray is lower. In general, measures result compatible in many tests, both with $L = 12$mm and $L = 3.8$mm injector, with more significant differences in case of greater Δp. This can be justify with the choked condition of the exit area of the injectors: the $L = 12$mm version reaches this condition "more easily" than the shorter one, thus with same differential pressures it is able to discharge a lower mass. However, it is clear that the reported results suffer from the small used quantities of N_2O, but the experimental facility did not permit higher values.

As the visual behavior investigation is concerned, tests have permitted an effective understanding of the effect of Δp on the spray morphology. The hole length does not affect the macroscopic shape of the flux, while the opening jet cone expands proportionally with the differential pressure. Figure 4.15 explains well this phenomenon, reporting two different tests conducted with the $L = 3.8$mm injector.

Some investigation with Shadowgraphy and high-speed cameras have been conducted to verify the applicability of the test facility. Preliminary results demonstrate that high speed rate monitoring is able to visually observe the small drops of nitrous oxide, thus giving more information on the spray dispersion after the injector exit area.

(a) $\Delta p = 4$ MPa. (b) $\Delta p = 0.5$ MPa.

Figure 4.15: Single hole $L = 3.8$mm injector spray comparison: a lower Δp determines a more narrow spray cone.

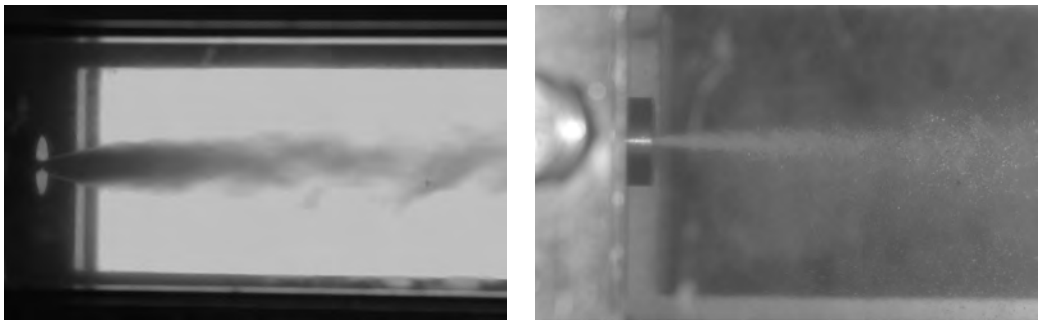

(a) Shadowgraphy. (b) High speed camera.

Figure 4.16: Shadowgraphy and high speed camera monitoring for single hole $L = 3.8$mm injector: density and droplets behavior can be monitored using these investigation techniques.

4.2.2 Swirl Injector

As described in previous sections of the present work, injection is one of the crucial parameters for the hybrid rocket performance determination. Among the various techniques for the performance increasing, swirl injectors are for sure one of the most promising. In [9] the stabilizing capability of this type of devices is studied, together with the higher performance, that they permit to develop. In this work the configuration of the injector is different from literature, but it should grant the same beneficial effects. Advantages interest the combustion properties, and in particular a swirled flux produces a stable combustion, thanks to the "vortex movement" of the oxidizer, which determines a more stable flame on the fuel surface. For this reason, the convective thermal exchange is increased, thus improving the final regression rate, and also this value is more uniform along the longitudinal direction of the combustion chamber: in this way, the oxidizer/fuel ratio is more constant along the grain surface.

The described promising characteristics have induced to start the development of these injectors, and the research work has started from their design and test. The tested injector configuration derives from the single hole version: it has the same body, but three tilted holes instead of one. The distribution of the holes should be on a circumference, which diameter is as close as possible to the fuel grain port diameter (in case of circular port): in this way, the flux of every hole is directly tangent to the grain surface, to take advantage of all the benefits of the swirled injection. The tilt of the holes has been set to 45°. The main characteristics of the tested swirl injector are as in the following table:

Tilt	45°
Holes #	3
Holes diameter	1 mm
Holes length	3.8 mm
Housing circumference	9 mm

As in case of singular hole injectors, the design has been done for a working pressure of 8 MPa, with a safety factor of 3, while the theoretical performance and fluid behavior have been predicted with fluid dynamics simulations (not described in the present work, see Figure 4.17 for an example of the results). To simulate the effect of the grain port, a Plexiglas pipe has been mounted at the outlet of the injector plate.

The diagnostics used during these tests is the same, that has been used dur-

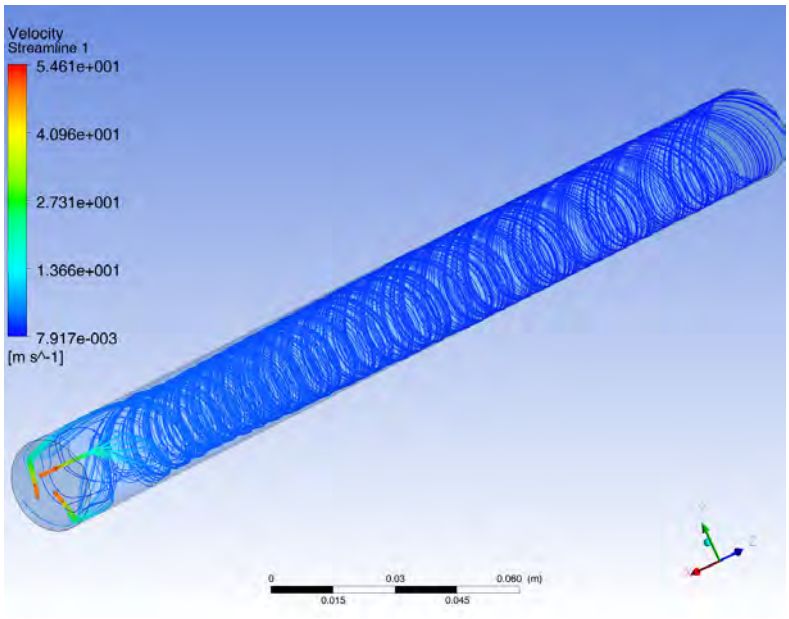

Figure 4.17: Fluid dynamics simulation of the 3 holes swirl injection performance.

ing single hole injector tests, and Table 4.7 reports the results of the conducted acquisitions.

From the reported data, tests can be divided into two main groups, on the basis of the total discharged mass: "high" Δp (2, 3 and 4 MPa), and "low" Δp (equal to 1 and 0.0 MPa). In the first group, the discharged masses are similar in all the different differential pressures, while a significant difference has happened with the lower pressure drops. This may refer to a choked condition of the injector plate with high Δp, which does not take place with the lower ones. It has to be noted, that the choked condition of an injector working with biphasic flow is not of simple investigation, due to the unpredictable physical characteristics of the flow: the density evolution throughout the hydraulic circuit and the injector hole may vary without repeatable behavior, due to the many influencing variables. Furthermore, the injector diameter is smaller than the single hole plate, thus cavitation can take place with lower pressure drop.

As the swirl behavior of the spray is concerned, the visual investigation through the windows of the discharge chamber demonstrates the effective vortex rotation in the generated flux. The Plexiglas pipe emphasizes this typical motion, and predicts which type of injection would take place in a port grain of the same dimension. On the other hand, the atomization of the fluid is more difficult to be analyzed, do to the reduced crossing section of the jet and to the transparent pipe itself, which seemed to badly influence the jet dispersion: liquid drops encounter the internal

	$\mathbf{P_t}$ [MPa]	$\mathbf{P_{dc}}$ [MPa]	$\mathbf{\Delta p}$ [MPa]	$\mathbf{P_t}$ [MPa]	$\mathbf{P_{dc}}$ [MPa]	$\mathbf{\Delta m}$ [kg]
	pre-test	pre-test	pre-test	post-test	post-test	(polynomial)
$\mathbf{\Delta p = 4}$ **MPa**	3,99	0,00	3,99	3,64	0,45	0,440 ± 2,12%
	3,99	0,00	3,99	3,61	0,44	0,436 ± 2,13%
	3,98	0,00	3,98	3,58	0,44	0,448 ± 2,09%
$\mathbf{\Delta p = 3}$ **MPa**	4,19	1,24	2,95	3,76	1,74	0,420 ± 2,18%
	3,92	0,95	2,97	3,54	1,45	0,404 ± 2,24%
	4,07	1,14	2,93	3,69	1,63	0,420 ± 2,18%
$\mathbf{\Delta p = 2}$ **MPa**	3,93	2,02	1,92	3,61	2,29	0,400 ± 2,26%
	3,98	2,08	1,90	3,64	2,34	0,404 ± 2,12%
	4,03	2,11	1,92	3,69	2,32	0,412 ± 2,21%
$\mathbf{\Delta p = 1}$ **MPa**	4,01	2,93	1,08	3,73	3,05	0,352 ± 2,45%
	3,94	3,05	0,90	3,66	3,15	0,324 ± 2,49%
	3,95	3,06	0,88	3,68	3,18	0,316 ± 2,57%
$\mathbf{\Delta p = 0,5}$ **MPa**	3,93	3,51	0,43	3,67	3,55	0,212 ± 2,89%
	3,98	3,52	0,46	3,74	3,58	0,216 ± 2,87%

Table 4.7: Experimental test results for 3 holes swirl injector.

wall of the pipe, and they mix together to each other, in a sort of recombination of the liquid phase. However, a macroscopic evaluation of the atomization rate has been possible from the opacity of the fluid in the pipe: the darker is the flux, the more liquid is present. Figure 4.18 illustrates a test in various phases of the discharge: the swirled movement is well notable, and also the differences in the density of the spray. Unfortunately, with the available diagnostics set-up, it has not been possible the quantification of the atomization rate capacity of the tested injector.

The atomization rate has been more evident with maximum pressure drop (4 MPa), while in other configurations the liquid phase has prevailed. This has permitted another interesting behavior of the jet: the pitch of the fluid thread

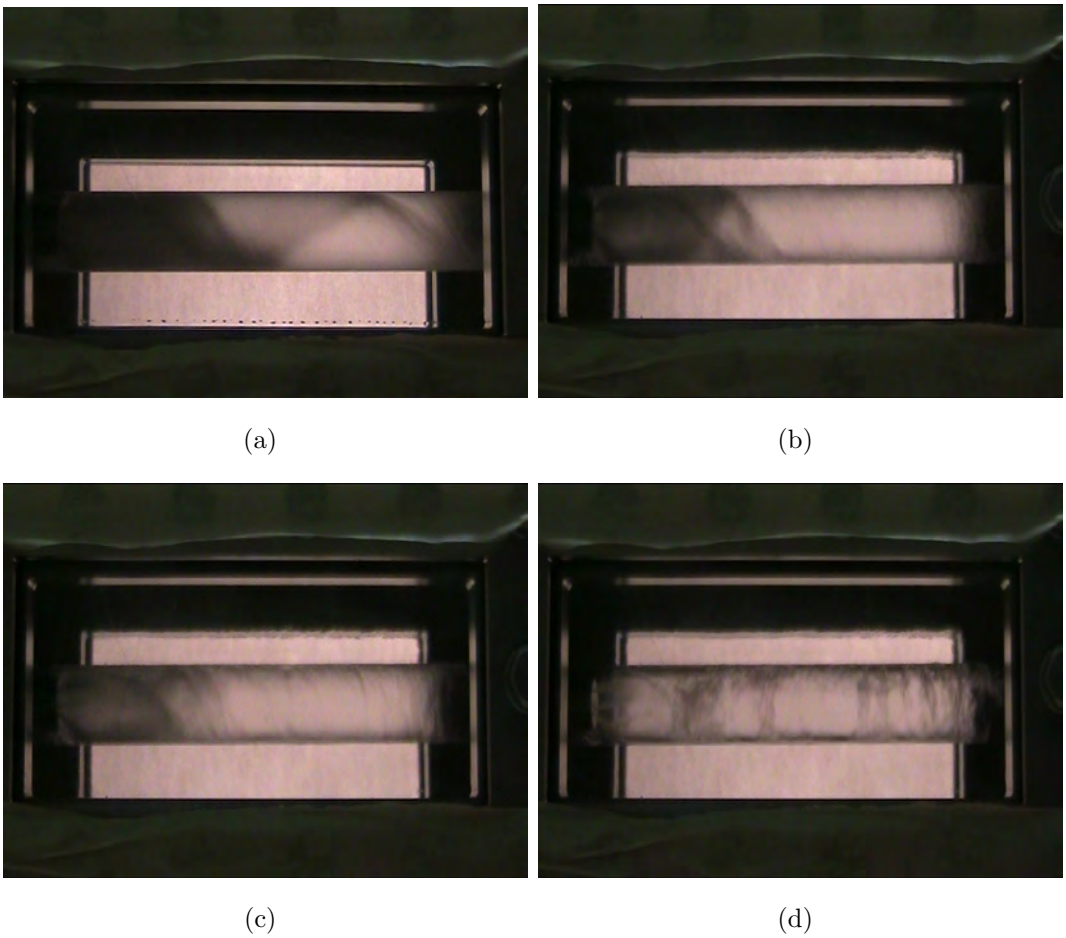

(a) (b)

(c) (d)

Figure 4.18: Swirl flux evolution for discharge test at Δp =1 MPa.

varies with the differential pressure, and in particular it is proportional to the Δp. Figure 4.19 compares two discharge tests at two different pressure drops: the main notable characteristics are the differences in the atomization effect and in the jet conformation. This is an important result, in order to adopt this injection technique during hot firing tests: higher Δp would give a better vaporization rate to the injected fluid, which would improve the mixing with the fluid, but a faster jet, which would reduce the time for the combustion reaction to take place. On the other hand, lower Δp would assure a slower jet, but with more liquid phase inside. An trade-off between the two solution would be necessary, together with a deep experimental investigation of the effect on complete motor performance development.

From the experimental results, the variation of the pitch of the fluid thread with respect to the discharge pressure value has been evaluated to be 6.3 mm/MPa (±

10%, uncertainty evaluated with propagation method on the following equation

$$\frac{\Delta_{pitch}}{\Delta p} = \frac{Lp_{i+1} - Lp_i}{p_{i+1} - p_i}$$

, with ± 1 mm on pitch length (Lp uncertainty, and ± 0.025 MPa on pressure value p).

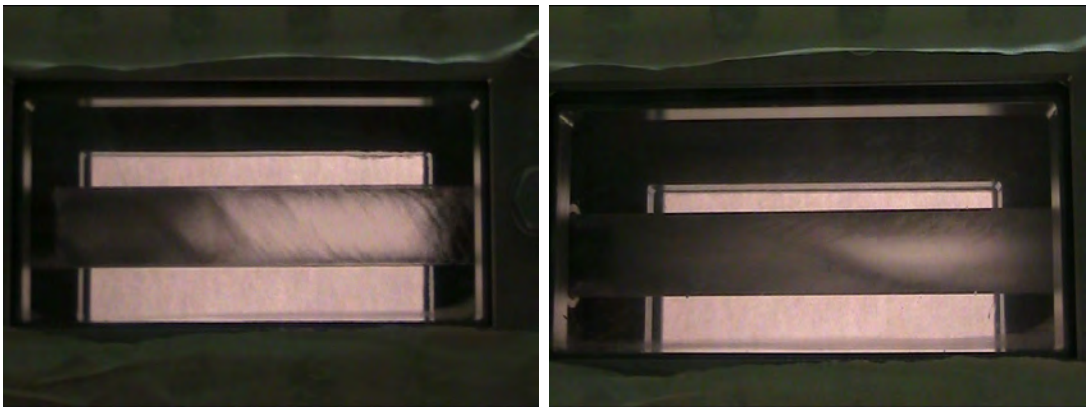

(a) 0.5 MPa (b) 4 MPa

Figure 4.19: Swirl flux comparison for discharge tests at different Δp: longer lengths of the the fluid thread pitch occur with higher pressure differences.

4.3 Mitigation Strategies

The injection behavior investigation has been conducted parallel to the first full scale test campaign, during which combustion instabilities have been detected (see par. 3.3.2) and determined the need of a deeper analysis of the phenomena. From the results of conducted tests, the initial configuration of the full scale motor have been changed. In particular, the L/D rate of the injection plate holes have been reduced, after the instabilities identification during the first part of the test campaigns. In fact, with the first injection plate, the motor behavior seemed to be affected by non optimal oxidizer injection, which caused the excitement of high amplitude pressure oscillations in the combustion chamber. For this reason, and from the tests on single hole injector, the injection plate have been changed: in the first version, the hole length was set to 12 mm (due to mechanical requirements, and as a first attempt design); in the second plate the holes have been shorten to 3.8 mm. This values are correspondent to the single hole versions for the described injection analysis.

As seen during discharge tests, the shorter injector grants lower vaporization within the hole, thus a jet with more liquid phase (higher discharged mass). On the other hand, the longer version is able to produce higher rate of vapor phase, but it don't reach the cavitation condition for the produced pressure drop between tank and combustion chamber. This means that the injected flux is less stable, thus badly influencing the combustion reaction with the fuel. For these reasons, it has been chosen a less performing injector, but able to produce a more stable jet. For the results on the developed performance during hot firing tests, please refer to section 3.3.2. Swirl injectors have not been tested in any firing experimental campaigns.

Chapter 5

Verification Tests

After the first test campaign, conducted on full scale motors, the combustion chamber internal geometry and fluid dynamics have been fixed, and the development of the rocket continued towards other technical characteristics, in order to obtain a propulsion system suitable for a possible application. Changes have interested the combustion chamber external layout and mounting interfaces, the injection plate, the hydraulic circuit and the oxidizer tanks. Two new different versions of the full scale motor have been successfully produced and tested, in the effort to check the effect of the modifications on motor performance, with particular attention to the combustion instabilities.

5.1 Full Scale Tests - 2nd phase

The modifications brought to the motor configuration for the second test campaign are summarized in the following description:

Combustion chamber The heavy ground test version have been simplified and lightened, and the structure has been adapted to the grain dimensions established during the 1st full scale test campaign (section 3.3.2). A unique cylinder contains the fuel paraffin wax grain, and the fore and aft ends permit an easy mounting of hydraulic circuit with injection plate and the nozzle, respectively. Steel has been used for all the external cases, for reasons of safety, manufacturing and availability.

Hydraulic circuit The hydraulic circuit has been totally changed, with respect to the version used during 1st test phase. The overall extension has been reduced, in order to keep the tanks next to the combustion chamber, and the

main oxidizer valve has been substituted with a custom version. The internal diameter of the piping system has been enlarged to reduce the pressure drops of the flow, and flexible pipes have been substituted by rigid tubes.

Oxidizer tanks Commercial steel reservoirs used during the first test campaign have been substituted with custom tanks, made of light alloys and composite materials: Anticorodal^{TM} Alluminum alloy for the internal liner, and fiberglass as external reinforcement. This choices have been made in order to adapt the oxidizer tanks to the real needed quantity of N_2O, to keep low their overall weight and to take confidence with lightweight materials.

The 2nd test campaign comprehended 5 firing tests, the results data of which are summarized in Table 5.1: in order to verify the performance of possible flight configuration, test FT5 has been conducted using final motor parts, which did not foresee any diagnostics mounting. From the visual monitoring of exhaust gases, the behavior seemed to be similar to all the previous tests.

The *uncertainty analysis* on calculated values (total impulse) has been conducted through the uncertainty propagation method, which has been applied to equations (2.8) described in chapter 2.

Due to the designing the tanks and hydraulic circuit, it was not possible to measure the exact burned oxidizer mass: rigid Aluminum piping did not allow the weighting of the tanks, as during the previous test campaign. Only the charged quantity of nitrous oxide has been measured, weighting directly the storage reservoir; during the tests, in fact, almost the entire content of tanks has been used: the motor functioned with liquid oxidizer in the first phase, and with the residual vapor phase in the final burning time. From the results data, it is possible to notice that the gas burning phase gives only small contribute to the overall performance.

Also during this test campaign, discharge and ignition tests have been conducted previously the firing tests in order to calibrate the injection performance and the igniters functioning. The main test results are described in the next paragraphs:

5.1.1 Tanks pressure

Pressure outlets were placed on the liquid phase section of the oxidizer tanks, just upstream the connecting pipes (as during 1st full scale test campaign). In this position, the dynamic component of pressure has been calculated, and it was

Test #	**Burning time – liquid phase (s ± 0,001s)**	**Burning time – final phase (s ± 0,001s)**	**Mean cc pressure (MPa ± 1%)**	**Total impulse (Ns)**	**Total impulse – liquid phase (Ns)**
FT1	4.05	2.00	2,269	59354 ± 5,15%	52444 ± 5,15%
FT2	4.01	2.37	3,478	60093 ± 4,68%	52427 ± 4,68%
FT3	4.05	2.00	2,703	57335 ± 5,15%	50645 ± 5,15%
FT4	4.05	2.06	2,466	57273 ± 5,06%	50029 ± 5,06%
FT5	–	–	–	–	–

Table 5.1: Resulting data for the 2nd full scale experimental campaign. *Total impulse – liquid phase* and *Specific impulse – liquid phase* are the rocket performance, limited to only liquid oxidizer discharge phase, *Total impulse* considers also the final vapor discharge phase.

negligible in all cases (0.04 MPa ± 1%). All the firing tests performed a similar behavior, and this is well described by Figure 5.1; the main discharge phases are as follows:

1. valve opening and fast pressure drop, due to the filling of the pipes empty sections, from the valve to the injection plate;

2. auto-pressurization effect in the tanks: part of the liquid vaporizes, and pressure is increased towards the saturation condition;

3. linear pressure decreasing during tanks emptying;

4. end of liquid phase;

5. vapor discharge phase, with lower thrust performance;

6. valve closing.

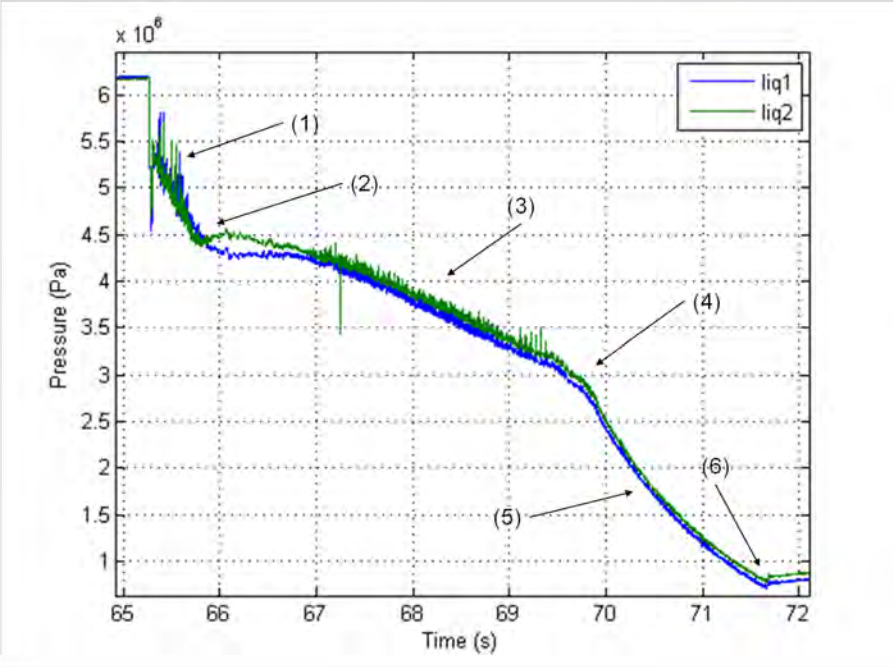

Figure 5.1: Oxidizer discharge phases during FT3.

5.1.2 Combustion chamber pressure

In the entire test campaign pressures in pre-combustion chamber and post-cc are characterized by the same trend, but different modulus. Mean pressure values in post-cc are 0.2 MPa (2 bar, ± 1%) lower than the correspondent value in pre-cc. This is due to the mixing plate, which has been installed after the final section of the fuel grain, prior the post-cc, which determined the described pressure drop. The behavior is represented in Figure 5.2, in which the following burning phases are present:

1. pressure increasing due to pyrotechnic igniters functioning (thermal flux entering the combustion chamber);

2. main valve opening and fast pressure increasing: starting of combustion reaction between wax and nitrous oxide;

3. end of liquid phase;

4. vapor phase burning time;

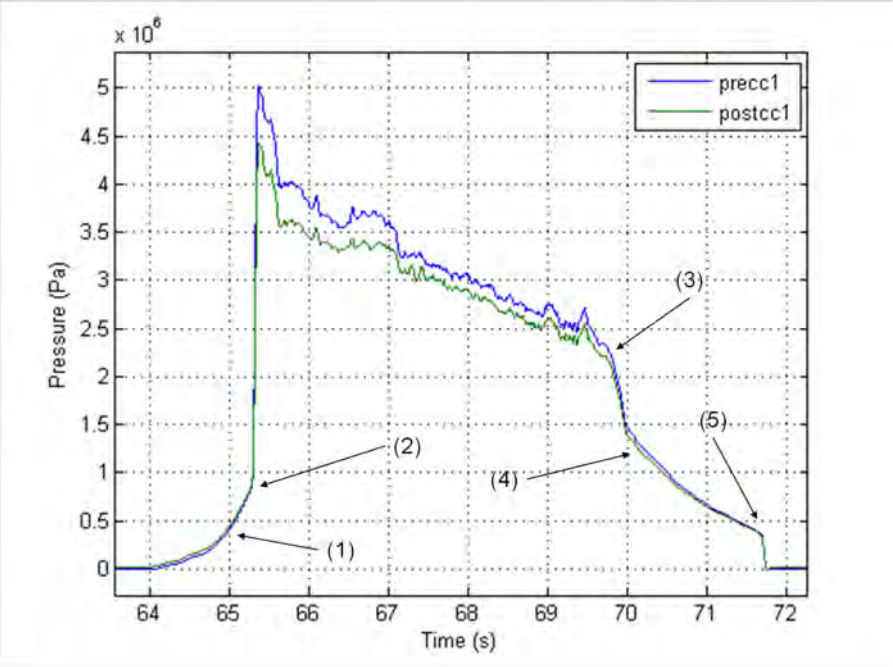

Figure 5.2: Pre-cc and post-cc pressures comparison for FT3.

5. closing of main valve.

Pressure data trends are similar during all the performed firing tests, thus confirming the repeatable performance developed by the motor. For the pressure oscillations discussion, please refer to further section 5.3.

Figure 5.3: Test FT4 during burning phase.

5.2 Full Scale Tests - 3rd phase

The aim of the last test campaign was to verify the performance of a "proto-flight" version of the hybrid rocket motor, which has been tested during the research program. In particular, a careful analysis of the combustion instabilities has been carried out, in order to have an accurate prediction of the stresses that this propulsion system would cause to an eventual payload.

Some modifications have interested again the motor configuration, and in particular the combustion chamber, which has adopted carbon fiber based composite materials for the external structure. Another aim of the tests was to verify the mechanical and thermal behavior of the most stressed parts, as the post-cc and nozzle section, which experience high combined stresses. Other design upgrades have interested the hydraulic circuit, the injection plate and the valve again, in order to have the most compact overall structure for the entire propulsion system.

After a first phase of discharge tests to verify the behavior of the oxidizer in the new version of the piping and valve, 9 hot firing tests have been carried out with a reduced sensors array, in order to test the real final subsystems. Table 5.2 summarizes the results of the test campaign.

The *uncertainty analysis* on calculated values (total impulse and specific impulse) has been conducted through the uncertainty propagation method, which has been applied to the equations (2.8) and (2.10), described in chapter 2. The uncertainty on the mean O/F values has been evaluated through the propagation method on the mean O/F ratio formula: $O/F = M_{ox}/M_f$, where M_{ox} and M_f are the weighted masses of the burned oxidizer and fuel, respectively.

The use of high performing final motor components have reduced the number of sensors, which have been mounted during the experimental investigation. This has not prevent from performing a rigorous analysis of the developed performance and instabilities, as it will be described later. The last motor version suffered some design issues, which affected in particular the connection between the carbon fiber combustion chamber and the hydraulic circuit for the oxidizer adduction (see *Notes* column for tests FT2, FT3, FT4, FT5 and FT6 in Table 5.2). The technical failures were due to the lower safety factors used during the "proto-flight" version design of the rocket components, and in general they determined lower performance (especially due to lower oxidizer mass flow rate, caused by leaks and breakages). As an example, see Figure 5.4, which reports the combustion chamber pressure pattern during FT2: the breaking of the nozzle section is clearly visible.

Test #	**Burned oxidizer mass (kg ± 0,06%)**	**Burned fuel mass (kg)**	**Mean O/F ratio**	**Mean cc pressure (MPa)**	**Burning time (s ± 0,001s)**	**Total impulse (Ns)**	**Mean Isp (s)**	**Notes**
FT1	9,4	1,55 ± 0,32%	5,7 ± 0,38%	2,25 ± 1,11%	2,77	21984 ± 1,90%	205 ± 2,00%	Ignition ok, visual stability of combustion, no valve closing, damaged nozzle
FT2	20,2	–	–	–	–	–	–	Ignition ok, break and ejection of nozzle section, oxidizer leak between motor head and valve connection, no valve closing
FT3	20,2	–	–	2,07 ± 1,21%	4,05	21139 ± 1,57%	–	Ignition ok, break of valve rear closing and large oxidizer leak from both aft section and connection with motor, no valve closing due to the failure
FT4	20,4	4,13 ± 0,12%	4,6 ± 0,18%	2,34 ± 1,07%	4,3	44270 ± 1,53%	184 ± 1,60%	Ignition ok, no oxidizer leaks, closing of main valve, deformed injection plate, connecting screws of motor head beyond yield point
FT5	22,0	4,6 ± 0,11%	4,5 ± 0,17%	2,42 ± 1,03%	4,41	48215 ± 1,51%	185 ± 1,58%	No valve closing, deformed injection plate, deformed parts in main valve and consequent break of seals
FT6	22,0	4,6 ± 0,11%	4,5 ± 0,17%	2,27 ± 1,10%	4,41	45035 ± 1,51%	173 ± 1,58%	No valve closing, oxidizer leak from connection between valve and motor head
FT7	21,7	–	–	–	–	–	–	No ignition due to malfunction of one igniter
FT8	22	4,6 ± 0,11%	4,5 ± 0,17%	3,92 ± 0,64%	4,41	50296 ± 1,51%	193 ± 1,58%	Valve closing at approx. 1 MPa (10 bar), break of sealing in head motor connection (no apparent leaking), non-deformed injection plate
FT9	19,7	–	–	–	–	–	–	Final motor parts test, no diagnostics

Table 5.2: Experimental data of the 3rd hot firing test campaign.

For these reasons, the experimental campaign has been performed with a parallel re-design activity for the inadequate components. Performance have been lower than the requirements during tests from FT1 to FT6, and this has been solved with an incremented oxidizer initial mass: last tests, FT8 and FT9, have been successful both in the thermal/mechanical behavior of the components and in the satisfaction of the performance requirements (FT8).

As the combustion chamber is concerned, the ignition phases are consistent during all the successful tests, while the patterns change towards the end of the

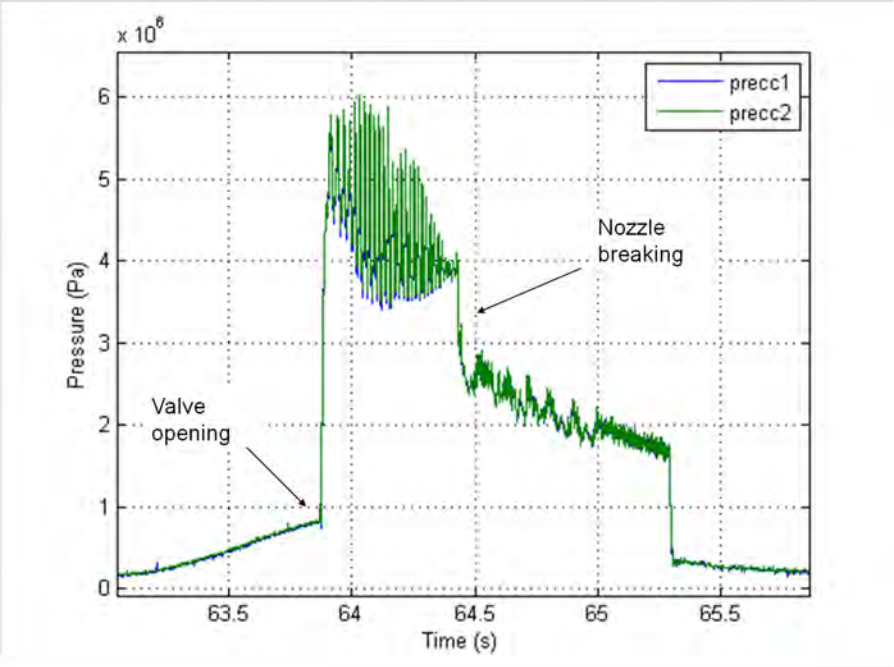

Figure 5.4: Pressure data for test FT2: nozzle breaking is clearly visible.

burning time. Figure 5.5 explain well the results, with a comparison of the measured combustion chamber pressure of the successful tests. It is notable the higher values obtained during test FT8, which was the first one without any oxidizer leak or structure failures, so the entire mass flow rate was adducted in the combustion chamber. With reference to the signal patterns, pressure oscillations develop only during the ignition of the motor burning, while they disappear after this initial transitory phase: for the analysis of the pressure instabilities occurred to the final motor version, please refer to the following section.

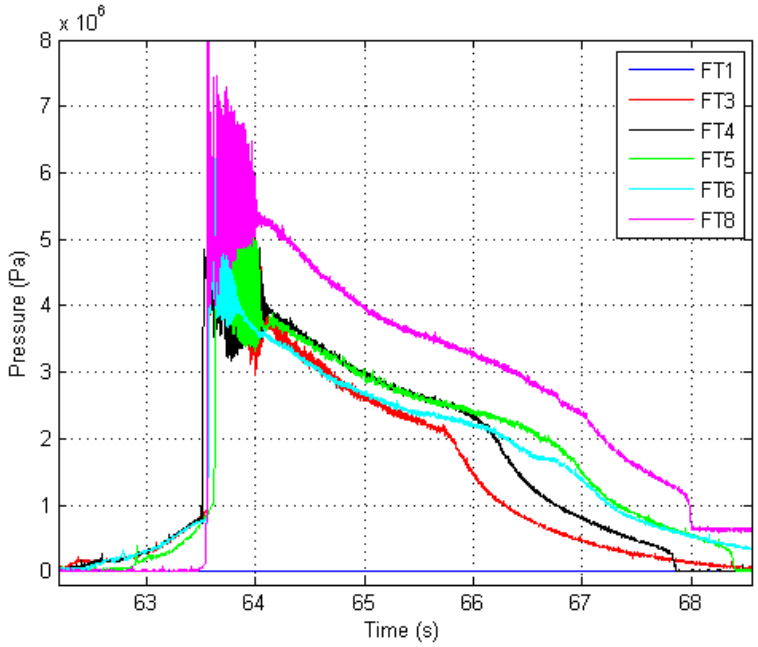

Figure 5.5: Pressure data comparison for the successful tests of the 3rd experimental campaign.

Figure 5.6: Test FT8 during burning phase.

5.3 Instabilities Analysis

During the **2nd test campaign** the typical encountered behavior is illustrated in Figure 5.7, which reproduces the time-frequency analysis of the pressure data for the combustion chamber, acquired during FT3. There is an initial unstable transient of 0.5 s, than the oscillations reduce for nearly 1 s before growing again and staying constant for the last 3 s of burn. The chamber pressure oscillates (50-60 % peak to peak) in a very coherent fashion at its fundamental frequency of approximately 45 Hz. The shape of the waves is non-linear: the rise of the pressure

is faster, and than the decay (Figures 5.8 and 5.9). The injector upstream pressure also participates in the coherent oscillations. Even though the injector pressure also participated in the oscillations, the wave forms are clipped at the lower end. This nonlinear behavior is commonly observed during *feed coupled instabilities*. This is due to the fact that high chamber pressures correspond to low mass fluxes and low pressures drops, while low chamber pressures correspond to high mass fluxes and high pressures drops. The fundamental frequency does not shift during the burning time, and its intensity is almost constant for the unstable behaviors of the test. The initial increase of the frequency is related to the pressure build up inside the chamber and the achievement of a quasi-steady state mass flow. The FFT analysis also indicates that the feed system coupled instabilities completely dominate the transient behavior, and the other low-frequency instability modes stay inactive during the entire test. This exclusion phenomenon is commonly observed in hybrid rocket systems. A number of higher harmonics (up to the 5th) of the fundamental mode are active with decreasing intensity.

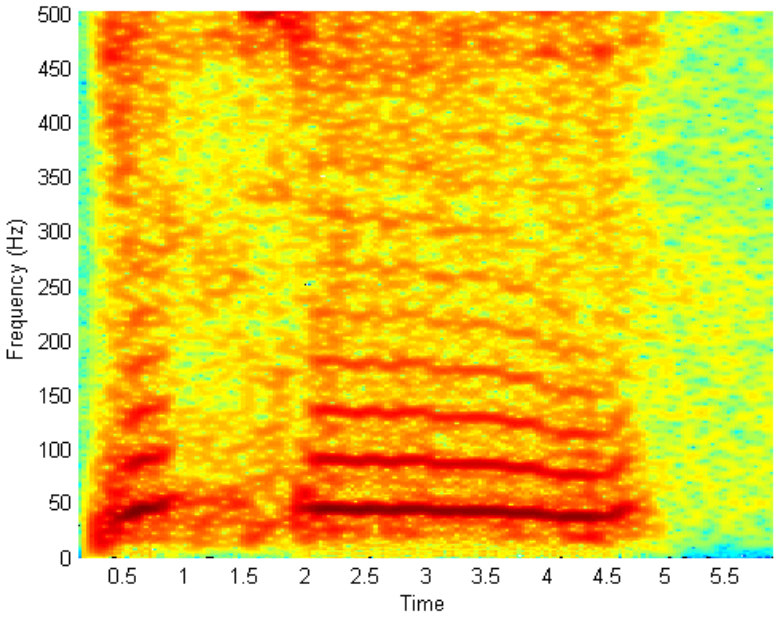

Figure 5.7: Frequency analysis of combustion chamber pressure for FT3.

The stability of the motor depends on the injector pressure drop, the chamber pressure, the nitrous oxide vapor fraction, the injection density and velocity. All these parameters affect the atomization and vaporization of the injected oxidizer. All these variables are slowly changing during the burn, affecting the stability of the system. If the system is near a critical condition, it is possible that a small

variation of the injection parameters moves the system "up and down" between a low unstable condition and a very high unstable one. This is particularly true if, as in this case, the various parameters influence the stability in opposite ways. This could explain the shift between higher and lower unstable conditions during the burn.

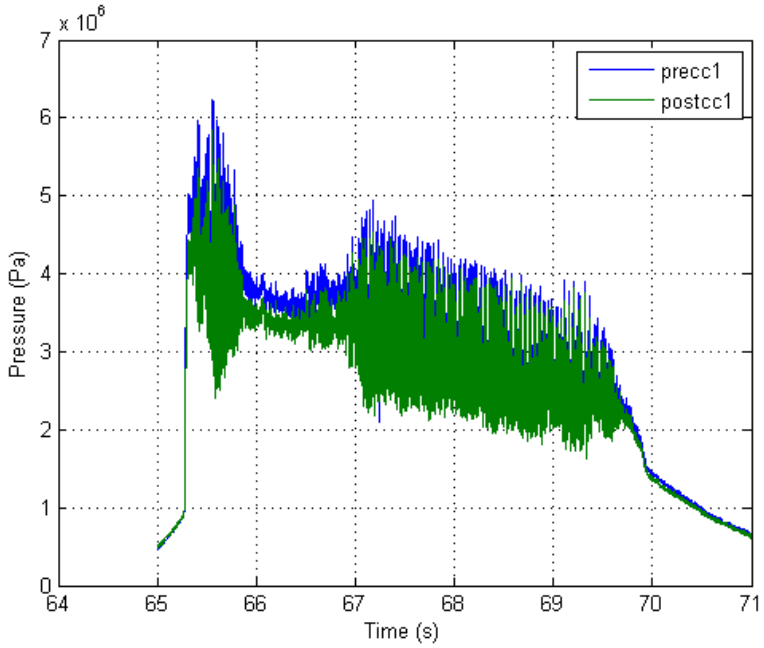

Figure 5.8: Pressure data in two different sections of the combustion chamber, for FT3.

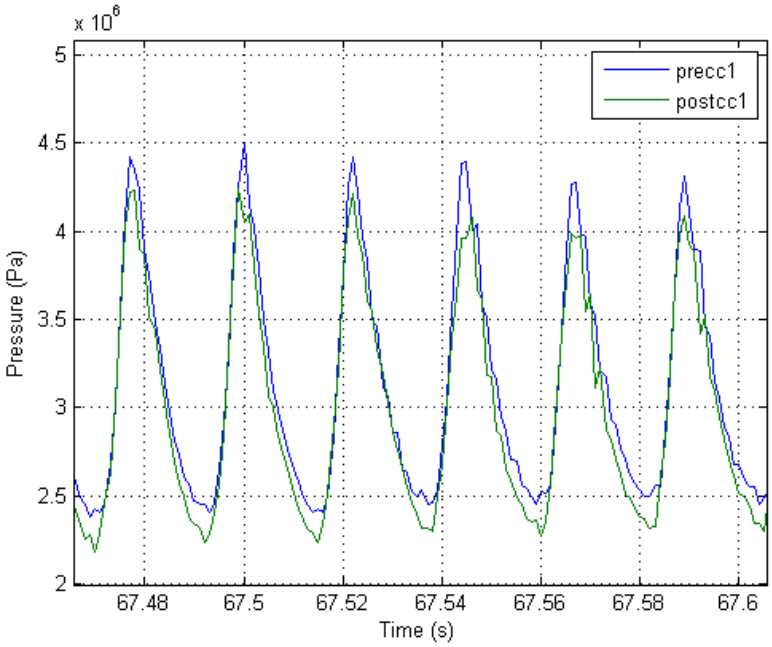

Figure 5.9: Zoom of previous graphic: pressure oscillations behavior is clearly visible.

Respect to the 2nd test campaign, during the final experimental investigation (**3rd test campaign**) a different injector plate has been used. The number and the diameter of the holes are the same (to have the same mass flow) but the disposition is different. The holes are placed in a slightly more uniform pattern. This change should modify a bit the injection behavior and the atomization/vaporization lag of the system. A reduced delay improve the stability of the motor, in fact the behavior is stable for almost the entire run, with the exception of the first 0.5 seconds (Figure 5.10). The initial behavior is similar to 2nd phase tests but after 0.5 s the system changes from an unstable to a stable condition and oscillations never occur again (Figure 5.11). The frequency of initial oscillations is a bit higher than in the previous campaign (nearly 50 Hz): this means that the system is more "rigid".From the experimental investigation, it seems that a substantial attenuation of the combustion instabilities has been achieved with a different distribution of the injection plate holes: the reason has not been definitively comprehended, and further investigations should be performed, in order to verify the physical processes, that govern such behavior.

Finally, there is a particular behavior, which has interested the first test of the 3rd campaign: during this initial reduced-burning time test, the same injection plate of the 2nd campaign has been used, but with a set of more powerful igniters (which have never been used again during the final campaign, due to some "hard

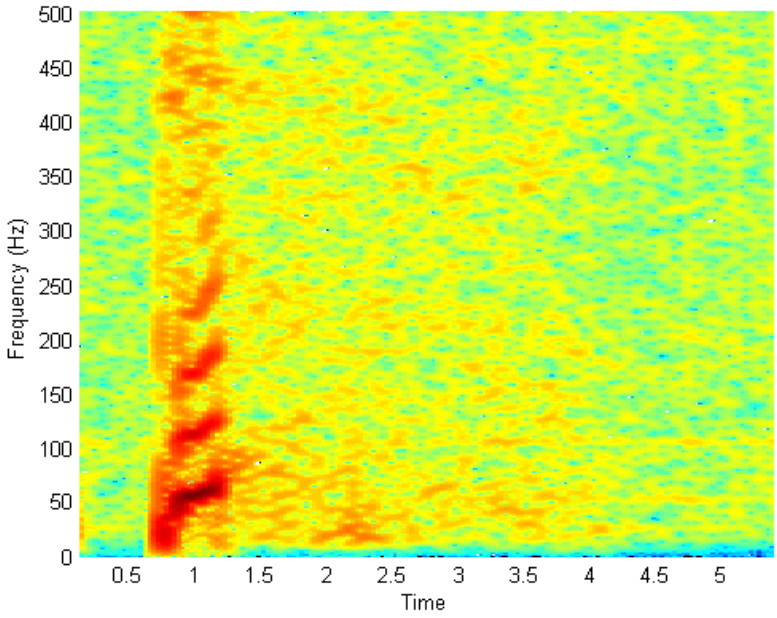

Figure 5.10: Frequency analysis of combustion chamber pressure for FT5.

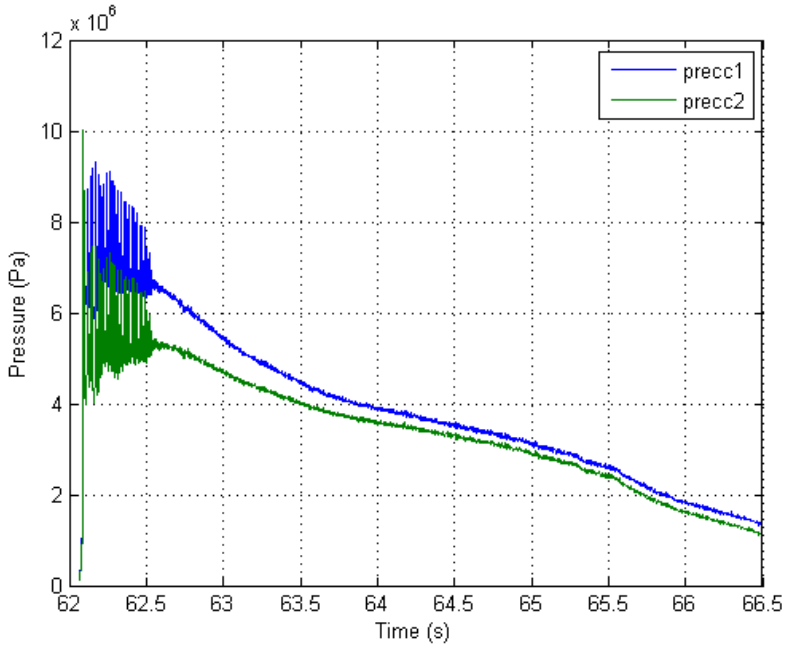

Figure 5.11: Pressure data in two different sections of the combustion chamber, for FT8.

starts" of the motor). To perform an initial short-lasting test, also the fill level of the tanks was different with respect to a complete one. Both things strongly influenced the pressure history during the burn, as shown in Figure 5.12. The initial pressure rise is steeper and the oxidizer discharge is faster. The tank is empty after a burning

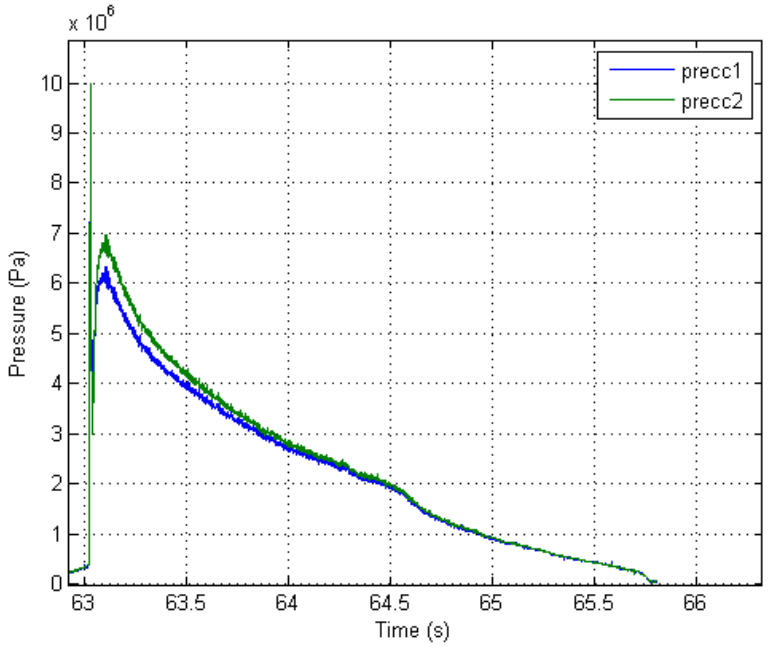

Figure 5.12: Pressure data in two different sections of the combustion chamber, for FT1.

time of only 1.5 s. Considering the preceding discussion, these changes surely have a strong impact on the stability of the motor and on the build up of pressure oscillations (and their amplification level) inside the combustion chamber.

Moreover the igniters influence not only the initial pressure but also the initial amount of heat released in the pre-cc. More heat means more vaporization of the liquid nitrous oxide, and this helps the achievement of a more stable combustion.

Chapter 6

Conclusions

In the present work a deep experimental investigation on hybrid rockets have been successfully conducted, with test campaigns on several different motor configurations. The aim of the research program was the performance characterization both of small and full scale motors, with particular attention on the combustion instabilities developed during the transitory ignition and burning phases. All the facility components, the test bench and the motor parts (hydraulic circuit, injection plate, ignition technique and combustion chamber) have been designed and produced at CISAS "G. Colombo". An accurate definition of the diagnostics systems, and its upgrade on the basis of the parameters of interest, have been done for all the different test phases. The analyses have been carried out with pressure data measured in different sections of the motor (oxidizer tanks, hydraulic circuit, pre- and post-injection, aft injection and combustion chamber), burned oxidizer and fuel masses, oxidant physical conditions: this final parameters were very important, since liquid nitrous oxide in biphasic – auto-pressurized state has been used. Basically, every motor version has been tested in three different test types:

- oxidizer "cold" discharge, to verify the performance of the hydraulic circuit;
- ignition tests, to calibrate the thermal flux that is necessary to correctly ignite the motor;
- "hot" firing tests, which comprehend all the functioning phases of a complete burning test.

The subject of the first experimental campaign was a small scale hybrid rocket (2000 Ns of total impulse), which served as a test bed to take confidence with testing of chemical propulsion systems, to calibrate the diagnostics set-up, to chose

the final ignition subsystem and to characterize the performance of different fuel grains: nylon, polyethylene, polyethylene wax and paraffin wax. Thanks to the high average regression rate obtained values (up to 3 mm/s), paraffin wax aided with EVA glue and carbon has been chosen as final material for the solid grain: its mechanical and thermal properties have demonstrated to be adapted for such an application, and its burning performance have allowed a simplified configuration of the grain, with respect to polymer materials. In fact, paraffin wax has been chosen also for the full scale motors, and single cylinder port has been able to perform the required propulsion performance (the same results would have required multi-port configuration, in case of polymer fuels). During ignition tests, two different solution have been tested: bi-propellant torch and pyrotechnical igniters; the first technique was useful to evaluate and calibrate the exact thermal flux to be used, in order to perform an instantaneous ignition of the motor at the oxidizer main valve opening.

The first full scale experimental investigation has been conducted on a ground hybrid rocket demonstrator, with 50 kNs of required total impulse. The design solutions have allowed the installation of several measurement sensors, in order to have complete and redundant diagnostics of the motor. Cold discharge tests have been useful for the verification of correct design of the adducting piping and the injection performance of the injection shower plate with high mass flow rates (up to 5 kg/s). Ignition tests have demonstrated the effectiveness of using multiple pyrotechnical igniters to correct start the burning reaction in the combustion chamber. During the hot firing tests, the propulsion performance have been measured, together with combustion efficiency and average regression rate values. The following considerations can be done:

- the designed propulsion system have satisfied the performance requirements of 50 kNs of total impulse.

- a high total motor efficiency has been reached adopting a specific mixing plate in the post-combustion chamber section. Values have been up to 90% of the theoretical prediction, and no particular influence has been demonstrated by different ignition tehcniques or pre-cc types. General lower values have been obtained with respect small scale tests, due to higher specific oxidizer flux (Gox of 200-300 kg/m^{2}s) and scale effect.

- average regression rate measured values have been 70% to 80% of the theoretical values, and this was due to different fuel composition (theoretical calculation did not take into account the EVA glue and carbon additives).

As the combustion stability is concerned, the first full scale motor in its initial testing phase suffered from a shifting behavior, in which two different equilibrium conditions alternate: one unstable condition, with high combustion efficiency, and a stable condition at lower efficiency. The reason of this unpredictable and random shifting behavior was the flip/unflip character of the oxidizer injection: in fact, after changing of the L/D ratio of the plate holes, the bimodal condition disappeared.

The injection behavior has been specifically analyzed through the set-up of a test facility, to perform discharge tests of different injector types, in many different discharge conditions. An important parameter to be monitored during this kind of experimental investigation was the mass flow rate of biphasic flow: due to unpredictable vapor fraction value, commercial sensors are not suitable for this application, so a dedicated measurement instrument has been designed and set-up. The functioning principle is the weighting of the storage tank prior, after and during the discharge. The weight data are then analyzed and numerically processed, and a time-dependent mass flow rate measurement has been possible. Characteristic performance of the designed instrument are as follows: 100 g/s full scale mass flow rate, with 2.5% accuracy and 25 Hz of bandwidth. The results of the conducted injection investigation have been applied to hot firing tests.

The last full scale experimental campaigns have served to check the performance of the motor, after the injection modifications, and for lightweight versions of the entire propulsion system, with particular attention on the instabilities mitigation. During the second full scale experimental investigation, the propulsive requirements have been satisfied, thanks to the corrected design of the injection plate. The motor behaved in similar manner during all the conducted tests, and from the instability point of view it presented another pressure oscillation pattern, with respect the first motor version. The fundamental frequency was about 45 Hz, and from the spectra pressure data in combustion chamber it has been possible to recognize the typical behavior observed during feed coupled instabilities.

The final test campaign subject was a possible “proto-flight” version of the hybrid rocket, in which compact design and lightweight materials have been used. From the fluid dynamics point of view, changes have interested the injection plate: it had the same number of holes with respect the previous motor configuration, but the pattern disposition was slightly more uniform. This solution has modified the injection behavior, and this resulted in a more stable combustion: in fact, the initial oscillations were quite similar to the previous motor configuration, but after the transitory ignition phase they disappear, and never occur again till the end of

the burning phase. The conducted analysis on this final motor version have been useful in the determination of the stresses, that would affect any possible payloads of the produced propulsion system.

During the Ph.D. research program, the following publications have been produced:

A. Bettella, M. Manente, E. Benini, Y. Guçlu, D. Curreli, **F. Moretto**, S. Martini, M. Pessana, T. Walloschek, M. De Rosa, T. Kachler, D. Pavarin,
Turbo-pump Pressurization Concept for Hybrid Propulsion Thrusters Application to Launch Vehicles,
44th AIAA/ASME/SAE/ASEE Joint Propulsion Conference & Exhibit, 21 - 23 July 2008, Hartford, CT, USA, AIAA Paper 2008-4934.

F. Moretto, A. Bettella, N. Bellomo, G. Parissenti, M. Pessana, D. Pavarin,
Feasibility Study of Hybrid Propulsion System for Sounding Rocket Application,
2nd Space Propulsion Conference, San Sebastian, Spain, 2nd-5th May 2010, paper SP2010_1842382.

N. Bellomo, A. Bettella, **F. Moretto**, F. Branz, M. Faenza, D. Papale, G. Venturelli, M. Pessana, D. Pavarin,
Feasibility Study for Throttleable Hybrid Rocket Motor for Soft Landing
2nd Space Propulsion Conference, San Sebastian, Spain, 2nd-5th May 2010, paper SP2010_1842370.

Bibliography

[1] Ronald W. Humble, Gary N. Henry, Wiley J. Larson,
Space Propulsion Analysis and Design.
2nd ed., Space technology series, The McGraw-Hill Companies, Inc. Primis Custom Publishing, New York, 1995.

[2] George P. Sutton, Oscar Biblarz,
Rocket Propulsion Elements.
7th ed., John Wiley & Sons, 2001.

[3] Martin J. Chiaverini, Kenneth K. Kuo,
Fundamentals of Hybrid Rocket Combustion and Propulsion.
Progress in Astronautics and Aeronautics, Frank K. Lu, Editor-in-Chief, Volume 218; American Institute of Aeronautics and Astronautics, Inc., Reston, Virginia, 2007.

[4] Ernest O. Doebelin,
Measurement Systems: Application and Design.
4th ed., McGraw-Hill, Singapore, 1990.

[5] Matthias Grosse,
Effect of a Diaphragm on Performance and Fuel Regression of a Laboratory Scale Hybrid Rocket Motor Using Nitrous Oxide and Paraffin.
45th AIAA/ASME/SAE/ASEE Joint Propulsion Conference & Exhibit, 2 – 5 August 2009, Denver, Colorado (USA).

[6] Enrico Geremia,
Analisi Sperimentale e Numerica del Comportamento dell'N_2O in un Sistema di Alimentazione per Endoreattori a Propellenti Ibridi - Experimental and Numerical Analysis of N_2O Behavior in the Feeding System

for Hybrid Rocket Motors.
Master of Science Thesis, Padua, Italy, 2009.

[7] D. Van Pelt, J. Hopkins, M. Skinner, A. Buchanan, R. Gulman, H. Chan, M. A. Karabeyoglu and B. J. Cantwell,
Overview of a 4-Inch Paraffin-Based Hybrid Sounding Rocket Program.
40th AIAA/ASME/SAE/ASEE Joint Propulsion Conference & Exhibit, July 2004, Fort Lauderdale, Florida (USA), paper AIAA-2004-3822.

[8] G. M. Faeth, L.-P. Hsiang and P.-K. Wu,
Structure and Breakup Properties of Sprays.
Int. J. Multiphase Flow, Vol. 21, Suppl. pp. 99-127, 1995.

[9] Justin M. Pucci,
The Effect of Swirl Injector Design on Hybrid Flame-Holding Combustion Instability.
38th AIAA/ASME/SAE/ASEE Joint Propulsion Conference & Exhibit, July 2002, Indianapolis, Indiana (USA), paper AIAA-2002-3578.

[10] Charles C. Jones, David D. Myre, James S. Cowart
Performance and Analysis of Vortex Oxidizer Injection in a Hybrid Rocket Motor.
45th AIAA/ASME/SAE/ASEE Joint Propulsion Conference & Exhibit, 2-5 August 2009, Denver, Colorado (USA), paper AIAA 2009-4938.

[11] M. Arif Karabeyoglu, Brian J. Cantwell and Greg Zilliac,
Development of Scalable Space-time Averaged Regression Rate Expressions for Hybrid Rockets.
41st AIAA/ASME/ASEE Joint Propulsion Conference, Tucson, AZ, USA, 10-13 July 2005, paper AIAA 2005-3544.

[12] Jonny Dyer, Eric Doran, Zach Dunn, Kevin Lohner, Greg Zilliac, Brian Cantwell,
Modeling Feed System Flow Physics for Self-Pressurizing Propellants.
43rd AIAA/ASME/SAE/ASEE Joint Propulsion Conference & Exhibit, 8-11 July 2007, Cincinnati, OH, USA, paper AIAA 2007-5702.

[13] Arif Karabeyoglu,
Thermal Transients in Hybrid Rocket Fuel Grains – Nonlinear Effects.
43rd AIAA/ASME/SAE/ASEE Joint Propulsion Conference & Exhibit, 8-11 July 2007, Cincinnati, OH, USA, paper AIAA 2007-5369.

[14] Martin J. Chiaverini, Kenneth K. Kuo, Arie Peretz and George C. Harting,
Regression-Rate and Heat-Transfer Correlations for Hybrid Rocket Combustion.
Journal of Propulsion and Power, Vol. 17, No. 1, January-February 2001.

[15] Gerald A. Marxman,
Combustion in the Turbulent Boundary Layer on a Vaporizing Surface.
Tenth Symposium (International) on Combustion, pp. 1387-1849, The Combustion Institute, 1965.

[16] M. Arif Karabeyoglu and D. Altman,
Dynamic Modeling of Hybrid Rocket Combustion.
Journal of Propulsion and Power, Vol. 15, No. 4, July-August 1999.

[17] Arif Karabeyoglu, Jose Stevens and Brian Cantwell,
Investigation of Feed System Coupled Low Frequency Combustion Instabilities in Hybrid Rockets.
43rd AIAA/ASME/SAE/ASEE Joint Propulsion Conference & Exhibit, 8-11 July 2007, Cincinnati, OH, USA, paper AIAA 2007-5366.

[18] M. A. Karabeyoglu, D. Altman and B. J. Cantwell,
Combustion of Liquefying Hybrid Propellants: Part 1, General Theory.
Journal of Propulsion and Power, Vol. 18, No. 3, May-June 2002.

[19] Arif Karabeyoglu and Jonny Dyer,
Nonlinear Combustion in Hybrid Rockets – Explanation of Spontaneous Shifting in Motor Operation.
45th AIAA/ASME/SAE/ASEE Joint Propulsion Conference & Exhibit, 2-5 August 2009, Denver, Colorado, USA, paper AIAA 2009-5218.

[20] C. Carmicino and A. Russo Sorge,
On the Role of Vortex Shedding in Hybrid Rockets Combustion

Instability.
44th AIAA/ASME/SAE/ASEE Joint Propulsion Conference & Exhibit, 21-23 July 2008, Hartford, CT, USA, paper AIAA 2008-5016.

[21] C. Carmicino and A. Russo Sorge,
The Effects of Oxidizer Injector Design on Hybrid Rockets Combustion Stability.
42nd AIAA/ASME/SAE/ASEE Joint Propulsion Conference & Exhibit, 9-12 July 2006, Sacramento, California, USA, paper AIAA 2006-4677.

[22] Kevin Lohner, Jonny Dyer, Eric Doran, Zachary Dunn and Greg Zilliac
Fuel Regression Rate Characterization Using a Laboratory Scale Nitrous Oxide Hybrid Propulsion System.
42nd AIAA/ASME/SAE/ASEE Joint Propulsion Conference & Exhibit, 9-12 July 2006, Sacramento, California, USA, paper AIAA 2006-4671.

[23] Alon Gany
Scale Effects in Hybrid Motors under Similarity Conditions.
32nd AIAA/ASME/SAE/ASEE Joint Propulsion Conference & Exhibit, 1-3 July 1996, Lake Buena Vista, FL, USA, paper AIAA 96-2846.

[24] S. Venkateswaran, C. L. Merkle
Size Scale-up in Hybrid Rocket Motors.
AIAA 34th Aerospace Sciences Meeting and Exhibit, Reno, NV, Jan 15-18, 1996, paper AIAA Paper 96-0647.

[25] O. Y. Park, C. T. Bryant and R. L. Carpenter
Performance Analyses of HPDP 250K Hybrids.
36th AIAA/ASME/SAE/ASEE Joint Propulsion Conference & Exhibit, 16-19 July 2000, Huntsville, Alabama, USA, paper AIAA 2000-3544.

At the end of this challenging period of work, I would like to express sincere thanks to the staff of the space propulsion group at CISAS, my colleagues, my friends:

Daniele, Alberto, Marco,
Enrico, Nicolas, Francesco, Marta, Martina, Marco,
Davide, Yaman, Andrea, Davide, Mattia, Fabio,
Stefano, Andrea.